PRICES SUBJECT TO CHANGE

(NASA-CR-114751) DEVELOPMENT OF ELECTRICAL FEEDBACK CONTROLLED HEAT PIPES AND THE ADVANCED THERMAL CONTROL FLIGHT EXPERIMENT Technical Summary (Dyna-Therm Corp.) CSCL 20M G3/33 46722

N74-32370

Unclas

dynatherm
CORPORATION

NASA CR 114,751

N74-32370

DTM-74-2

TECHNICAL SUMMARY REPORT

for

DEVELOPMENT OF ELECTRICAL FEEDBACK CONTROLLED HEAT PIPES AND THE ADVANCED THERMAL CONTROL FLIGHT EXPERIMENT

by Walter B. Bienert

May 1974

Prepared under Contract NAS2-6227

by

Dynatherm Corporation
One Industry Lane
Cockeysville, Maryland

for

National Aeronautics and Space Administration
Ames Research Center

FOREWORD

This report presents the summary of the "Development of Electrical Feedback Controlled Heat Pipes and the Advanced Thermal Control Flight Experiment." The work was performed by Dynatherm Corporation under NASA Ames Research Center Contract NAS2-6227 and under the direction of Mr. J. P. Kirkpatrick, the NASA Technical Monitor.

Since the preparation of the draft of this report the ATFE Flight Experiment was launched aboard the ATS-F satellite. Initial telemetry data indicate that the experiment is achieving its objective successfully.

TABLE OF CONTENTS

TABLE OF CONTENTS (Cont'd)

LIST OF FIGURES

LIST OF FIGURES (Cont'd)

LIST OF FIGURES (Cont'd)

LIST OF TABLES

1. INTRODUCTION

The program described in this report consisted of two major tasks:

- Development of the Technology of Feedback Controlled Variable Conductance Heat Pipes
- Design, Fabrication, and Qualification of an Advanced Thermal Control Flight Experiment (ATFE)

The concept of feedback controlled variable conductance heat pipes (FCHP) had been studied analytically during a previous contract (Ref. 1). While evaluating both passive (mechanical) and active (electrical) feedback systems, it became apparent that the latter offers better control capability and is more suitable for aerospace applications. The objective of the first task of the present program was thus to develop the necessary technology for flight qualification of an electrical FCHP.

The Advanced Thermal Control Flight Experiment is designed to demonstrate the performance of this new thermal control component in a space environment. In addition, the temperature control aspects of a passive thermal-diode heat pipe and of a phase-change material (PCM) also will be evaluated. The ATFE will be flown aboard the Applications Technology Satellite (ATS-F), which is scheduled for launch in May 1974. While the ATFE is an experiment designed to provide performance data for the components mentioned above, it is also a thermal control system that can be used to provide temperature stability of spacecraft components in future applications.

A summary of the program milestones and of the intermediate steps which led to the flight qualification of the ATFE is provided in Section 2 of this report. The results of the Technology Development Phase are presented in Section 3, and an in-depth discussion of the ATFE system design and qualification is provided in Section 4.

2. PROGRAM MILESTONES AND SUMMARY

The program was initiated during August 1970. During the technology development phase, a comprehensive analytical model of an electrical FCHP was developed and breadboard experiments were conducted to verify and amplify the model.

An active FCHP is shown schematically in Figure 2.1. It is basically a gas-controlled wicked-reservoir heat pipe that utilizes an electronic controller and a reservoir heater to adjust its thermal conductance. An increase in heat source temperature, caused by an increase in heat load and/or sink condition, results in an error signal to the controller and causes it to turn off the power to the reservoir heater. The corresponding decrease in reservoir temperature, and therefore in the vapor pressure of the working fluid in the reservoir, results in an increase in the effective storage volume thereby allowing more noncondensible gas to enter. This causes the gas-vapor interface to move toward the reservoir, thus increasing the condenser conductance and ultimately reducing the source temperature. The continual adjustment of the conductance by regulation from the controller can provide essentially absolute temperature control under broad variations in heat load and sink conditions.

The analytical model, which was developed under this program, describes the performance of a FCHP both under steady-state and transient conditions. The steady-state performance can be adequately handled through a closed form analysis, while a computer program (FEDCON) was developed to perform transient performance calculations. Also, in order to get a better general understanding of the response characteristics of a FCHP than that afforded by a numerical analysis, a highly simplified closed form transient model was developed. Comparison of computer solutions and

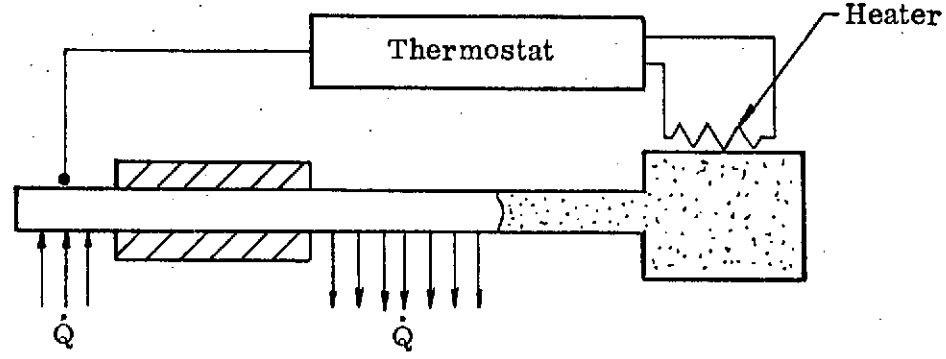

FIGURE 2.1

SCHEMATIC OF ELECTRICAL FEEDBACK CONTROLLED VARIABLE CONDUCTANCE HEAT PIPE

results from the closed form model showed that the latter gives adequate first order answers to a particular design problem.

Two breadboard models of electrically controlled FCHP's were fabricated and tested. Initial tests were conducted with manual control of the reservoir heater; later, automatic on-off control was used; and finally a proportional controller was employed. The effects of variations of the heat load and of the sink temperature were studied with these experiments. Also, different thermal masses of the heat source were employed in order to evaluate transient response characteristics. The test results correlated very well with the predictions by the analytical models; and, as a result, the technology of FCHP's was considered developed to a point where incorporation of such a system into a flight experiment was justified.

Definition of the ATFE flight experiment started early in the program. Basically, the ATFE (Figure 2.2) consists of a solar absorber, a thermal diode, a simulated equipment package that contains phase-change material (PCM box), an electrical feedback-controlled variable conductance heat pipe (FCHP), and a space radiator. Supporting hardware, not shown in Figure 2.2, are a solid-state electronics module, temperature sensors, foil heaters, support structure, and thermal insulation.

The ATFE is mounted in the east wall of the ATS-F earth-viewing module with only the outboard surfaces of the solar absorber and radiator exposed to the external environment. Three-axis stabilization and the geosynchronous orbit result in an incident solar flux that rises and sets over a 12-hour period and is followed by 12 hours of darkness, similar to the solar cycle experienced by a fixed point on Earth's surface. The absorbed solar energy is used to simulate power dissipation during an electrical duty cycle and is transported from the absorber to the PCM box by the diode heat pipe.

ADVANCED THERMAL CONTROL FLIGHT EXPERIMENT (ATFE)

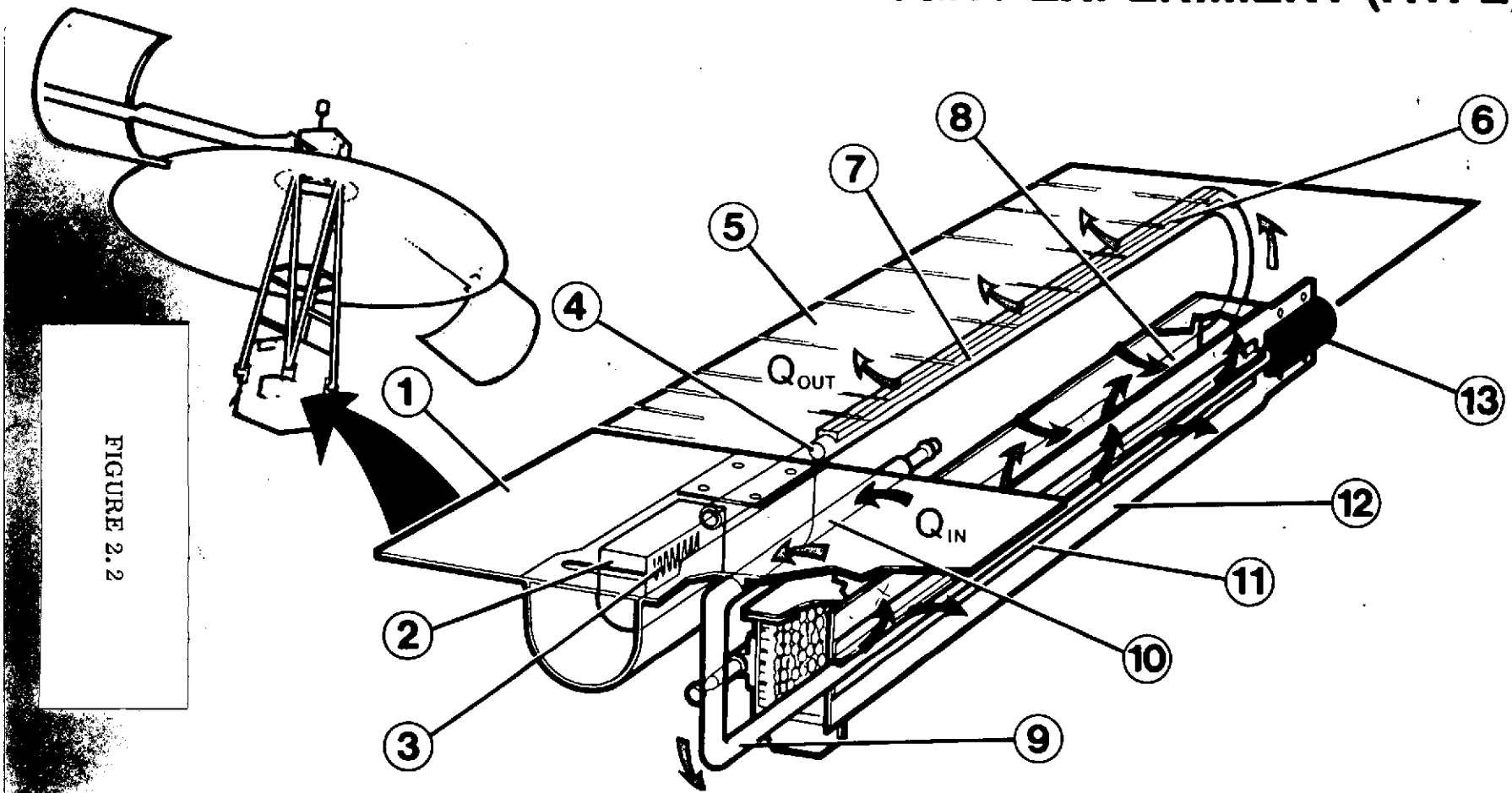

FIGURE 2.2

1 SOLAR ABSORBER
2 GAS RESERVOIR
3 CONTROL HEATER
4 GAS/VAPOR INTERFACE
5 RADIATOR
6 FEEDBACK CONTROLLED HEAT PIPE (FCHP)
7 FCHP CONDENSER SECTION
8 FCHP EVAPORATOR SECTION
9 THERMAL DIODE HEAT PIPE
10 DIODE EVAPORATOR SECTION
11 DIODE CONDENSER SECTION
12 PHASE CHANGE MATERIAL (PCM) BOX
13 LIQUID RESERVOIR

This energy first melts the PCM, which is octadecane with a melting point of 28°C. When melting has been completed, the energy then passes through the PCM box to the FCHP, which transports it to the space radiator. During the cycle, temperature control of the diode/PCM box interface is provided by the FCHP whose temperature control set point is 29°C. The FCHP system senses the temperature at the interface and correspondingly regulates the heat rejection to space to accommodate the variations in both the thermal load and the thermal boundary conditions at the radiator. As the shadow period is approached, the diode and FCHP decrease their conductance to minimize the heat loss from the PCM box to space. Thermal energy released by freezing the PCM is used to compensate for heat lost during the transient shutdown of the diode and FCHP and to provide temperature stability during part of the shadow period. When all the PCM has frozen, the temperature of the equipment shelf decreases at a rate that depends on the heat capacity of the PCM box and its parasitic heat leaks. The amount of octadecane provided in the PCM box is designed to permit cooling of the PCM box to approximately 0°C. This allows the evaluation of the PCM melting point stability in zero gravity.

Initial sizing of the absorber panel, the PCM box, and the radiator was made using a computer code ATFETA, which established preliminary design data associated with the thermal response of elements in the ATFE. More detailed analysis was conducted later in the program. For instance, a trade-off study between amount of PCM and diode conductance was performed and the effects of the different coatings on absorber and radiator were evaluated. Also, detailed failure analyses were conducted in order to assess the impacts of failures of either the diode or the FCHP on obtaining meaningful data from the flight experiment.

With respect to the PCM box, a breadboard model of a representative section was fabricated and tested. The results were correlated to within 5% of the analytical predictions.

Three complete systems of the ATFE experiment were fabricated and tested -- an Engineering Model, Qualification Model, and the Flight Model. In addition, a nonfunctional structural model was delivered to the spacecraft contractor (Fairchild Industries, Inc.) for integration testing with the Thermal Structural Model (TSM) of the ATS spacecraft. The on-off temperature controller, the command circuitry, and signal conditioning for the ATFE telemetry were developed by ITE, Inc., under subcontract to Dynatherm.

The Engineering Model was delivered to NASA ARC in December 1971. Ambient functional tests, thermal vacuum tests, and qualification level vibration tests were performed at Ames. Results of the ambient test demonstrated the ability of the thermal diode to transport the required 20 watts in the forward mode. The ability of the FCHP to transport 20 watts was also demonstrated.

Steady-state and 24-hour orbital cycle tests were conducted in the thermal vacuum. Solar simulation was accomplished by applying power to heaters attached to the underside of the absorber and radiator panels. In general, individual components and the complete experiment performed in accordance with experiment objectives. As a result of these tests, several design changes were made on the Qualification and Flight Models. The changes dealt mostly with improving the insulation in order to reduce heat leaks from the PCM shelf. These heat leaks and losses, during the transient shutdown of the diode, depleted the PCM shelf of its stored energy sooner than predicted. During the Engineering Model tests, the reservoir heater power required to maintain control

was approximately 4.5 watts as compared to the 2.8 watts provided by the controller. The increased power requirement was due to conduction losses from the reservoir along the heat pipe tube to the radiator fins. Consequently, the design of the subsequent models was modified to include a low conductance section in this area and the 2.8 watts proved adequate.

After evaluation of the test results from the Engineering Model, a Critical Design Review (CDR) was held at NASA GSFC. Two major modifications to the ATFE design were recommended at the CDR:

- The absorber length was increased by 1 inch and the radiator length decreased. This modification increased the thermal input to the experiment and ultimately the thermal throughput of the feedback controlled heat pipe.
- The Electronics Module was relocated to the outside of the Experiment so that it is thermally coupled to the spacecraft. This was done in order to isolate the module from the excessively low temperatures experienced by the absorber and radiator during the shadow period.

Fabrication of the Qualification and the Flight units was started following the CDR. Engineering evaluation tests were performed at Fairchild Industries with the ATFE interfaced with the ATS-F Experiment Integration Unit (EIU). The EIU is used to simulate the spacecraft's electrical interface.

The Qualification Unit was subjected to Qualification Level tests at NASA ARC during August 1972. Thermal vacuum and vibration were two major areas of testing.

The ATFE satisfied all acceptance criteria for all tests performed. The only one continuing problem encountered was the early depletion of the energy stored in the PCM. Even with the insulation improved, the PCM provided thermal control for only five hours of the freezing period as opposed to a predicted twelve hour period based on a calculated 2-watt leak. The only corrective action considered was to provide additional insulation in the Flight Unit.

Fabrication of the Flight Unit was completed in January 1973. During the thermal vacuum testing at ARC, the thermal diode of the Flight Unit did not completely turn off, thus creating an additional heat leak from the PCM shelf. This partial failure of the diode could either be attributed to slightly different thermal coupling between diode and PCM shelf or to an intrinsic problem in this particular diode. Since it was impossible to distinguish between the two causes, the thermal coupling was improved and the diode was replaced by that from the Qualification Unit (which had functioned properly). The Flight Unit was then retested at ARC and satisfied all acceptance criteria.

Part of the qualification and acceptance test program was testing for electromagnetic interference (EMI) susceptibility. The levels of the RF energy radiated by the spacecraft were not available until shortly before the tests commenced. As a result, EMI shieldings had to be installed empirically during the tests until the specified interference levels were met.

Since the Qualification Unit served as a back-up for the Flight Unit, it also had to be retrofitted with EMI shielding and the diode from the Flight Unit had to be installed into the Qualification Unit. Because these modifications represented significant changes in the system, this model was also subjected to requalification tests at ARC. These tests were conducted during October 1973. The Qualification Unit now exhibited the

same partial failure of the diode which indicated that the problem formerly encountered with the Flight Model had been intrinsic with the particular diode and had not been caused by poor thermal coupling in the assembly. Since all other functional test objectives were met with the Qualification Unit, it was decided to use it in its present status as a flight back-up. The philosophy behind this decision was that only a slim chance exists that it had to be used as a back-up. If this need were to arise a new diode could conceivably be installed in time. But even if the Qualification Unit had to be flown in its present condition, significant flight data would be obtained.

The Qualification Unit is presently in NASA storage, and the Flight Unit has been integrated with the ATS-F spacecraft in preparation for the May 1974 launch.

3. TECHNOLOGY DEVELOPMENT

A major objective of this program was the development of the technology of Feedback Controlled Variable Conductance Heat Pipes (FCHP) and Phase Change Material (PCM) packages for storage of latent heat. A large fraction of the analytical and experimental effort was expended toward FCHP's, primarily because its technology was completely unexplored at the beginning of the program. Some background information on PCM packages had been available. Thus, the development effort in that area was directed toward a breadboard model of the same basic design as was to be employed in the ATFE Flight Experiment.

With regard to the FCHP, some of the results have already been published (Ref. 3 and Ref. 4). An outline of the theory was also provided in the Heat Pipe Design Handbook (Ref. 5). The following sections of this report present the theory of FCHP's in a self-consistent form including those aspects which have already been reported.

The steady-state behavior of a FCHP is discussed in Section 3.1. It is followed by the derivation of analytical models for the transient characteristics in Section 3.2. Both an approximate closed form solution and a numerical computer model are discussed. The results of breadboard experiments supporting the analysis are given in Section 3.3. Finally, the breadboard development of PCM packages is summarized in Section 3.4.

3.1 Steady-State Analysis of FCHP's

An electrically controlled FCHP is shown schematically in Figure 3.1. It is basically a gas-controlled wicked-reservoir heat pipe that utilizes an electronic con-

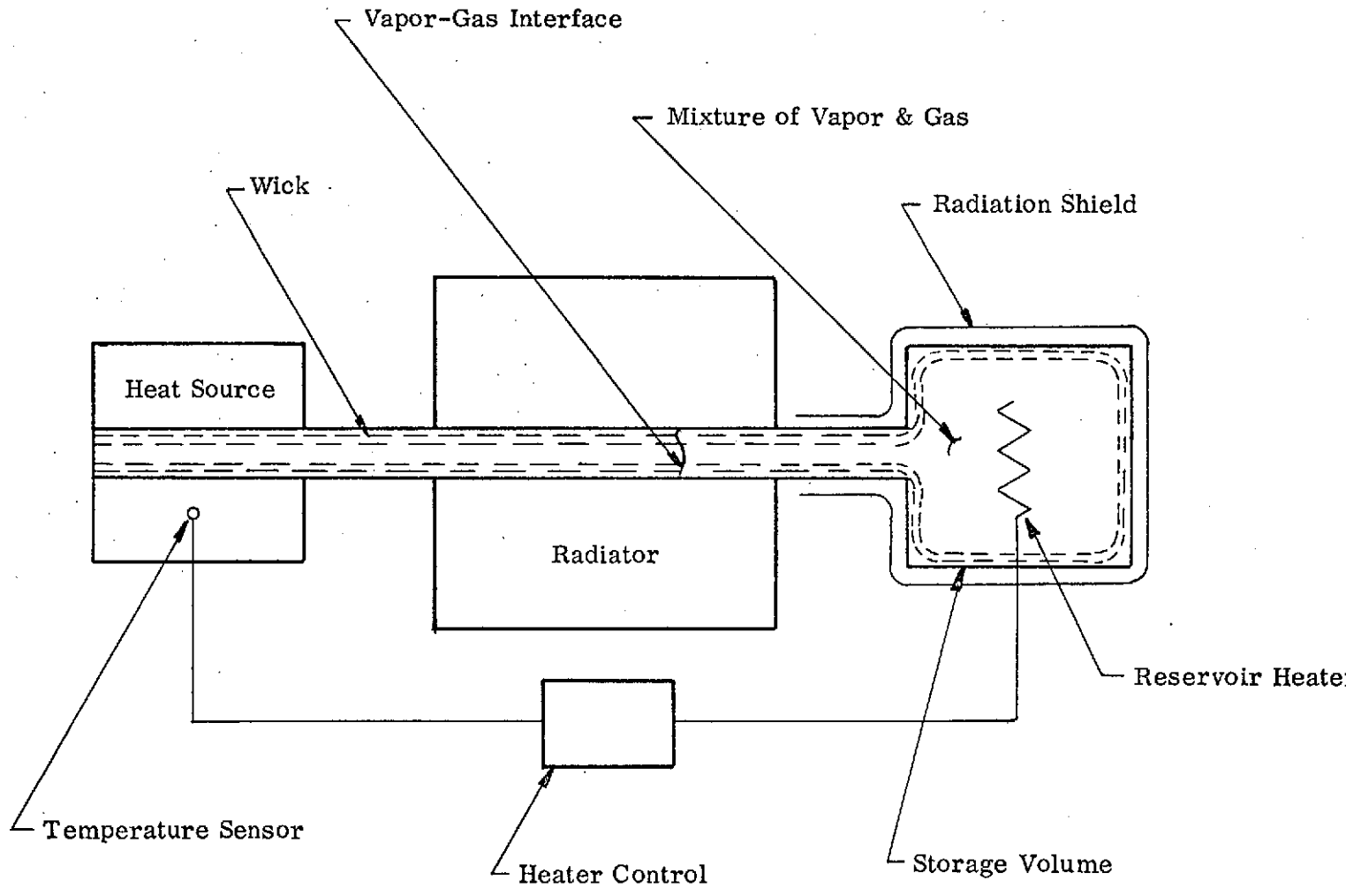

FIGURE 3.1

ELECTRICAL FEEDBACK CONTROLLED VARIABLE CONDUCTANCE HEAT PIPE SYSTEM

troller and a reservoir heater to adjust its thermal conductance. An increase in the heat source temperature caused by an increase in heat load and/or sink temperature results in an error signal to the controller causing it to reduce the power to the reservoir heater. The corresponding decrease in reservoir temperature and therefore in the partial pressure of the working fluid in the reservoir allows more noncondensible gas to enter the reservoir. This causes the gas-vapor interface to move toward the reservoir, thus increasing the active condenser length and ultimately reducing the source temperature. Unlike in a passive variable conductance heat pipe in which the vapor pressure provides an internal reference for control, the FCHP senses the source temperature and controls it directly with an external reference (e.g., a thermostat).

A FCHP provides inherently better control of the source temperature than a passive variable conductance heat pipe. The latter is limited to controlling the vapor temperature. If the thermal resistance between the heat source and the vapor is appreciable, variations in heat load may yield intolerable fluctuations in temperature of the source even if the vapor temperature remained absolutely constant. The FCHP actually permits a lowering of the vapor temperature with increasing heat load to compensate for the higher temperature drop through the heat source resistance.

An analytical model of an FCHP must account for changes in the heat load and in the sink temperature. The theory presented in References 3, 4, and 6 properly describe the control performance under such conditions. However, for the purpose of determining the required reservoir volume, an ideal FCHP was always assumed. It is one in which the maximum reservoir temperature equals the vapor temperature (all noncondensible gas is displaced from the reservoir in the "low power-low sink" condition) and in which the minimum reservoir temperature equals the prevailing

sink temperature. Such an ideal FCHP does require the smallest reservoir for a given set of conditions, but it is not necessarily the most practical one. The following, more general model places fewer restrictions on the range of reservoir temperatures. The ideal FCHP is included as a special case in the general analysis.

The analysis is based on satisfying conservation of mass of the noncondensible gas and on a pressure balance between vapor and vapor-gas mixture (Ref. 5). Figure 3.2 shows schematically the "high" and "low" operating conditions of a FCHP. Other assumptions, such as the existence of a sharp vapor-gas interface, are also discussed in the references.

The "high" operating condition corresponds to maximum heat load and highest sink temperature. Since this requires the highest conductance of the heat pipe, the entire condenser will be active and all of the noncondensible will be compressed within the reservoir. The pressure balance yields for the mass of the noncondensible:

$$m_g = \frac{V_r}{R_g} \frac{1}{T_{r,h}} \left[p_v (T_{v,h}) - p_v (T_{r,h}) \right] \tag{1}$$

The "low" operating condition corresponds to minimum heat load and lowest sink temperature. This requires the lowest conductance of the heat pipe; and, consequently, the maximum condenser blockage will occur. Pressure balance and conservation of mass yields:

$$m_g = \frac{V_c}{R_g} \frac{1}{T_{o,l}} \left[p_v (T_{v,l}) - p_v (T_{o,l}) \right] + \frac{V_r}{R_g} \frac{1}{T_{r,l}} \left[p_v (T_{v,l}) - p_v (T_{r,l}) \right] \tag{2}$$

By combining these two equations, the following general expression for the required reservoir size is obtained:

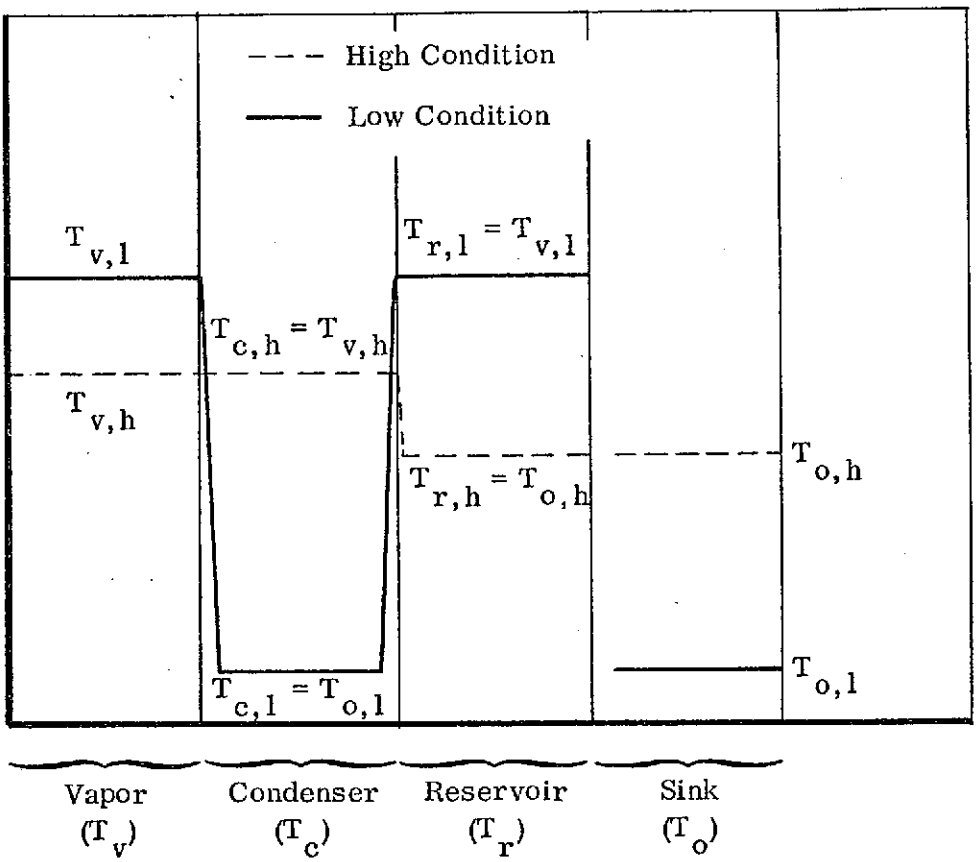

FIGURE 3.2

SCHEMATIC TEMPERATURE DISTRIBUTION
IN A FCHP DURING "LOW" AND "HIGH" CONDITIONS

$$\frac{V_c}{V_r} = \frac{T_{o,l}}{p_v(T_{v,l}) - p_v(T_{o,l})} \left\{ \frac{p_v(T_{v,h}) - p_v(T_{r,h})}{T_{r,h}} - \frac{p_v(T_{v,l}) - p_v(T_{r,l})}{T_{r,l}} \right\} \quad (3)$$

Up to this point, no restrictions have been placed on the reservoir temperature, except that it may not exceed the vapor temperature since reverse heat pipe action would then occur. Note also that the subscripts "l" and "h" for the reservoir temperature do not indicate its lowest or highest value, respectively. On the contrary, at the "low" operating condition, the reservoir will be at its highest temperature and visa versa.

Equation 3 gives the ratio between the maximum blocked condenser volume and the reservoir volume. For design purposes, the total required condenser volume must also be known. At the high condition we have:

$$Q_h \sim V_{c,t} (T_{v,h} - T_{o,h}) \quad (4)$$

And at the low condition:

$$Q_l \sim (V_{c,t} - V_c) (T_{v,l} - T_{o,l}) \quad (5)$$

From (4) and (5) the total required condenser volume is obtained:

$$\frac{V_c}{V_{c,t}} = 1 - \frac{Q_l}{Q_h} \frac{T_{v,h} - T_{o,h}}{T_{v,l} - T_{o,l}} \quad (6)$$

Finally, in order to close the analytical model, the vapor temperatures are related to the heat source temperatures as follows:

$$T_{s,h} = T_{v,h} + R_s Q_h \quad (7)$$

$$T_{s,l} = T_{v,l} + R_s Q_l \quad (8)$$

Equations 3, 6, 7, and 8 completely describe the control performance of a FCHP under varying load and sink conditions.

The ideal FCHP, as described in the references, is one in which at the low condition the noncondensible is completely displaced from the reservoir. This requires that:

$$T_{r,l} = T_{v,l} \tag{9}$$

i.e., that the reservoir temperature equals the vapor temperature at the low condition. At the high condition, the reservoir temperature of the ideal FCHP will be equal to the prevailing sink temperature:

$$T_{r,h} = T_{o,h} \tag{10}$$

Equation 10 defines the lowest temperature which the reservoir can practically assume. Ideally, all noncondensible will be contained within the reservoir under this condition and the entire condenser will be active.

After substituting Equations 9 and 10 into 3, the following expression for the required reservoir size of an ideal FCHP is obtained:

$$\frac{V_c}{V_r} = \frac{p_v (T_{v,h}) - p_v (T_{o,h})}{p_v (T_{v,l}) - p_v (T_{o,l})} \frac{T_{o,l}}{T_{o,h}} \tag{11}$$

The last expression is identical to the one given in Reference 3 for the reservoir requirements of an ideal FCHP.

The requirements for an ideal FCHP -- i.e., the conditions imposed on the reservoir temperature by Equations 9 and 10 -- are often not very realistic for a practical system. The first requirement, namely, that the reservoir temperature equals the vapor

temperature at the low condition, has several drawbacks. Firstly, it may require an excessive amount of auxiliary power to the reservoir. Secondly, with the reservoir completely devoid of noncondensible and being wicked at the same time, it will act as a secondary heat pipe. Thus, in a practical heat pipe, the reservoir temperature at the low condition (when it reaches its maximum value) may be less than the vapor temperature.

At the high condition, where the reservoir temperature ideally should be equal to the sink temperature, different restrictions exist. In some applications, it may not be possible for the reservoir to ever attain that minimum temperature. The ATFE flight experiment is a good example of this case. Heat leaks from the absorber to the reservoir limited the lowest attainable reservoir temperature to a value much above the sink temperature. Even more important, during transients from the low to the high condition, the time required for the reservoir to reach its lowest temperature may be unacceptable. As a result, large overshoots of the source temperature may occur.

Because of the above considerations, an off-ideal design of an FCHP may frequently be more desirable. Such a design will, of course, require a larger-than-optimum reservoir volume. The general Expression 3 describes the reservoir requirements for any specified range of reservoir temperatures. Two special cases of an off-optimum design are of interest to the designer. In the first one, the available auxiliary power for the reservoir is limited and the reservoir is not heated all the way up to the vapor temperature at the low condition. But at the high condition it can achieve the sink temperature. For this case we have:

$$T_{r,l} < T_{v,l} \tag{12}$$

$$T_{r,h} = T_{o,h} \tag{13}$$

Substituting these conditions into Equation 3 yields the following expression for the required reservoir size:

$$\frac{V_c}{V_r} = \frac{T_{o,l}}{p_v(T_{v,l}) - p_v(T_{o,l})} \left\{ \frac{p_v(T_{v,h}) - p_v(T_{o,h})}{T_{o,h}} - \frac{p_v(T_{v,l}) - p_v(T_{r,l})}{T_{r,l}} \right\} \tag{14}$$

In this special case, the reservoir temperature is raised by the auxiliary heater to a value which is less than the vapor temperature but obviously higher than the sink temtemperature -- i.e., $T_{r,l} > T_{o,l}$ -- because otherwise it would become a passive VCHP.

In the other case of an off-optimum design, auxiliary power requirements are not the limiting consideration. Instead, fast response during a transient change from one operating condition to another may be important. Hence, the lowest reservoir temperature should be higher than the sink temperature; but the highest reservoir temperature can be equal to the vapor temperature. In this case, the limiting reservoir temperatures are given by:

$$\begin{aligned} T_{r,l} &= T_{v,l} \\ T_{r,h} &> T_{o,h} \end{aligned} \tag{15}$$

The required reservoir size then becomes:

$$\frac{V_c}{V_r} = \frac{p_v(T_{v,h}) - p_v(T_{r,h})}{p_v(T_{v,l}) - p_v(T_{o,l})} \cdot \frac{T_{o,h}}{T_{r,h}} \tag{16}$$

To illustrate the above design equations, the reservoir requirements for a typical case are plotted in Figures 3.3 and 3.4. The example applies approximately to the specifica-

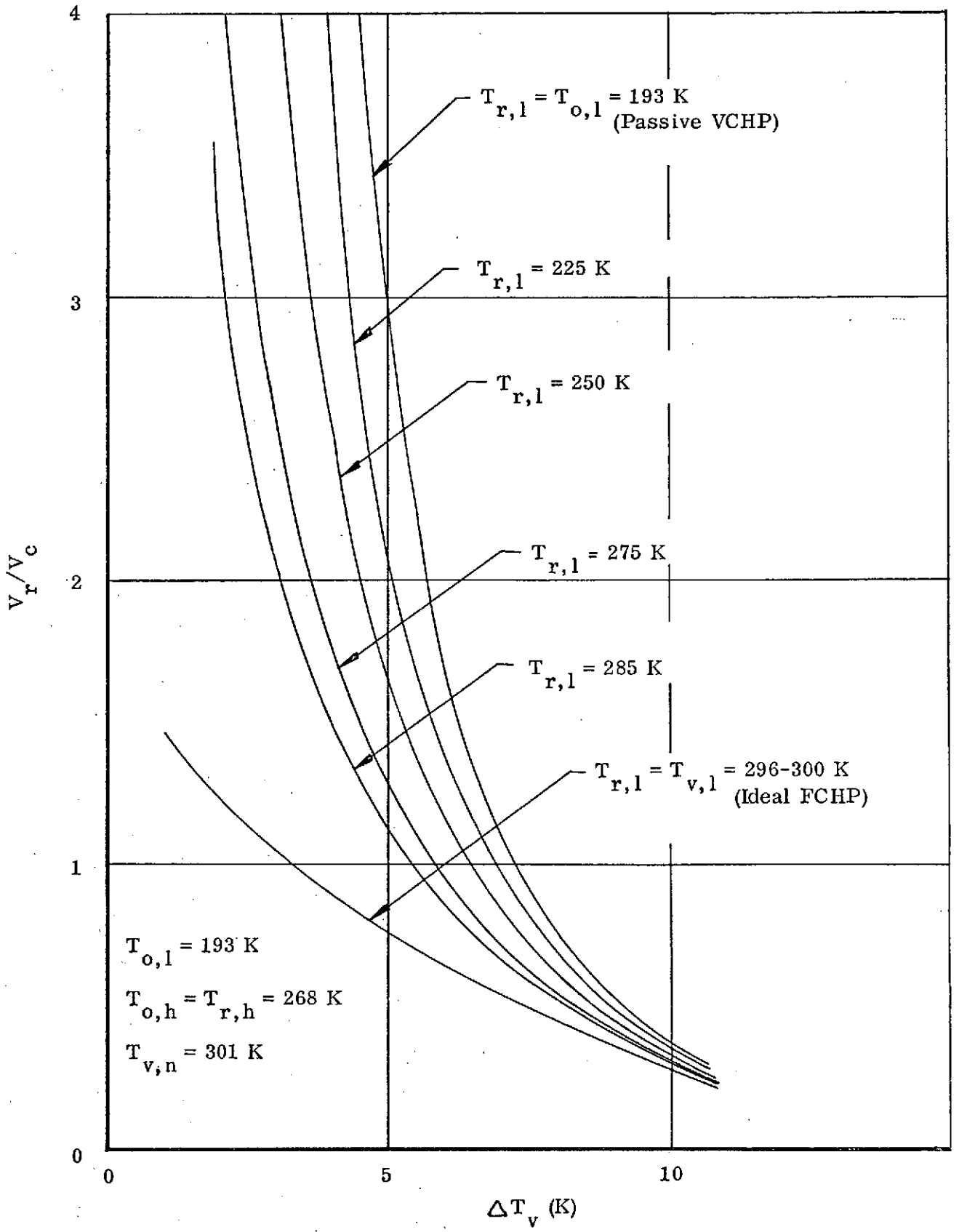

FIGURE 3.3

RESERVOIR REQUIREMENTS FOR NON-IDEAL FCHP
(RESERVOIR TEMPERATURE AT HIGH CONDITION
EQUALS SINK TEMPERATURE)

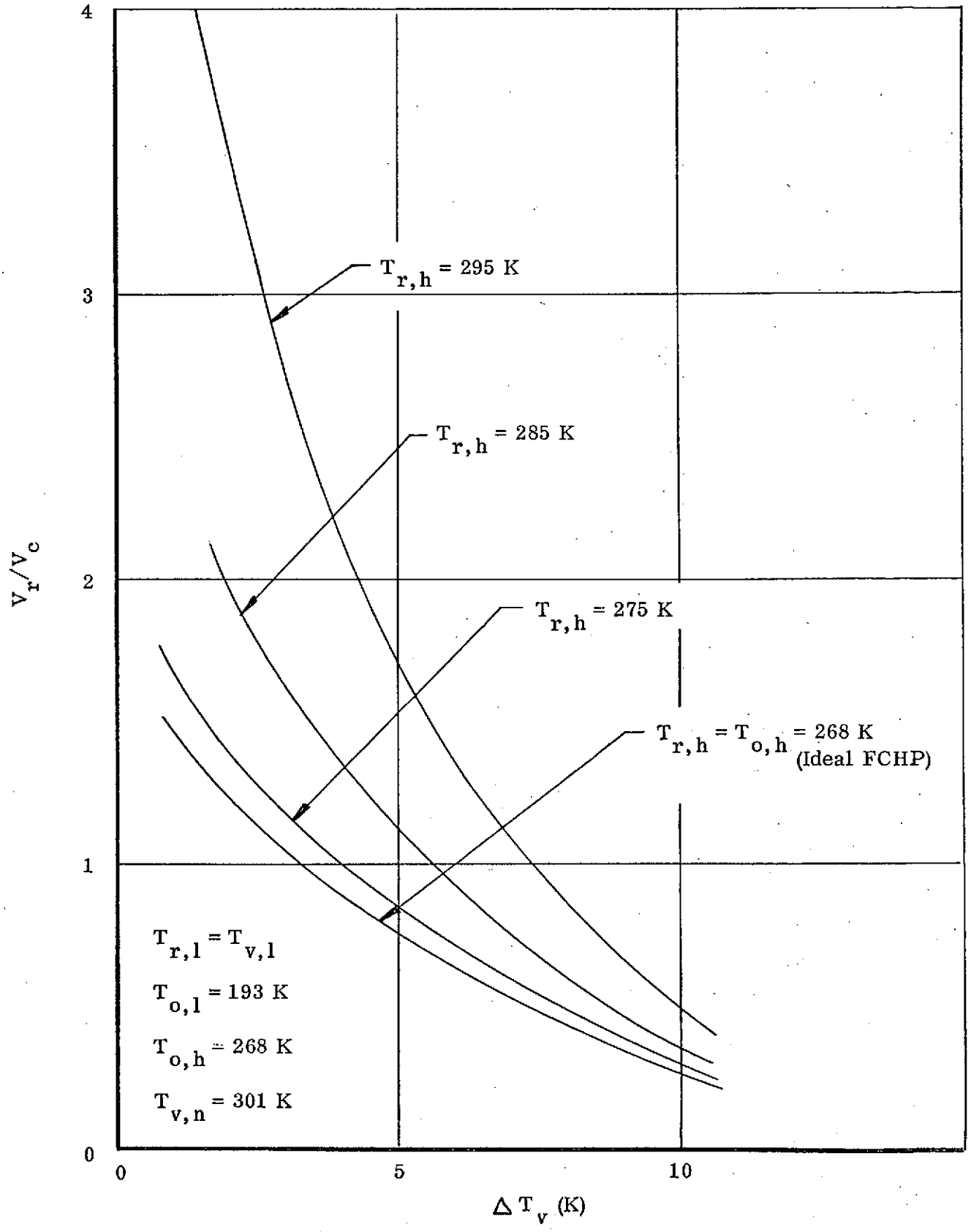

FIGURE 3.4

RESERVOIR REQUIREMENTS FOR NON-IDEAL FCHP
(RESERVOIR TEMPERATURE AT LOW CONDITION
EQUALS VAPOR TEMPERATURE)

tions for the ATFE flight experiment. Typical variations of the sink temperature in the ATFE are between $-80^{o}C$ and $-5^{o}C$. The working fluid is methanol and the nominal vapor temperature was selected to be $28^{o}C$. In these figures, the required reservoir volume (normalized with respect to the maximum blocked condenser volume) is plotted against ΔT_v, the variation of the vapor temperature. Note that ΔT_v and the nominal vapor temperature $T_{v,n}$ are related through:

$$T_{v,h} = T_{v,n} + \frac{\Delta T_v}{2} \tag{17}$$

$$T_{v,l} = T_{v,n} - \frac{\Delta T_v}{2} \tag{18}$$

Figure 3.3 depicts the case where auxiliary power is at a premium; i.e., where the maximum reservoir temperature at the low condition is less than the vapor temperature. Also shown is the limiting case which corresponds to the ideal FCHP.

Figure 3.4 represents the other case. Here the lowest reservoir temperature, at the high condition, is shown as a parameter. Again, the limiting case is that of the ideal FCHP which is, of course, identical to the one in Figure 3.3.

Figure 3.5 shows the ratio of blocked-to-total condenser volume for the same operating conditions. The fact that the blocked condenser volume is usually less than the total required condenser volume has been mostly neglected in the literature. But a proper design must account for it, and the important design parameter for selecting the storage volume should be $V_r/V_{c,t}$ rather than V_r/V_c. As shown in Figure 3.5, the ratio of $V_c/V_{c,t}$ is always identical to unity if the heat load varies from zero to a maximum value. The ratio of $V_c/V_{c,t}$ is smallest if the heat load is constant and only the sink conditions vary.

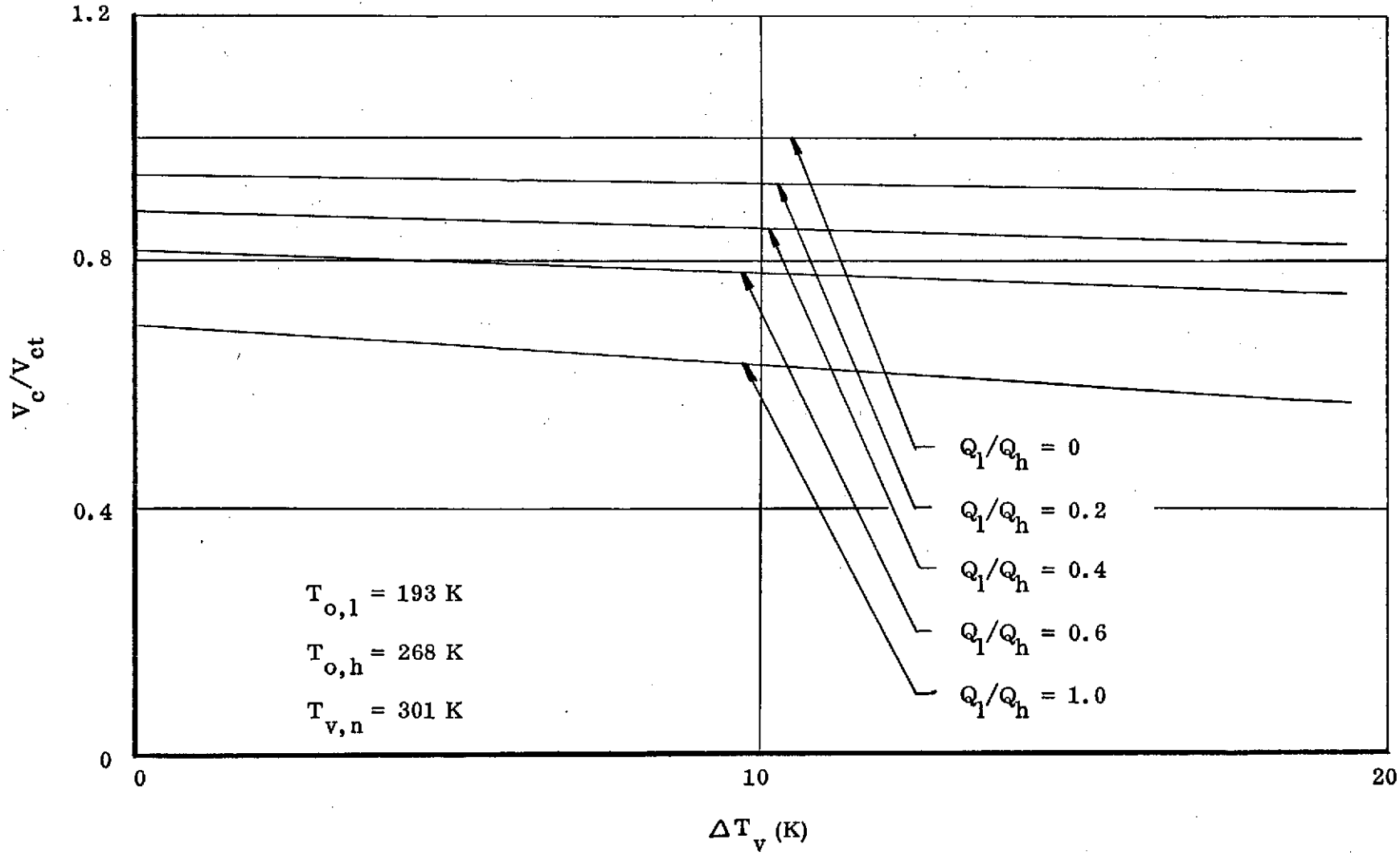

FIGURE 3.5

RATIO OF BLOCKED-TO-TOTAL CONDENSER VOLUME

The preceding paragraphs dealt with the design selection of the storage reservoir. Such selection will always be made on the basis of expected extreme values of sink and heat load variations. Once the system has been designed, the steady-state performance at other than the extreme conditions is of interest. In principle, this information can be obtained from the design equations for the reservoir (3, 11, 14, and 16). But these equations do not contain the most important parameter describing the control performance; namely, ΔT_v explicitly. Sometimes it is also desirable to assess quickly what benefits or penalties, in terms of control performance, are obtained by changing the reservoir size.

The described information can easily be obtained by rearranging the design equations and solving them for ΔT_v, the control performance of the FCHP. Since the vapor temperature appears in these equations through the vapor pressure of the working fluid, an approximation must be used to solve the equations for ΔT_v.

For small variations of the vapor temperature, the vapor pressures at the high and low condition may be expressed as follows:

$$p_v (T_{v,h}) = p_v (T_{v,n}) + \frac{\Delta T_v}{2} \frac{dp_v}{dT} (T_{v,n}) \tag{19}$$

$$p_v (T_{v,l}) = p_v (T_{v,n}) - \frac{\Delta T_v}{2} \frac{dp_v}{dT} (T_{v,n}) \tag{20}$$

The above linear approximations can be substituted into Equations 3, 11, 14, and 16; and an explicit solution for ΔT_v obtained for each case. Although the algebra associated with the substitutions is straight forward, the effort is rather tedious and the resulting summary equations are fairly lengthy. A listing of these equations is therefore reserved for the Appendix.

Without reproducing the performance equation here, it is noteworthy to mention that in all cases the control performance ΔT_v is inversely proportional to the slope of the vapor pressure curve. That is, the equations all are of the type:

$$\Delta T_v \sim \frac{1}{\ln \frac{dp_v}{dT}} \tag{21}$$

The conclusion then is that the best control performance (smallest ΔT_v) is achieved with working fluids which have a steep vapor pressure curve at the operating temperature. This fact was recognized earlier for the case of passive self-controlled VCHP's and reported in Reference 6.

Typical results of a performance analysis are given in Figures 3.6 and 3.7. Again the same sink variations and nominal vapor temperature as apply to the ATFE have been used. Basically, the last two figures are mirror images of Figures 3.3 and 3.4, with ΔT_v plotted as a function of reservoir size. Figure 3.6 corresponds to the case where the maximum reservoir temperature at low conditions assumes different values than in an ideal FCHP. The group of curves in Figure 3.6 is bracketed by two extreme cases. The lowest curve (lowest ΔT_v) corresponds to the ideal FCHP. The highest curve (largest ΔT_v) represents the control performance of a passive VCHP. Note also that,with feedback control, ΔT_v may assume negative values. This means that the vapor temperature at the low condition can be higher than at the high condition. It is precisely this feature which gives FCHP's their excellent control performance. As pointed out in References 2, 3, and 6, the FCHP controls the source rather than the sink temperature. If the heat load varies and the impedance between source and heat pipe is finite, a negative change of the vapor temperature is necessary in order to attain near absolute control.

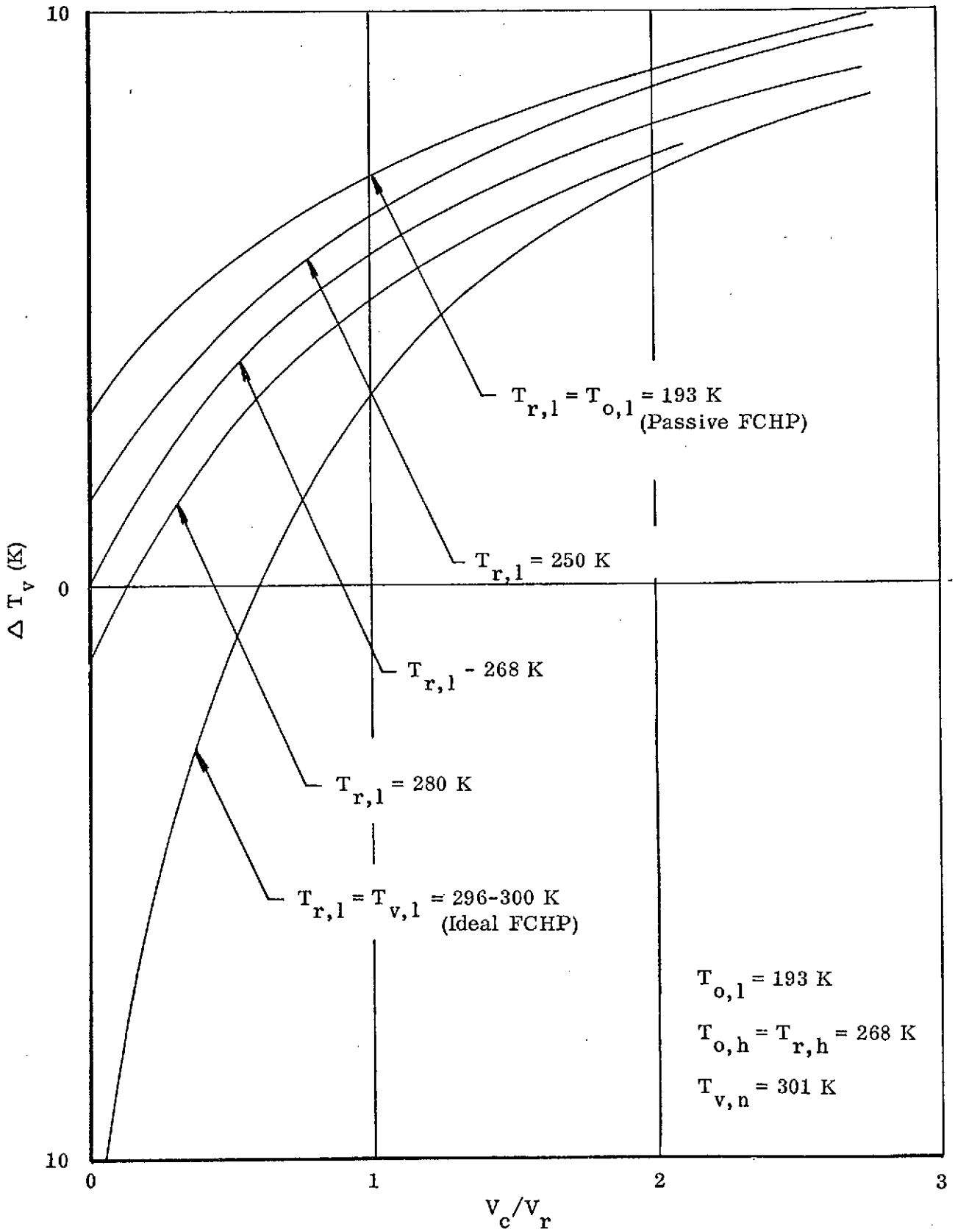

FIGURE 3.6

FCHP PERFORMANCE ANALYSIS
(RESERVOIR TEMPERATURE AT HIGH CONDITION
EQUAL TO SINK TEMPERATURE)

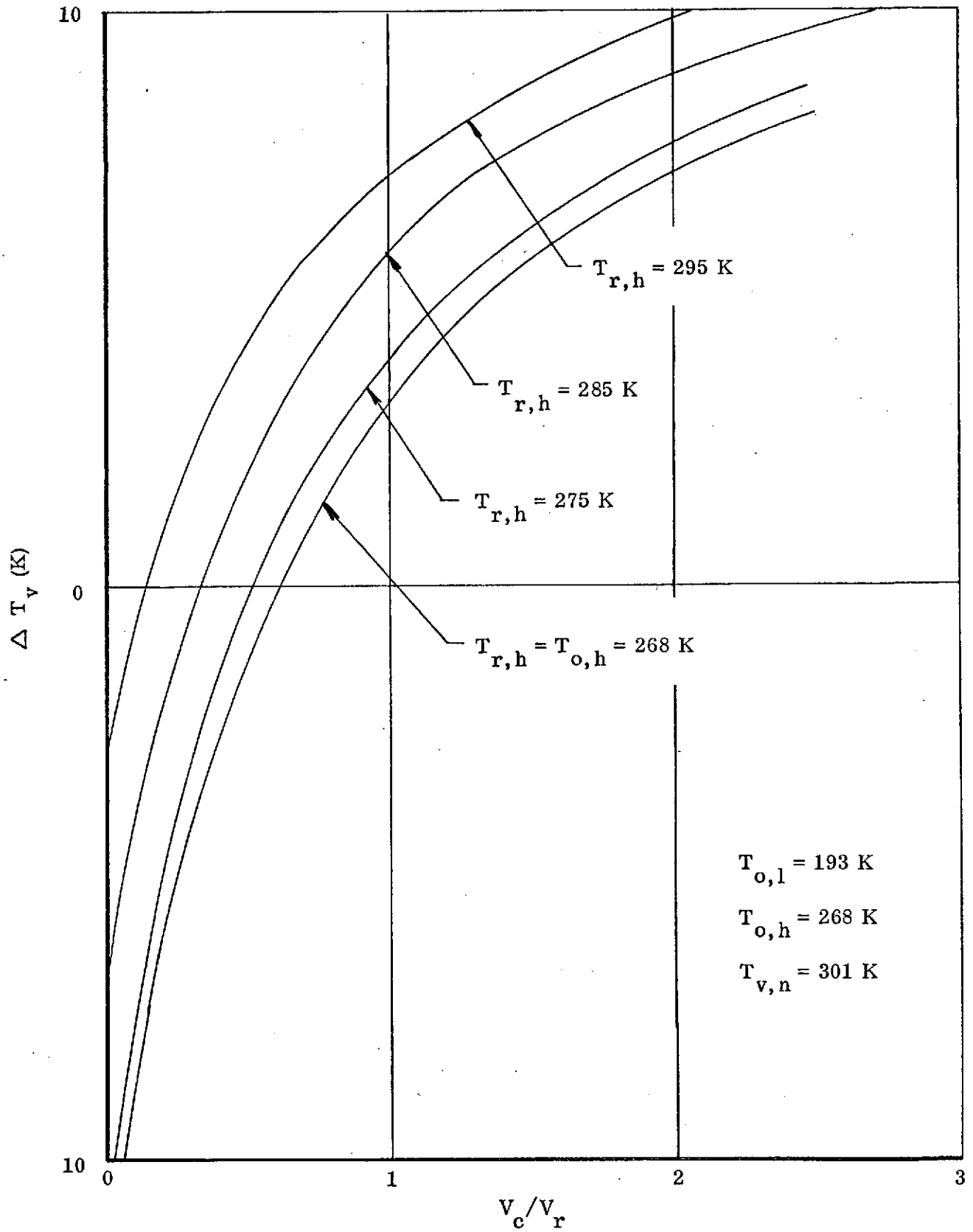

FIGURE 3.7

VCHP PERFORMANCE ANALYSIS
(RESERVOIR TEMPERATURE AT LOW CONDITION
EQUALS VAPOR TEMPERATURE)

The difference in control capability between an ideal FCHP and an equivalent passive VCHP is shown in Figure 3.8. The variation of the sink temperature is plotted as a function of highest sink temperature for two cases--an infinite storage reservoir ($V_c/V_r = 0$) and a typical practical reservoir size ($V_c/V_r = 0.1$). For the limiting case of an infinite storage reservoir, the FCHP always has a negative ΔT_v up to the point where the highest sink temperature approaches the vapor temperature. The passive system, on the other hand, always displays a positive ΔT_v.

The preceding analysis is concerned mostly with control of the vapor temperature. Ultimately, of course, the source temperature must be controlled. Vapor and source temperature are related through Expressions 7 and 8. By employing these equations together with the ones for the vapor temperature, the required analysis can readily be performed.

3.2 Closed Form Transient Analysis of FCHP's

The transient response characteristics of an ideal active feedback controlled heat pipe system have been determined for a step change from a low power/low sink condition to a high power/high sink condition or vice versa. This step change represents the worst case in terms of the system's response in that control of the heat source requires that the temperature of the storage reservoir must go from approximately the source temperature to a temperature approaching the high sink condition or vice versa. In other words, in controlling the heat source when the system is subjected to either of the above step changes, the maximum variation of the storage temperature must be realized. Since the heat source can respond no more rapidly than the storage volume, the above step change represents the worst case.

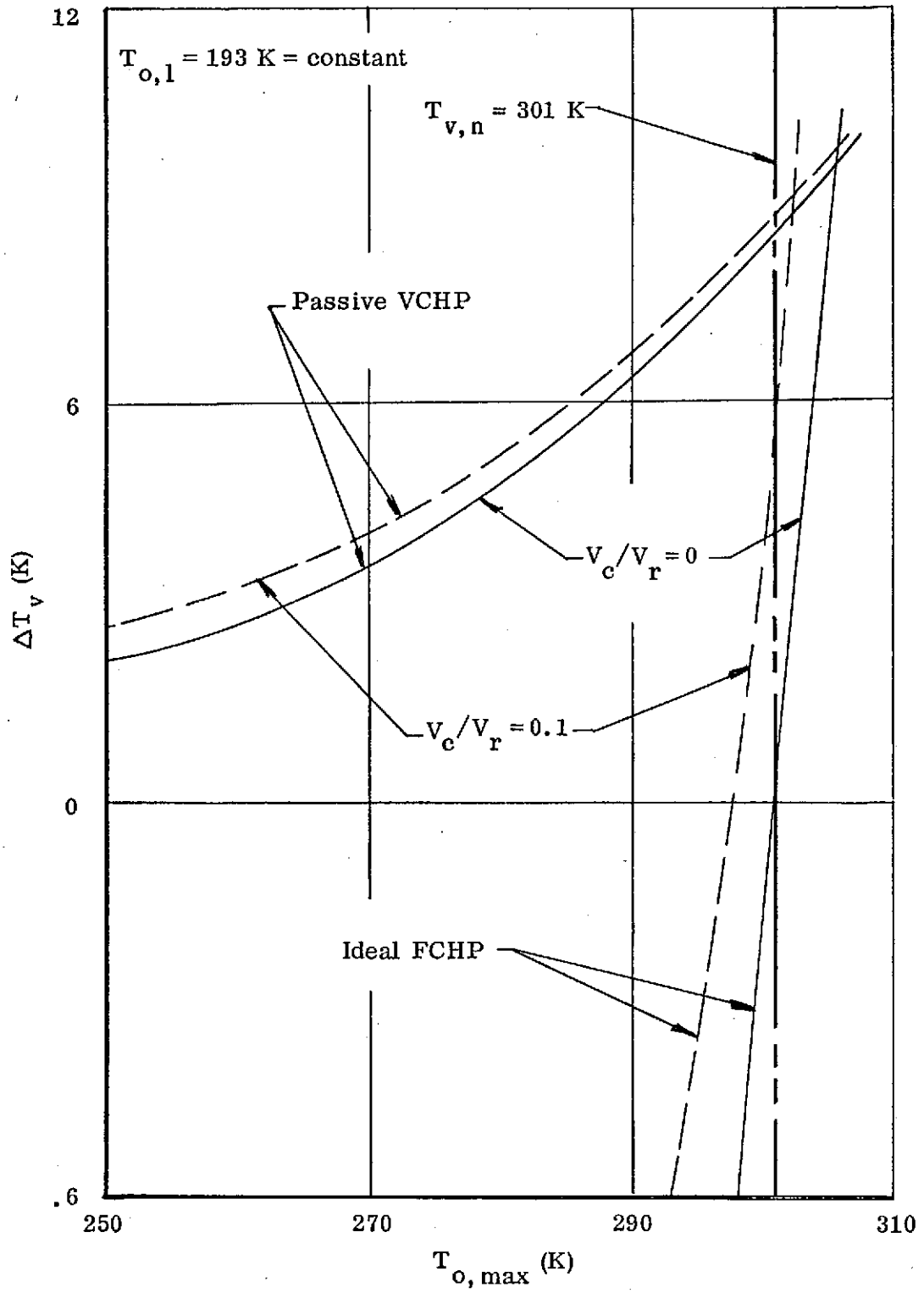

FIGURE 3.8

PERFORMANCE COMPARISON OF FCHP AND PASSIVE VCHP
(ΔT_v AS A FUNCTION OF SINK TEMPERATURE AT HIGH CONDITION)

The equations governing the transient behavior of a feedback controlled variable conductance heat pipe system are highly nonlinear. In order to get a better general understanding of the response characteristics of feedback controlled systems than that afforded by solving a system of nonlinear equations, the following simplifying assumptions have been made in performing the analysis:

- The mode of heat dissipation is convection. This eliminates the fourth order terms associated with radiation and permits the response of the storage temperature to be determined explicitly.

- The recovery of the vapor temperature occurs at the same rate as that of the storage temperature; i.e., for the case of going from the low power/low sink to the high power/high sink condition:

$$\frac{T_v - T_{v,h}}{T_{v,i} - T_{v,h}} = \frac{T_r - T_{r,h}}{T_{r,l} - T_{r,h}} \tag{22}$$

  This implies that the vapor temperature responds instantaneously to changes in the storage temperature and is valid provided that the time constant ($\tau = m c_p R$) of the condenser section is small relative to that of the storage volume ($\tau_c / \tau_r \ll 1$). This will be the case generally since the thermal resistance (R_r) between the reservoir and the sink will be quite large relative to the thermal resistance (R_c) between the vapor and the sink in order to minimize the auxiliary power requirements. This assumption eliminates the nonlinearities associated with the variable conductance.

- An ideal (i.e., zero deadband) on/off controller is used.

Subject to the above assumptions, the transient response of an active feedback controlled heat pipe is determined from the following equations for the case of a step change from the low power/low sink condition to the high power/high sink condition.

At the storage volume:

$$Q_r = (m\, c_p)_r \frac{dT_r}{dt} + (h\, A)_r (T_r - T_{o,h}) \tag{23}$$

With an ideal on/off controller, the auxiliary power will immediately go to zero ($Q_{r,h} = 0$) when the step change is effected. The conductance (h A) of the storage volume is determined from the low power/low sink condition. At this steady-state condition, ideally, the storage temperature should equal the vapor temperature in the heat pipe corresponding to the low power; i.e.,

$$T_{r,l} = T_{v,l} \tag{24}$$

And the auxiliary power must be such that:

$$Q_{r,l} = (h\, A)_r (T_{r,l} - T_{o,l}) \tag{25}$$

Hence, the insulation requirements for the storage volume are determined from:

$$(h\, A)_r = \frac{Q_{r,l}}{T_{v,l} - T_{o,l}} \tag{26}$$

Solving the above equations and applying the second assumption gives the recovery of the storage temperature and the vapor temperature of the heat pipe as:

$$\frac{T_r - T_{o,h}}{T_{r,l} - T_{o,l}} = \frac{T_v - T_{v,h}}{T_{v,i} - T_{v,h}} = e^{-t/\gamma_r} \tag{27}$$

where:

$$\tau_r = \frac{(m\ cp)_r\ (T_{v,1} - T_{o,1})}{Q_{r,1}} \tag{28}$$

As indicated by Equation 27, the storage temperature and therefore the vapor temperature are single values and vary exponentially with time. In an actual case of going from a low power/low sink to a high power/high sink condition, the vapor temperature would first increase to some maximum value consistent with conservation of energy and mass of the noncondensible. It would then begin to decrease to its steady-state value as the storage temperature responds to the auxiliary heat input. Equation 27 does not account for the fact that the vapor temperature will rise/decrease to a maximum/minimum at some time after a change in load and/or sink condition. However, a conservation solution is obtained if, instead of using the steady-state value of vapor temperature corresponding to the original load and/or sink condition as the initial condition (e.g., $T_{v,i} = T_{v,1}$), a value is used which is based on adjustment of the interface to the new load and/or sink conditions without any recovery due to a change in the temperature of the storage volume.

At the heat source:

$$Q_{s,h} = (m\ c_p)_s \frac{dT_s}{dt} + \frac{T_s - T_v}{R_s} \tag{29}$$

Substitution of Equation 27 into 29 and integrating gives the response of the source temperature as:

$$\Psi = \frac{T_s - T_{s,n}}{T_{v,i} - T_{v,h}} = \frac{1}{1 - \frac{\tau_s}{\tau_r}} \left(e^{-t/\tau_r} - e^{-t/\tau_s}\right) \tag{30}$$

where it has been assumed that the system is designed to give absolute control of the source temperature. Also:

$$\tau_s = (m\, c_p\, R)_s \tag{31}$$

If the initial vapor temperature $T_{v,i}$ is set equal to its value just prior to the step change ($T_{v,i} = T_{v,l}$), the response of the source temperature is obtained explicitly as:

$$T_s = T_{s,n} + \frac{R_s\,(Q_h - Q_l)}{1 - \frac{\tau_s}{\tau_r}}\,(e^{-t/\tau_r} - e^{-t/\tau_s}) \tag{32}$$

The response of the source temperature to a step change from a high power/high sink condition to a low power/low sink condition is the same as the above, provided that the maximum auxiliary power is just sufficient to achieve thermal equilibrium of the storage volume at the low power/low sink condition (i.e., $Q_{r,\max} = Q_{r,l}$). This results in identical response for both step changes.

The maximum overshoot/undershoot, associated with the above response, is determined by differentiating Equation 30 with respect to time and is:

$$\psi_p = \frac{T_{s,p} - T_{s,n}}{T_{v,i} - T_{v,h}} = \left(\frac{\tau_r}{\tau_s}\right)^{\beta} \tag{33}$$

where:

$$\beta = \frac{1}{1 - \frac{\tau_r}{\tau_s}} \tag{34}$$

The corresponding time for the maximum overshoot/undershoot is determined from:

$$\frac{t_p}{\tau_s} = \frac{1}{1 - \frac{\tau_s}{\tau_r}} \ln \frac{\tau_r}{\tau_s} \qquad (35)$$

Analysis of Equation 33 indicates that the ratio τ_r/τ_s should be as small as possible in order to reduce the magnitude of the maximum overshoot/undershoot. This will also improve the recovery of the source temperature to changes in heat load and/or sink conditions. In general, the best performance will be attained by having the time constant of the storage volume as small as possible. The most efficient way of doing this is to effectively reduce the heat capacity of the storage reservoir. A reduction in the reservoir's insulation (i.e., in the resistance between the reservoir and the sink) improves the response to increase in heat load and/or sink temperature; however, it results in an increase in the auxiliary power required in order to accommodate the low power/low sink condition.

The maximum overshoot/undershoot (Ψ_p) to a simultaneous step change in heat load and sink condition versus τ_r/τ_s is presented in Figure 3.9. The corresponding time (t_p) at which the maximum overshoot/undershoot occurs is also shown in Figure 3.9. As expected, τ_p increases with increasing τ_r/τ_s which implies that the time for the heat source temperature to recover increases as τ_r/τ_s increases. The transient response of the heat source is shown in Figure 3.10 for the case where τ_r/τ_s is equal to one. Reference to Equation 30 shows that for the step change from a low power/low sink condition the parameter Ψ and therefore the source temperature increases exponentially until the maximum overshoot is reached. After this time, Ψ decreases exponentially and becomes asymptotic to zero as time goes to infinity.

In addition to the maximum overshoot and the time to maximum overshoot, one other performance characteristic of importance is the recovery time (t_R). This param-

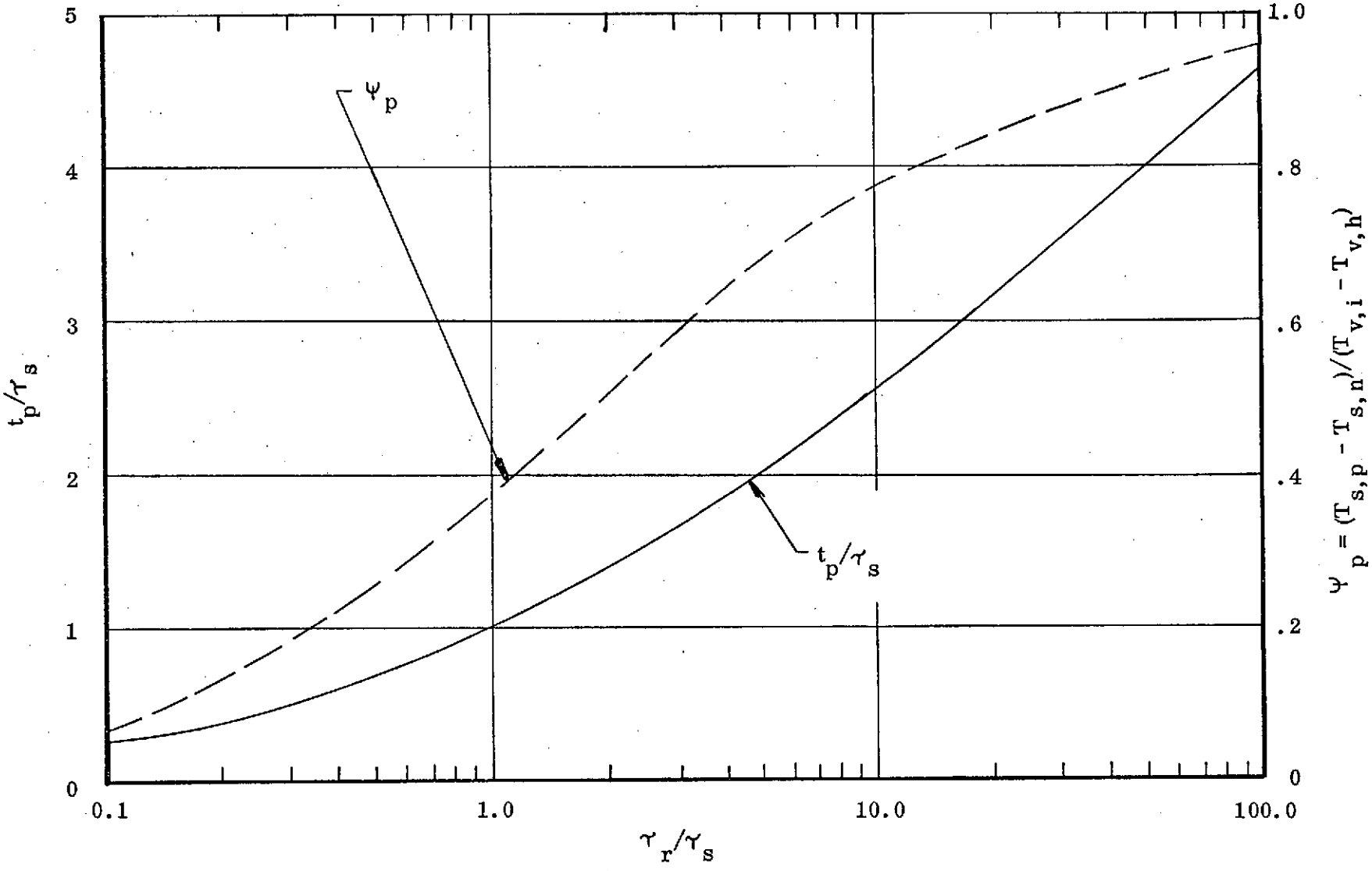

FIGURE 3.9

NORMALIZED TEMPERATURE AND TIME ASSOCIATED
WITH MAXIMUM OVERSHOOT/UNDERSHOOT

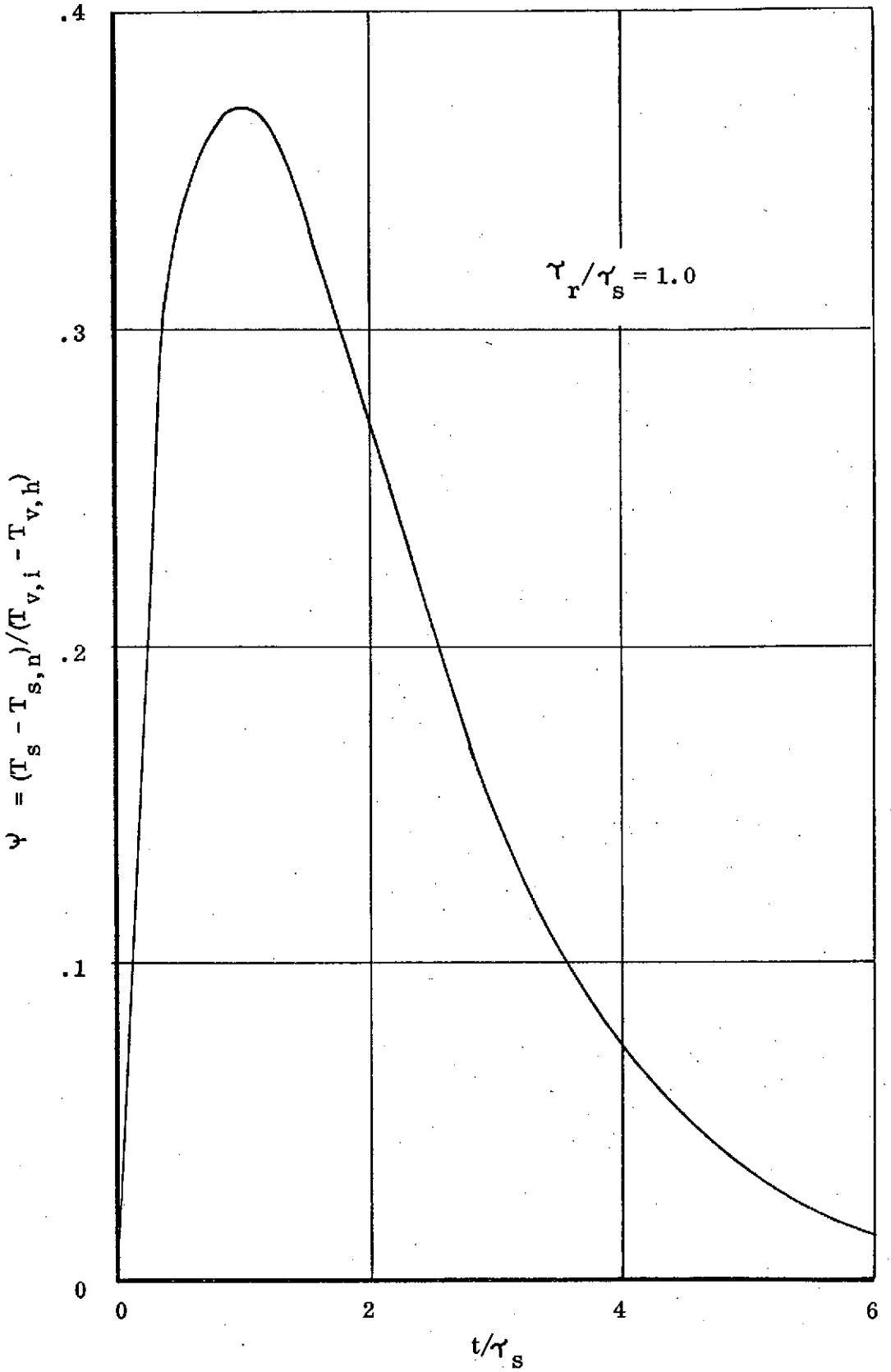

FIGURE 3.10

TRANSIENT RESPONSE OF HEAT SOURCE TEMPERATURE

eter is defined as the time required for the controlled variable to come to within some specified absolute percentage of its final value and therefore remain less than the specified percentage. The ratio of the recovery time to the time constant of the heat source (t_R/τ_s) versus τ_r/τ_s is shown in Figure 3.11 for various values of percentage of recovery (Ψ_R). It can be seen from this figure that for values of τ_r/τ_s much above 1.0, the ratio t_R/τ_s increases rapidly with increasing τ_r/τ_s.

As an example of the use of these figures, consider the performance specification that source temperature will recover to within $\pm 1^{\circ}C$ within 15 minutes. Hence:

$$t_R = 15 \text{ minutes}$$

$$T_{s,R} - T_{s,n} = 1^{\circ}C$$

Assume:

$$T_{v,i} - T_{v,h} = 10^{\circ}C$$

$$\tau_s = 1 \text{ minute}$$

Thus:

$$t_R/\tau_s = 15$$

and:

$$\Psi_R = 0.1$$

Figure 3.11 is entered with the above values of t_R/τ_s and Ψ_R, and the value of τ_r/τ_s required to satisfy the above specifications is 6.6 or:

$$\tau_r = 6.6 \text{ minutes}$$

Therefore from Figure 3.9:

$$\Psi_p = 0.72$$

or:

$$T_{s,p} - T_{s,n} = 7.2^{\circ}C$$

and:

$$t_p = 2.2 \text{ minutes}$$

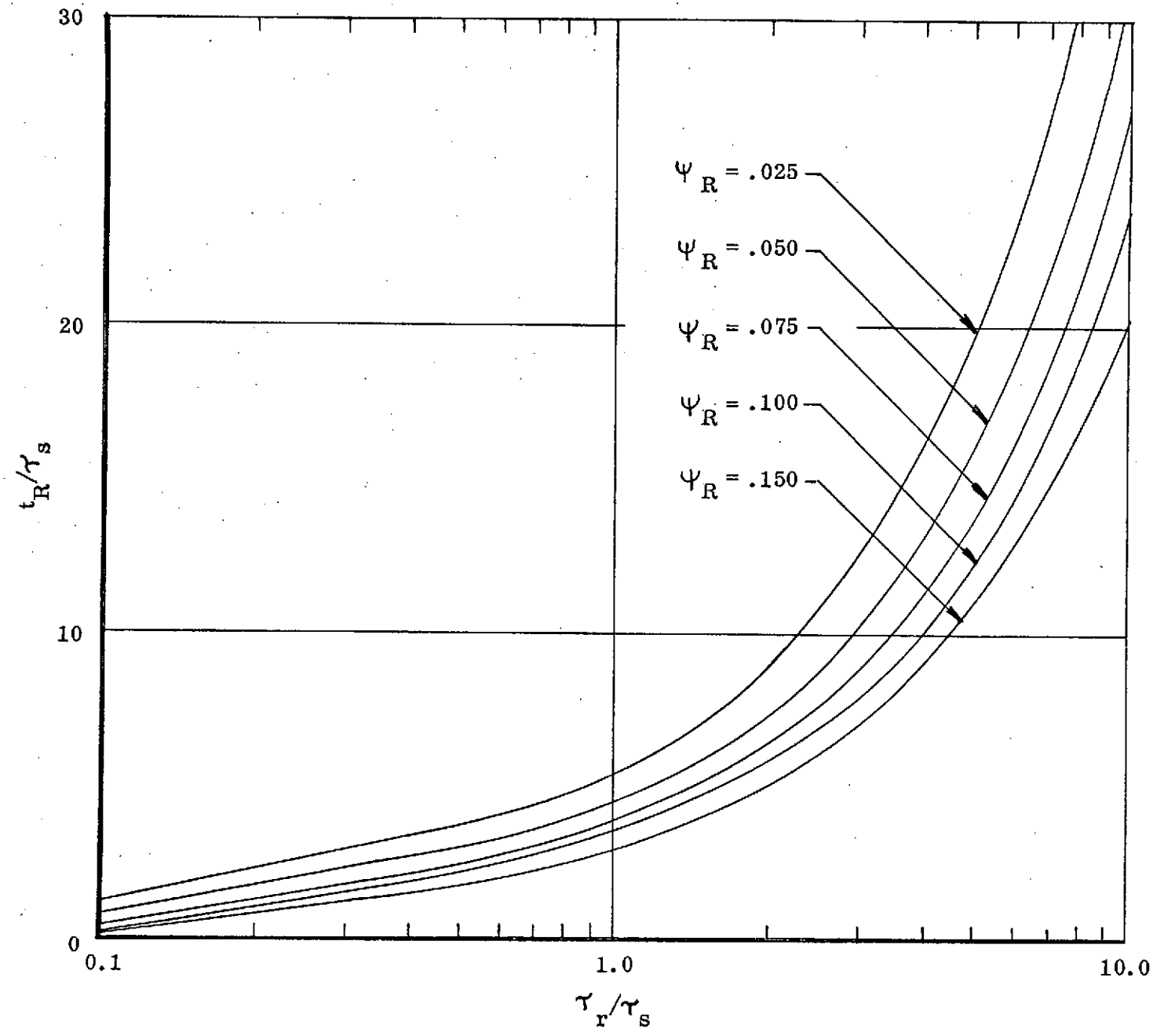

FIGURE 3.11

RECOVERY TIME OF HEAT SOURCE TEMPERATURE

If the above overshoot is unsatisfactory, then a compromise between increased recovery time and/or percentage of recovery and reduced overshoot must be made in arriving at a final design.

3.3 Numerical Transient Analysis of FCHP's

The transient performance of a FCHP can be described by a system of simultaneous nonlinear equations. The mathematical model upon which the equations are based is shown schematically in Figure 3.12.

The following assumptions have been used in defining the model:

- The noncondensible gas obeys the ideal gas equation of state.
- Mass diffusion is negligible; i.e., a sharp interface exists between the working fluid vapor and the noncondensible gas at the beginning of the inactive part of the condenser.
- Conduction along the heat pipe wall is negligible.
- The inactive part of the condenser instantaneously assumes the sink temperature when it becomes inactive.
- Heat dissipation to the sink can be described by the convection equation.
- The entire condenser length is active at the high power condition.

Details of the mathematical model are given in Appendix B. The set of nonlinear equations has been programmed in Fortran IV for solution on a digital computer. The program FEDCON is described in the appendix along with a flow diagram, a description of input cards, and a program listing. The program FEDCON has been used to correlate

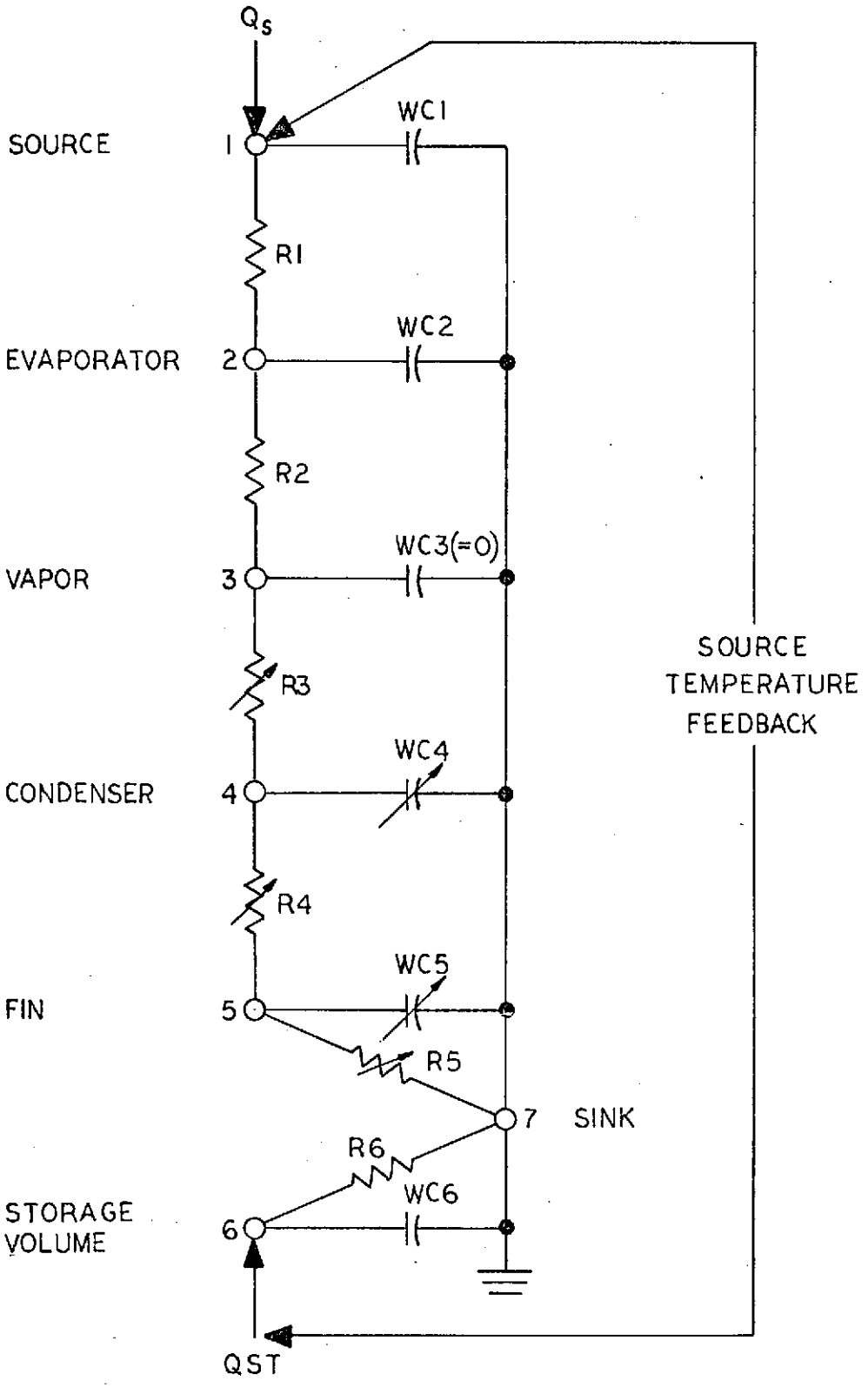

FIGURE 3.12

THERMAL MODEL FOR ELECTRICAL FEEDBACK CONTROLLED HEAT PIPE SYSTEM

test data obtained with a breadboard model of a FCHP. These results are presented in the following sections.

3.4 Breadboard Testing of FCHP

During the Technology Development Phase of the program, two breadboard models of FCHP's were fabricated and tested. The experimental model used for the data correlation is shown in Figure 3.13. The heat pipe contained an annular wick configuration. Several layers of 200-mesh screen were attached to the inner wall of the storage volume. This screen was interconnected with the annular wick in a transition section between the condenser and the reservoir. Water was used as the working fluid and the noncondensible was argon. The auxiliary heater consisted of resistance wire tightly wrapped around the storage reservoir. The latter was insulated with fiber glass insulation approximately 1.5 cm thick. An on/off controller with a $\pm 0.25^{o}C$ deadband was used to regulate the auxiliary power, and a thermistor was used as the feedback temperature sensing element.

Fiber glass tape was wrapped around the evaporator section of the heat pipe in order to increase the thermal resistance (R_s) between the heat source and the vapor. An aluminum cylinder weighing 185 grams, and wrapped with a heater wire over its length, was clamped around the heat pipe over the fiber glass tape to simulate a heat source. Its effective heat capacitance was 186 watt-sec/^{o}C. Two thermocouples and the control thermistor were attached to the outside diameter of the cylinder.

When conducting the tests, the heat pipe system was inserted within a 5-cm diameter copper tube which was surrounded by a water bath. Cooling of the heat pipe was affected by circulating water from the bath to copper fins which were brazed to

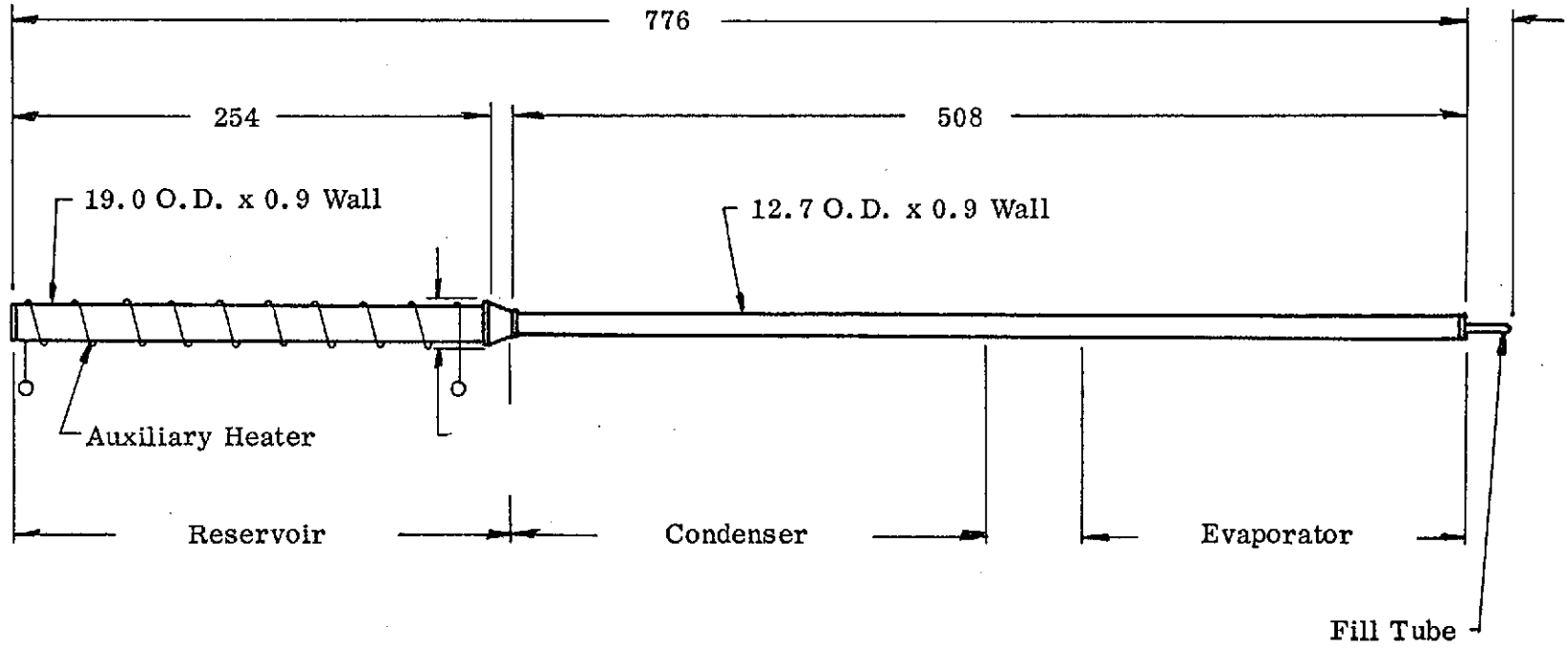

FIGURE 3.13

BREADBOARD MODEL OF ELECTRICAL FEEDBACK CONTROLLED HEAT PIPE

the heat pipe along the 25 cm condenser section. This setup permitted the storage reservoir and the heat pipe to see the same sink temperature while, at the same time, allowing the reservoir to be insulated from the convective cooling of the condenser section, therein reducing the auxiliary power requirements.

The effective reservoir volume (void volume) of the breadboard design was 57.7 cm^3 and the vapor volume of the condenser was 15.1 cm^3 resulting in a ratio of $V_r/V_{c,t} = 3.87$. Nominal high power/high sink and low power/low sink operating conditions were as follows:

Q_l = 15 watts	$T_{o,l} = 5^oC$	$T_{s,l} = 84^oC$
Q_h = 75 watts	$T_{o,h} = 30^oC$	$T_{s,h} = 84^oC$

The nominal heat source temperature control point (84^oC) had been chosen such that, for the particular gas charge, absolute control was achieved when the temperature of the storage reservoir at the high power/high sink condition was essentially equal to the sink temperature. Similarly, at the low power/low sink condition, the auxiliary power was just sufficient to achieve absolute control at the nominal source temperature. But for the given set of parameters, the reservoir temperature at the "low" condition was less than the vapor temperature. Thus the breadboard model was not optimized for a minimum reservoir; but, rather, it fell into the first category of off-ideal designs described in Section 3.1.

The minimum ratio of $V_r/V_{c,t}$ required for the stated operating condition would have been 1.49 (Equation 11). By selecting a larger reservoir ($V_r/V_{c,t} = 3.87$), the maximum required reservoir temperature was only 68^oC instead of 82^oC for an ideal FCHP. This was in keeping with the goal of minimizing the auxiliary power. Conversely,

by using a different gas charge, the same heat pipe could have been operated in a different mode. There, at the low condition, the reservoir is heated up to the vapor temperature; but, at the high condition, it remains warmer than the sink temperature. As discussed in Section 3.1, this latter mode is more desirable if auxiliary power is readily available but short transients are desired.

In the selected design, the auxiliary power was on throughout the entire transient during a step change from high to low condition. Conversely, the auxiliary power was off throughout the entire transient associated with the step decrease. This set of test conditions (high power/sink to low power/sink or vice versa) represents the limiting case in that the total variation in reservoir temperature from high sink temperature to the system vapor temperature or vice versa must be realized in order to achieve control. This is also the worst case in terms of the transient response since the auxiliary power is just sufficient to achieve control.

3.4.1 Experimental Test Data

Steady-state axial temperature distributions during high and low conditions are shown in Figures 3.14 and 3.15. Superimposed on the test points in these figures are the calculated distributions using FEDCON. The test conditions correspond to the nominal high and low conditions listed before; i.e., variations in power from 15 to 75 watts and simultaneous variations in sink temperature from 5 to 30^{o}C. At the low power/low sink condition, the gas-vapor interface is located at the beginning of the condenser section (between TC's #4 and #5). The average temperature of the storage volume is less than the vapor temperature (TC #3) at this condition indicating that the breadboard is not an ideal FCHP. TC #11 is less than TC #10 due to a conduction effect associated with end losses. Similarly, the gradient between TC #10 and TC #8 indicates conduction

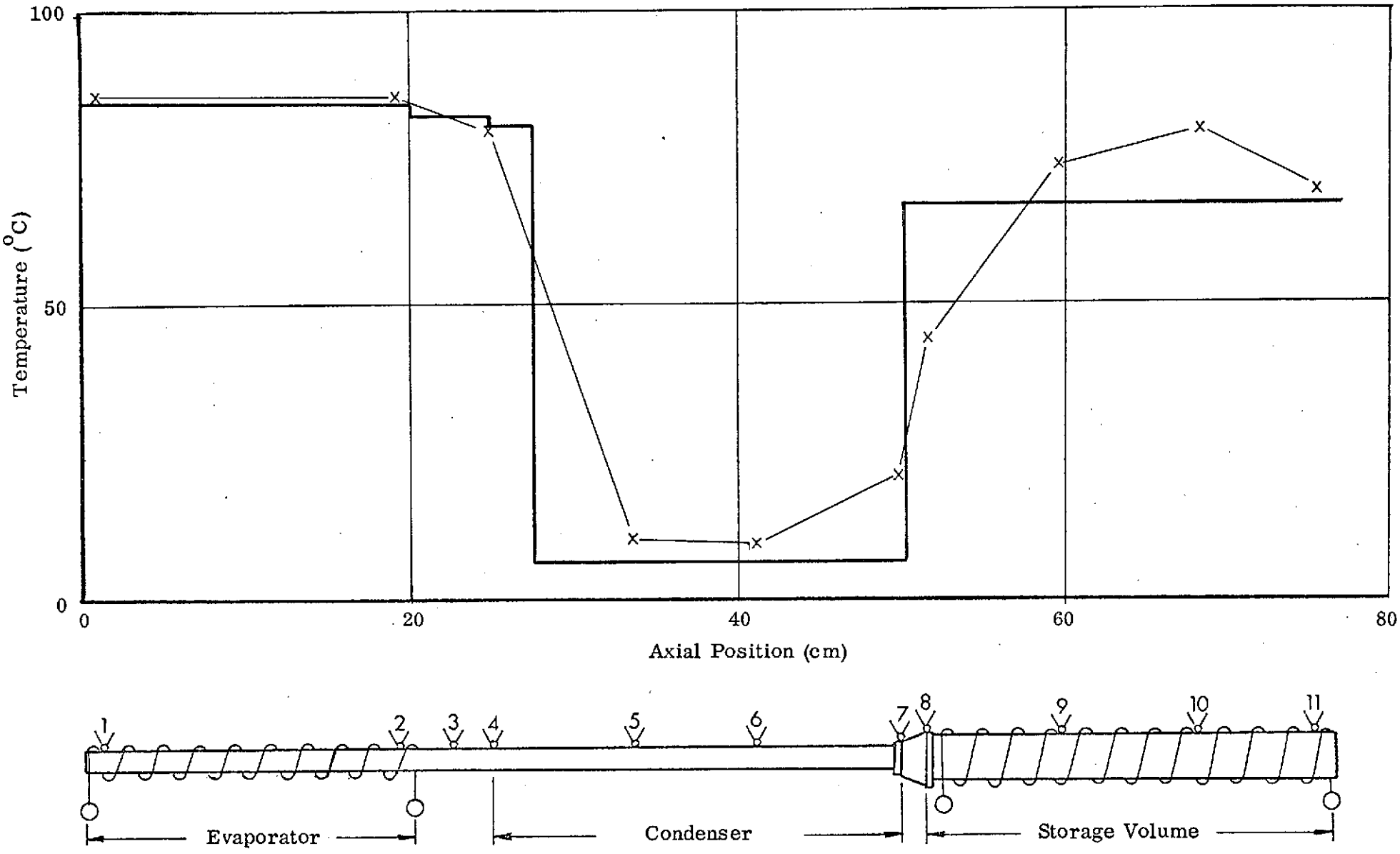

FIGURE 3.14

PREDICTED AND EXPERIMENTAL STEADY-STATE AXIAL TEMPERATURE DISTRIBUTION
(LOW POWER/LOW SINK)

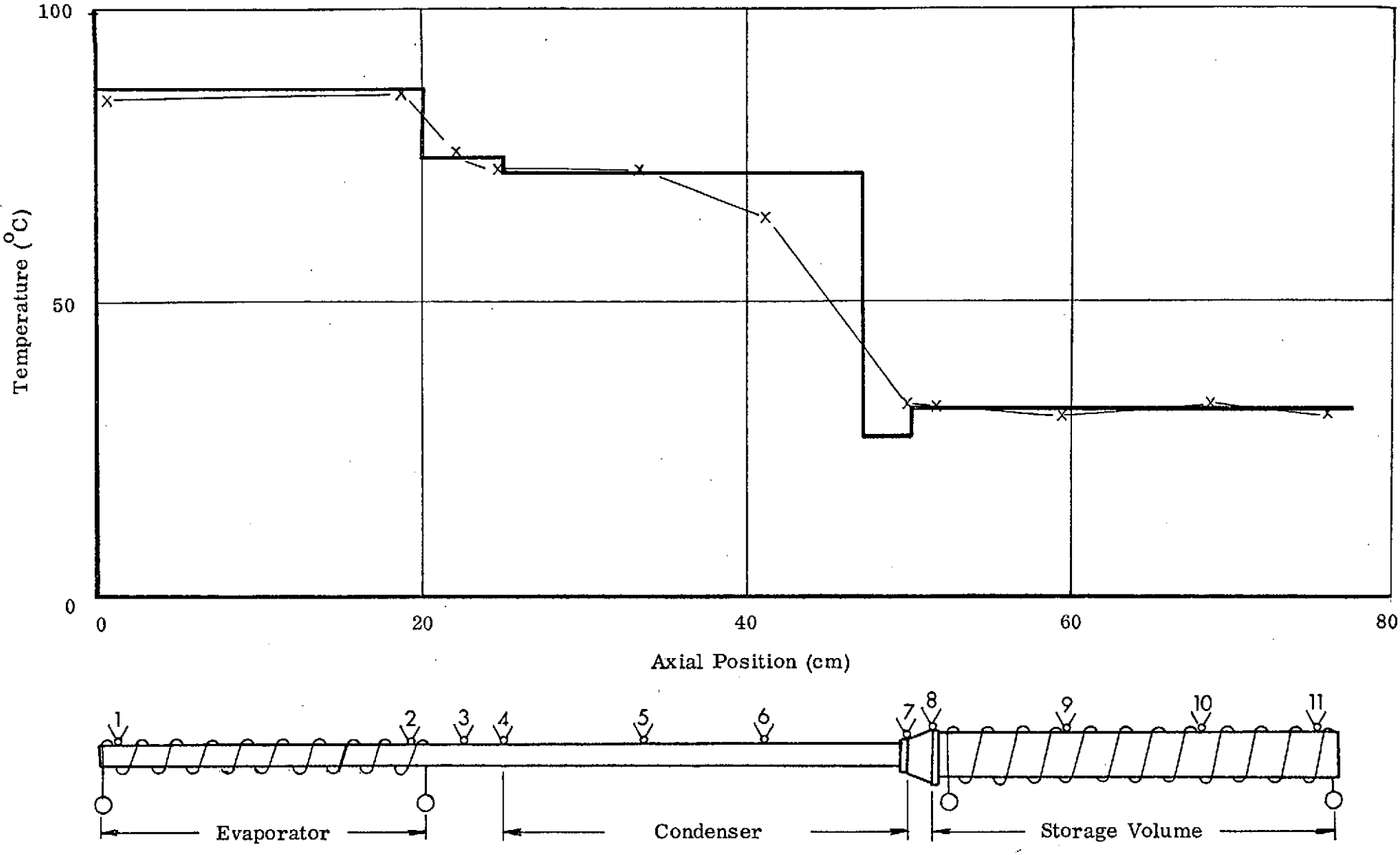

FIGURE 3.15

PREDICTED AND EXPERIMENTAL STEADY-STATE AXIAL TEMPERATURE DISTRIBUTION
(HIGH POWER/HIGH SINK)

losses from the storage volume to the condenser section. Except for a slight conduction effect from the condenser section to the storage volume, the reservoir is essentially at a uniform temperature less than $2^{o}C$ above the sink temperature for the steady-state high power/high sink case. For this power and sink condition and particular gas charge, the active condenser length extends over approximately two-thirds of the total condenser.

The difference between the source temperature and the vapor temperature at the high power/high sink condition is $11^{o}C$. Thus, the thermal impedance (R_s) between the heat source and the vapor is $0.133^{o}C$/watt. Consequently, an ideal variable conductance heat pipe with no feedback ($V_{st} \rightarrow \infty$) would experience a $\pm 6^{o}C$ variation in source temperature under the same test conditions. The actual experimental system without feedback could have controlled the vapor to within $\pm 4.3^{o}C$ and the source to within $\pm 8.3^{o}C$.

The transient response of the "simulated" heat source to simultaneous step changes from a low power/low sink condition to a high power/high sink condition and vice versa is shown in Figure 3.16. The corresponding response of the storage reservoir is shown in Figure 3.17. As can be seen, essentially absolute control of the source temperature is achieved for the two step changes. This control was attained for variations in power ranging from 15 to 75 watts and simultaneous variations in sink temperature from 5 to $30^{o}C$. The auxiliary power required to maintain the heat source at the set point ($84^{o}C$) at the low power/low sink condition was approximately 8.5 watts.

The maximum overshoot of the heat source temperature was $9^{o}C$, while the maximum undershoot was $11^{o}C$. The time for the heat source temperature to settle

FIGURE 3-16

RESPONSE OF SOURCE TEMPERATURE

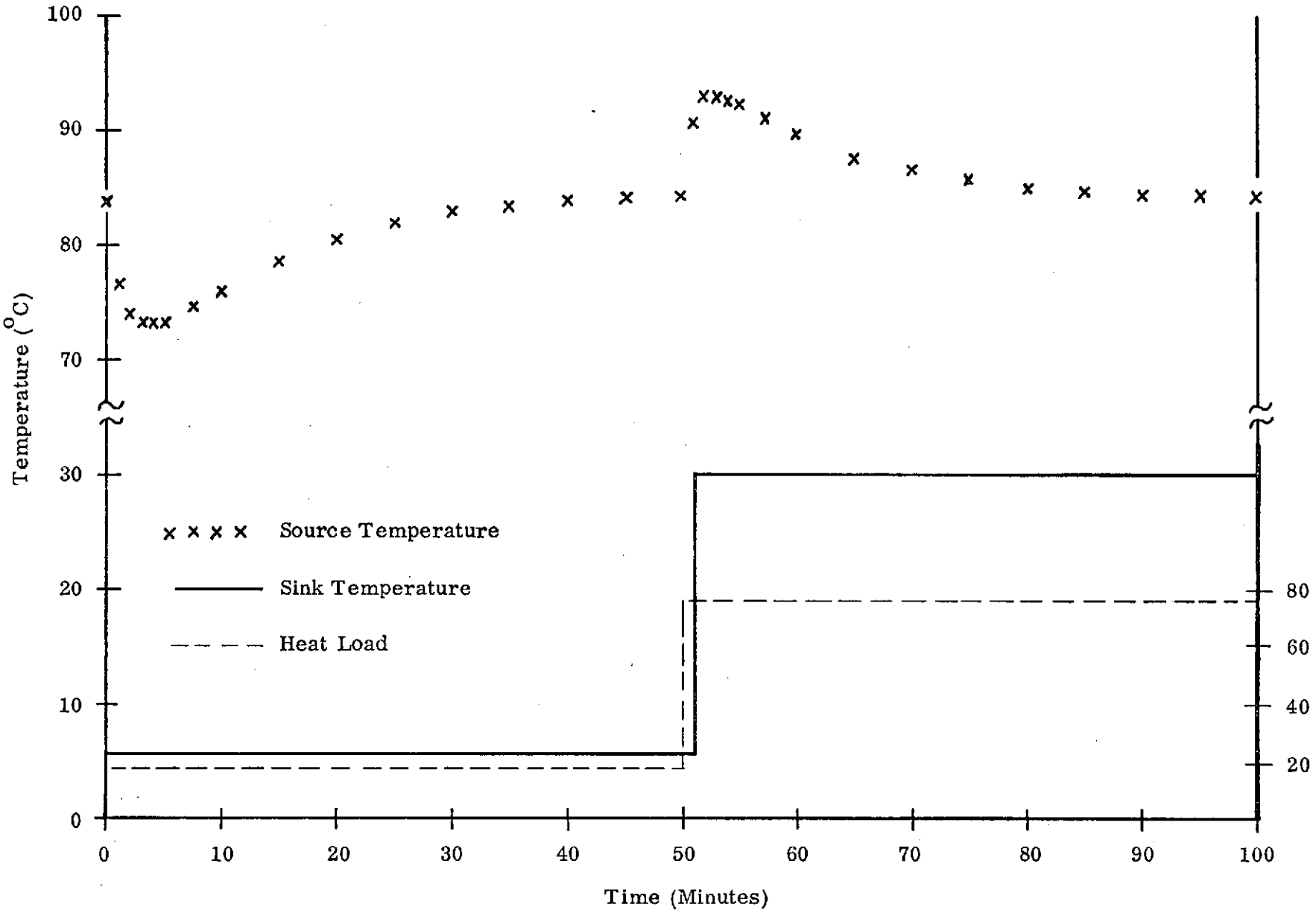

FIGURE 3.17

RESERVOIR TEMPERATURE RESPONSE

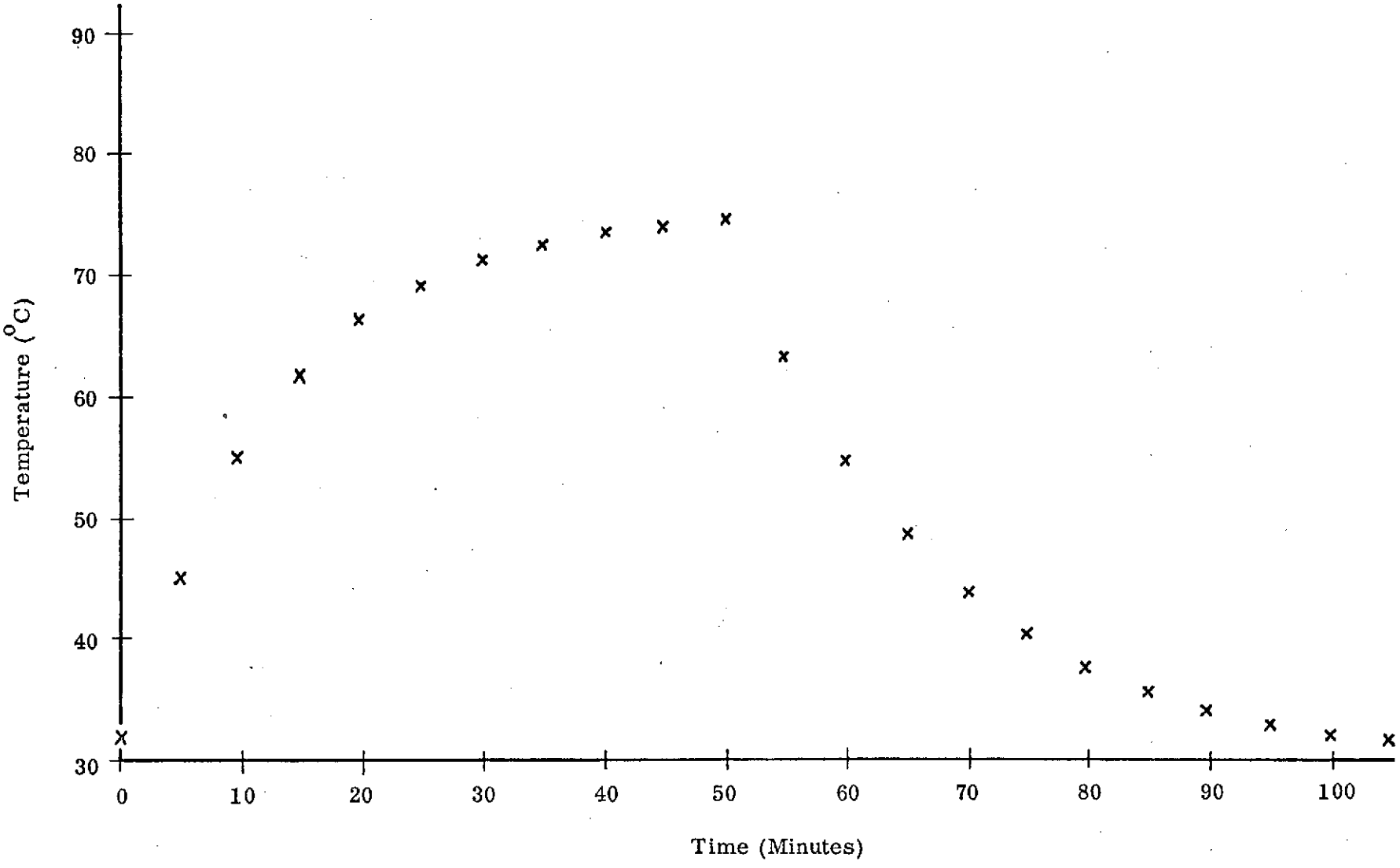

to within $1^{o}C$ of its final steady-state value was 29 minutes for the step increase and 36 minutes for the case in which power and sink temperature were decreased.

The difference between the overshoot and undershoot and the different recovery times for the two cases can be attributed to the effect of the vapor pressure on the response of the system. Although the response of the storage temperature is essentially identical for both cases, initially the change in the vapor pressure in the storage volume is less than for the case where the reservoir temperature increases from the sink condition (i.e., step change from high power/high sink to low power/low sink). Consequently, initial adjustment of the interface is not as rapid for the step change from high to low power/low sink; and, therefore, the undershoot is greater than the overshoot which in turn leads to longer recovery times.

3.4.2 Correlation of Transient Response

The experimental transient data has been correlated using both the nonlinear solution (FEDCON) and the closed form solution which predicts transient performance in terms of the individual time constants of the heat source and storage volume. The calculated heat source temperature response for both solutions is compared with the experimental data in Figure 3.18. The predicted and experimental storage temperature responses are also shown in this figure. A linear average of TC's #9, #10, and #11 is used to define the experimental storage temperature. Predicted and experimental heat source response characteristics are compared in Table 3.1.

The correlation based on the nonlinear solution was established by adjusting the mass of noncondensible gas charge such that the calculated and experimental reservoir temperature are identical at the high power/high sink steady-state condition. As indicated in Figure 3.18, the method of correlation results in almost exact duplication of

FIGURE 3.18

PREDICTED AND EXPERIMENTAL TRANSIENT RESPONSE

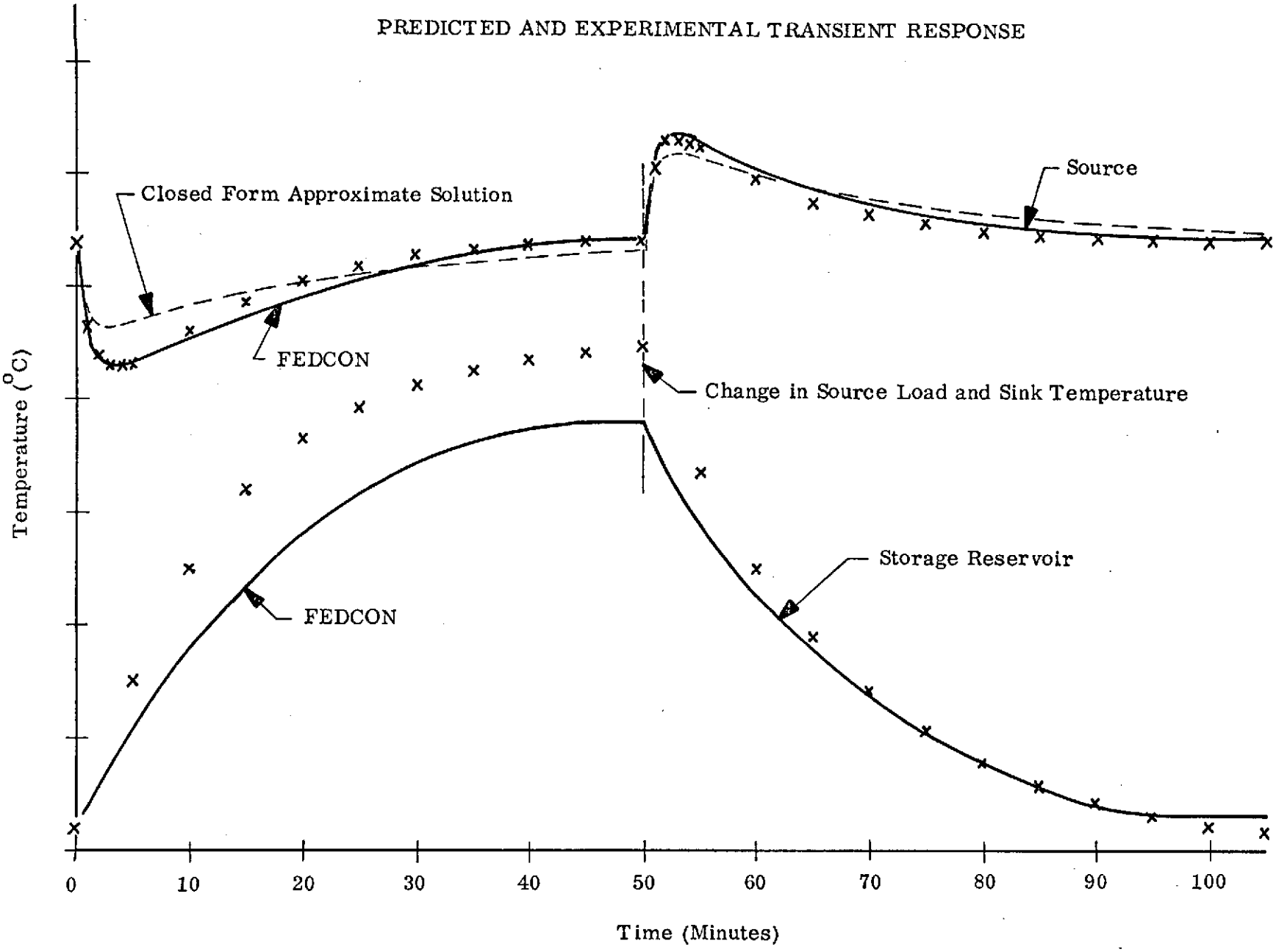

STEP CHANGE	DATA SOURCE	$T_{s,p}$ (^{o}C)	t_p (Minutes)	t_R* (Minutes)
High to Low Power/Sink	Experimental	73.0	3.0	33
	FEDCON Predicted	72.5	3.0	35
	Closed Form Predicted	76.0	2.5	45
Low to High Power/Sink	Experimental	93.0	2.5	28
	FEDCON Predicted	93.5	2.5	32
	Closed Form Predicted	92.0	2.5	45

*The recovery time (t_R) is defined here as being the time required for the source temperature to settle to within $1^{o}C$ of its steady-state value after a change in power/sink conditions.

TABLE 3.1

COMPARISON OF PREDICTED AND EXPERIMENTAL RESPONSE CHARACTERISTICS

the response of the heat source and reservoir temperatures for the step change to high power/sink.

The correlation of the step change to low power/low sink with FEDCON was obtained by using an "empirical" auxiliary power. This empirical power was calculated based on the known impedance between storage volume and sink and represents the minimum power which is required to achieve steady-state control of the source temperature. The empirical auxiliary power is 4.7 watts as compared to 8.5 watts which was required in the test. This difference can be attributed to the conduction loss from the storage volume to the condenser section which is approximately 4.5 watts. This heat loss to the condenser and therefore the auxiliary power requirement can be reduced by only applying the auxiliary power over the latter part of the storage reservoir as opposed to applying power over its entire length. Results previously obtained for similar test conditions, but with the auxiliary power applied to the latter one-third of the reservoir, showed that less than 6 watts were required to maintain steady-state control. The auxiliary power could also be minimized by reducing the diameter of the transition section and making it longer, therein more effectively decoupling the reservoir from the condenser cooling.

The predicted response determined from the closed form solution is also shown in Figure 3.18. This solution is based solely on energy considerations and assumes that the recovery of the vapor temperature occurs at the same rate as that of the reservoir temperature. The closed form solution expresses the response of the source temperature in terms of the time constants of the heat source (τ_s) and the storage volume (τ_r).

For this experimental model, the time constant of the heat source is 43 seconds

and that of the storage volume is 1370 seconds. Calculated results show a shorter time to maximum undershoot of the source temperature than that observed for the experimental system. Furthermore, the analytical solution predicts less overshoot/undershoot than the experimental data shows. The differences are due to the fact that the system vapor temperature and therefore pressure are assumed to respond immediately to a change in power and/or sink temperature. In reality, the vapor temperature may experience a slight overshoot/undershoot before it begins to recover. This is particularly true for the step change from high to low power/sink. In this case, initial changes in the storage volume result in only small storage vapor pressure changes. These, in turn, have less effect on the system vapor and source temperatures than in the opposite case (where the reservoir has to decrease from approximately the source temperature in order to achieve control). In either case, the recovery of the vapor depends on how fast the storage volume responds relative to the heat source. Thus, the mathematical model will give better correlation at low values of τ_r/τ_s since the more rapidly the reservoir responds relative to the heat source the faster the interface will adjust and, therefore, the better the assumption becomes that there is no overshoot/undershoot of the vapor temperature (its recovery is identical to that of the reservoir).

The recovery times, predicted by the closed form solution, are longer than those observed experimentally. This is a result of neglecting conservation of mass in the mathematical model. The predicted recovery is dependent upon the storage temperature asymptotically approaching its final steady-state value. In the real system, the vapor temperature (and therefore the source temperature) approach their nominal value before the storage temperature reaches its equilibrium value. This is due to the fact that, near the extreme points, small deviations of the storage tempera-

ture have little effect on vapor and source temperature.

The closed form solution is not nearly as accurate as the nonlinear analysis which includes conservation of mass and the associated properties of the gas and working fluid. However, it is sufficiently accurate to be used as a preliminary design guide for a controlled system.

3.5 PCM Development

The design of the PCM equipment shelf, which is part of the ATFE experiment, was preceded by the development and testing of a scaled-down breadboard model. Its design is shown in Figure 3.19. The package geometry is similar to that required in the ATFE. The package serves as an equipment mounting platform. Solar heat is transferred from an absorber panel to the equipment platform by a thermal diode heat pipe attached to the top plate of the platform. An electrical feedback-controlled heat pipe transfers the heat from the platform to a radiator. The feedback controlled heat pipe is used to control the platform during the periods of solar input. The diode, aside from transferring heat to the platform during this period, minimizes heat losses during the shadow period. The purpose of the fusible material is to provide close temperature control during the shadow period. At this time, the fusible material freezes therein, releasing its latent heat of fusion to make up for the heat losses and thereby maintain the equipment platform at constant temperature.

The breadboard model consisted, essentially, of an aluminum box and face plates and two compartments which contained a partially expanded honeycomb core and fusible material. Octadecane ($C_{18}H_{38}$) was chosen as the fusible material. It has a well defined melting point at 28°C and a heat of fusion of 246 watt-sec/g. Partially expanded

FIGURE 3.19

BREADBOARD MODEL OF
FUSIBLE MATERIAL PACKAGE

All Dimensions in Millimeters

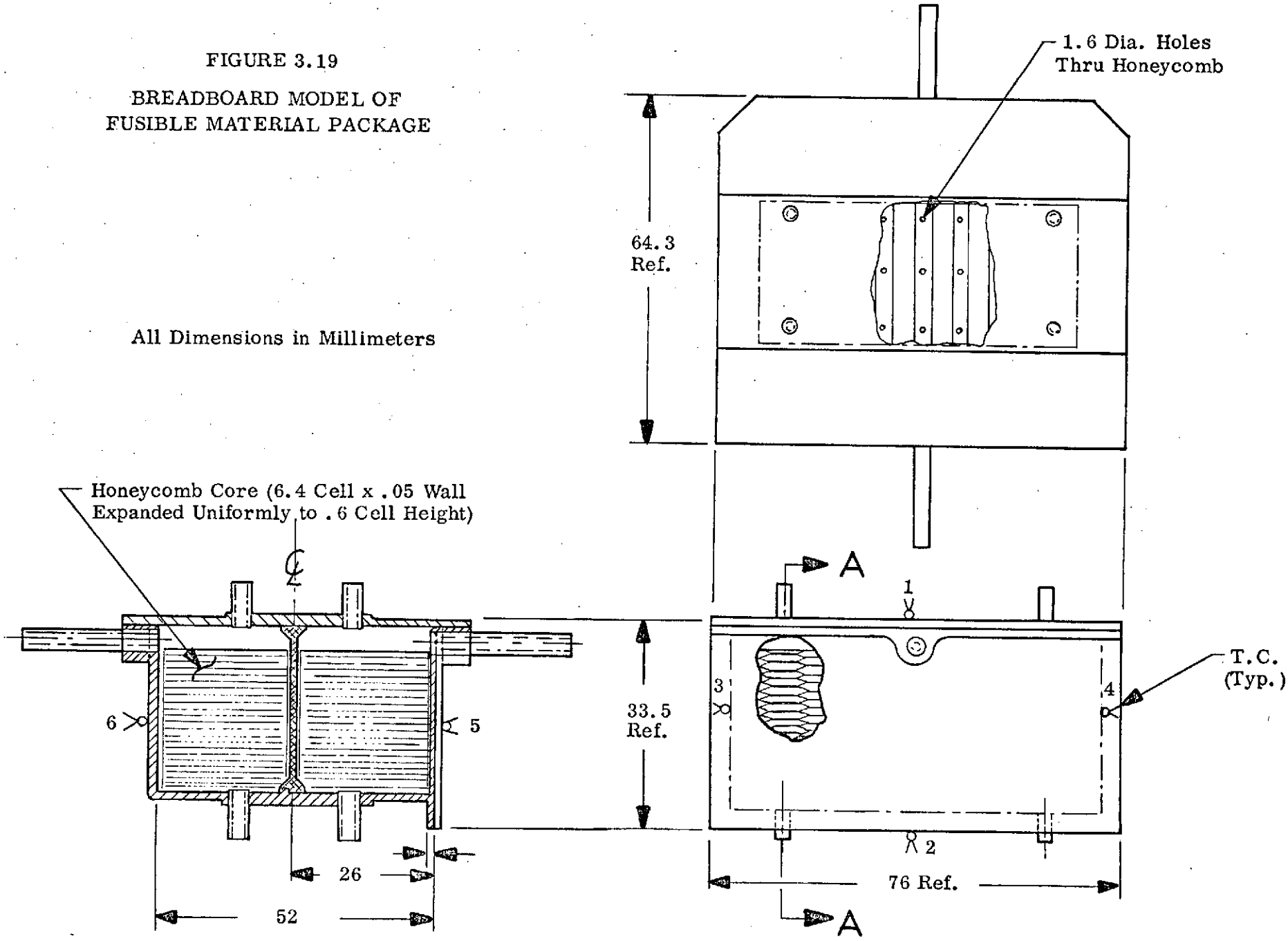

Section A--A

honeycomb was used to increase the effective conductivity and diffusivity of the fusible material. During periods when the fusible material freezes, its heat is transferred to the aluminum webs which separate the individual compartments. The individual compartments are used to reduce the heat transfer length through the fusible material/honeycomb core. As the transfer length is reduced, the amount of honeycomb required for optimum thermal performance is also reduced.

A void of approximately 15% was located at the top of the package between the honeycomb core and the face plate at which heat was to be applied. This void was sized to accommodate the expansion of the liquid fusible material in the event that the feedback controlled heat pipe in the ATFE fails and the package reaches the corresponding failure mode temperature of 127°C. The smallest characteristic dimension of the void is larger than the largest dimension of a single honeycomb cell. As a result, based on energy considerations associated with the surface tension of the liquid, the fusible material will preferentially fill only the honeycomb cell in a zero "g" space environment. Without having designed the void in this manner, a vapor space could form around the periphery of the individual compartments between the honeycomb and the solid aluminum members. This would result in poor conduction to the fusible material which, in turn, would reduce its effectiveness in providing thermal control.

Two fill holes (1/16" diameter) were drilled through each cell of the unexpanded honeycomb as indicated in Figure 3.19. The holes are required to fill the entire honeycomb core with the fusible material. An evacuation and a fill tube were located on opposite sides of the package for charging purposes. An adhesive film (FM-1000) was used to bond the honeycomb and provide a vacuum seal for the breadboard model. Subsequent units were welded to guarantee a reliable leak-tight seal.

The breadboard was charged with 54 grams of octadecane. A technical grade of the material was chosen because it provides more nucleation sites and facilitates solidification better than a purer grade. A tape heater was attached to the heat input side and thermocouples were located as shown in Figure 3.19. The package was precooled in a refrigerator to assure complete solidification of the PCM, and then the transient temperature profiles were monitored on a multipoint recorder at various input power levels. The objective of the melt tests was to determine the effectiveness of the design in terms of transferring the heat to the PCM. Also, the overall resistance between heat input side, heat output side, and PCM was of interest.

The temperature transients during a typical melt test are shown in Figure 3.20. From these data (only the temperatures at the heat input and output sides are shown), an energy balance and a value of the conductances can be obtained. The results of two tests at different input powers are summarized in Table 3.2.

TABLE 3.2

RESULTS OF PCM BREADBOARD MELT TESTS

	Test #1	Test #2
Gross Heat Input (watts)	5.25	12.7
Heat Loss at MP (watts)	1.90	1.9
Net Heat Input (watts)	3.35	10.8
Time Required to Melt (minutes)	55	20
Energy to Melt (watt-minutes)	184	216
Latent Heat in PCM (watt-minutes)	217	217
Heat Input Resistance (^{o}C/watt)	0.58	0.39

FIGURE 3.20

EXPERIMENTAL MELT CURVE OF BREADBOARD PCM BOX

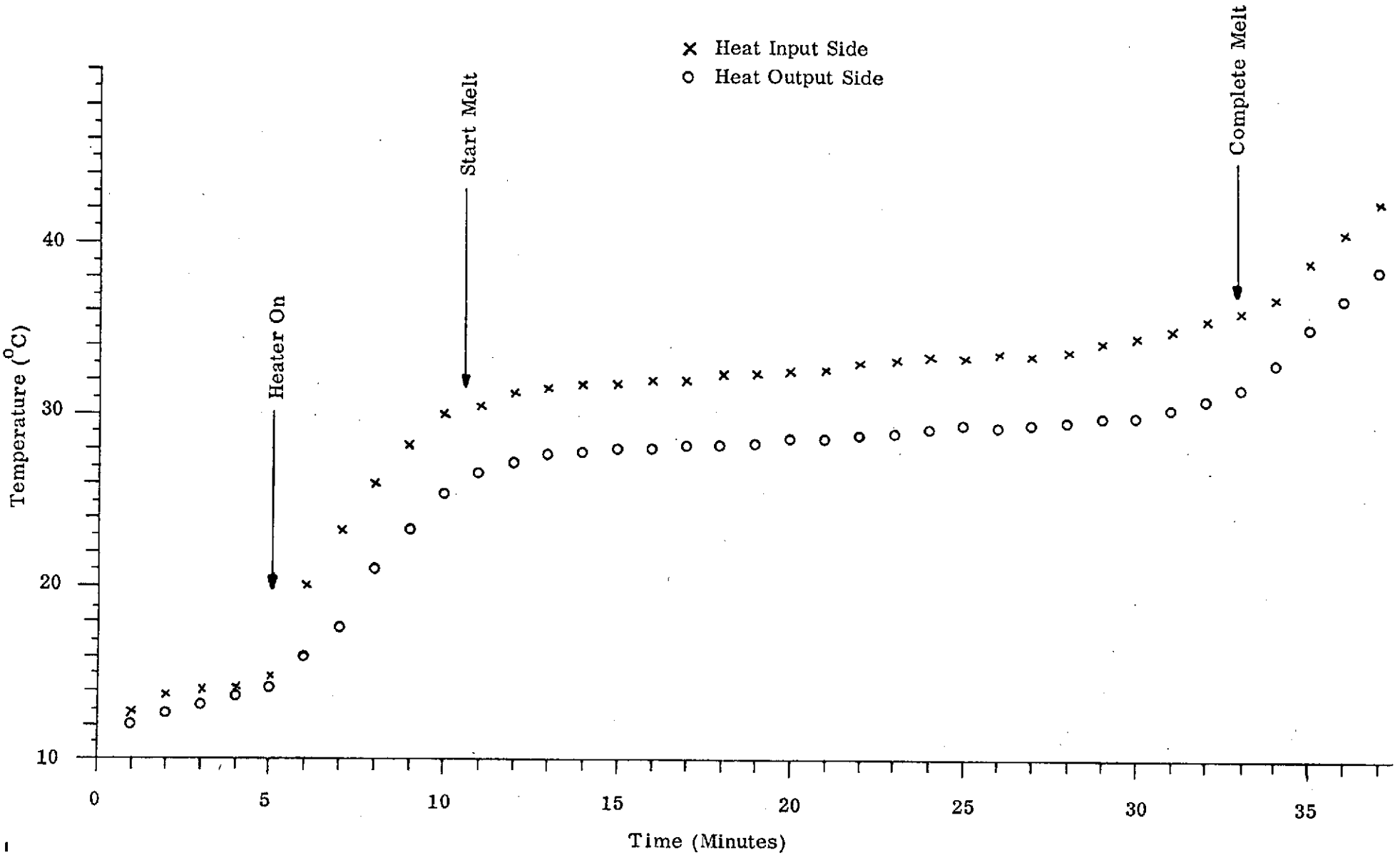

The measured energy required to melt the PCM compares favorably with its latent heat of fusion. This indicates that the conductive paths are adequate to transport the heat to the individual PCM cells and that all or most of the PCM melts before the temperature of the box rises significantly above the melting temperature. The heat input resistances shown in Table 3.2 were evaluated by using the difference between the highest temperature on the input side and the melting temperature. The discrepancy between the two values could be due to instrumentation error or a shift in the melting temperature. In fact, the two resistances would be identical if the actual melting temperature were 28.6°C instead of 28.0°C.

The thermal resistance during solidification (heat output resistance) should be identical to the input resistance provided that the freezing and melting patterns are the same. If the average measured melting or freezing resistance is extrapolated to the 18-inch long PCM shelf of the ATFE, a value of 0.065°C/watt is obtained. The resistance between input and output side (not measured during our tests) would be somewhat higher but less than twice the individual resistances.

4. ATFE FLIGHT EXPERIMENT

4.1 System Description and Design Summary

The objective of the Advanced Thermal Control Flight Experiment (ATFE) is to test (in a space environment) three recently developed thermal control devices:

- Active Feedback Controlled Heat Pipe (FCHP)
- Passive Thermal Diode Heat Pipe
- Phase-Change Material Storage Container (PCM Box)

A pictorial schematic of the experiment is shown in Figure 2.2 and a functional diagram is given in Figure 4.1. Basically, the ATFE consists of a solar absorber, a thermal diode, a simulated equipment package that contains phase-change material (PCM box), a feedback controlled variable conductance heat pipe (FCHP), and a space radiator. The ATFE will be flown aboard the Applications Technology Satellite (ATS-F). It is mounted in the east wall of the ATS-F earth-viewing module (EVM) with only the outboard surfaces of the solar absorber and radiator exposed to the external environment. Photographs of the front and back view of the assembled ATFE are shown in Figures 4.2 and 4.3.

The ATS spacecraft is three-axis stabilized and in a geosynchronous near-equatorial orbit. This results in an incident solar flux that rises and sets over a 12-hour period followed by 12 hours of darkness. The flux profile, which is shown in Figure 4.4, is similar to the solar cycle experienced by a fixed point on the earth's surface with the exception of two discontinuities. The discontinuity at 09:20 hours is caused by attenuation of the solar intensity when the shadow of the 30-foot latticed antenna falls on the east wall of the EVM. The discontinuity near earth midnight is seasonal; it is caused by earth

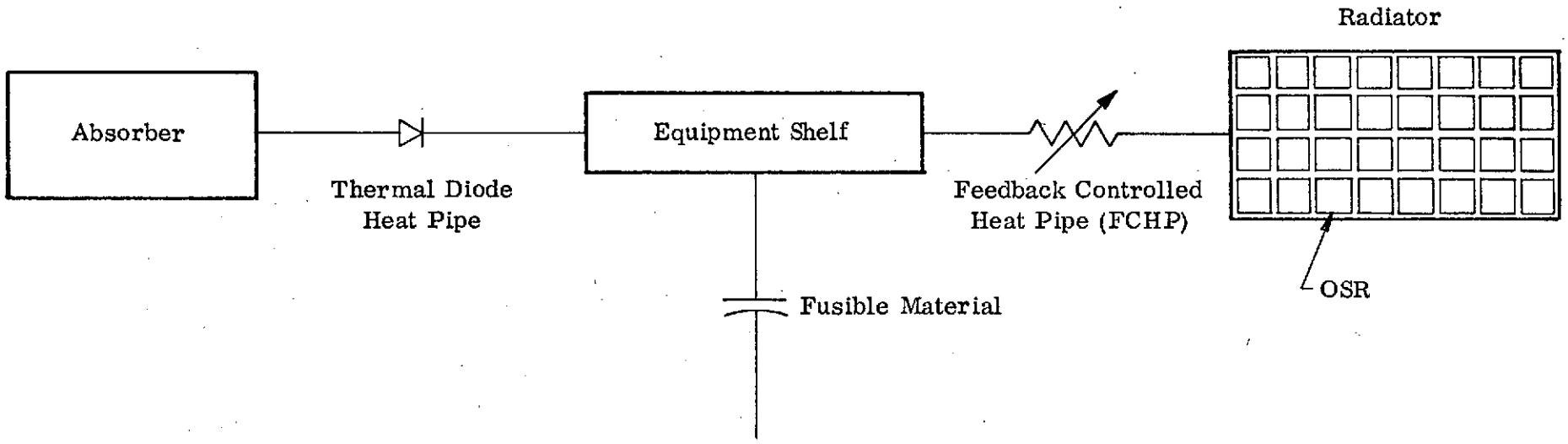

FIGURE 4.1

FUNCTIONAL DIAGRAM OF ATFE EXPERIMENT

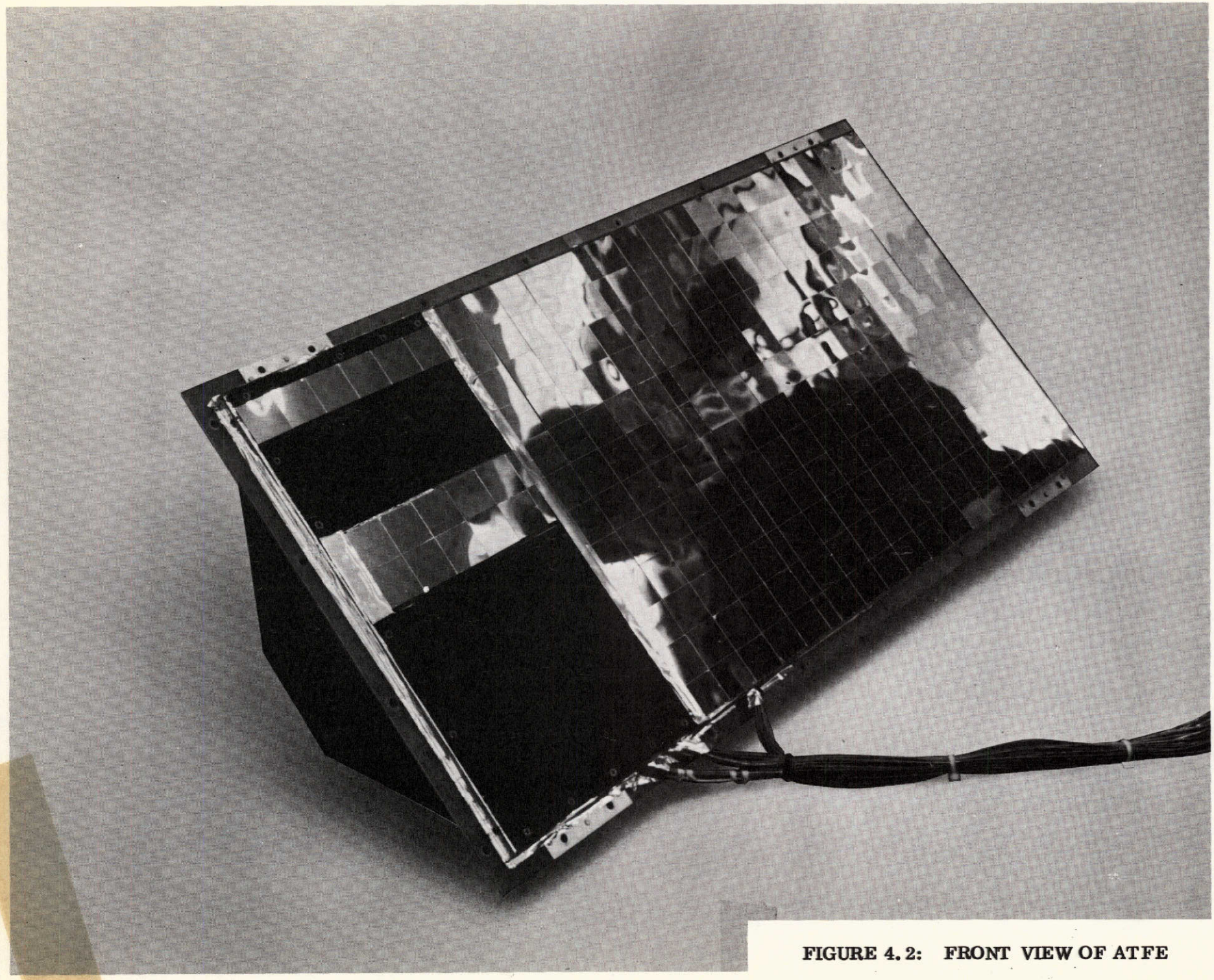

FIGURE 4.2: FRONT VIEW OF ATFE

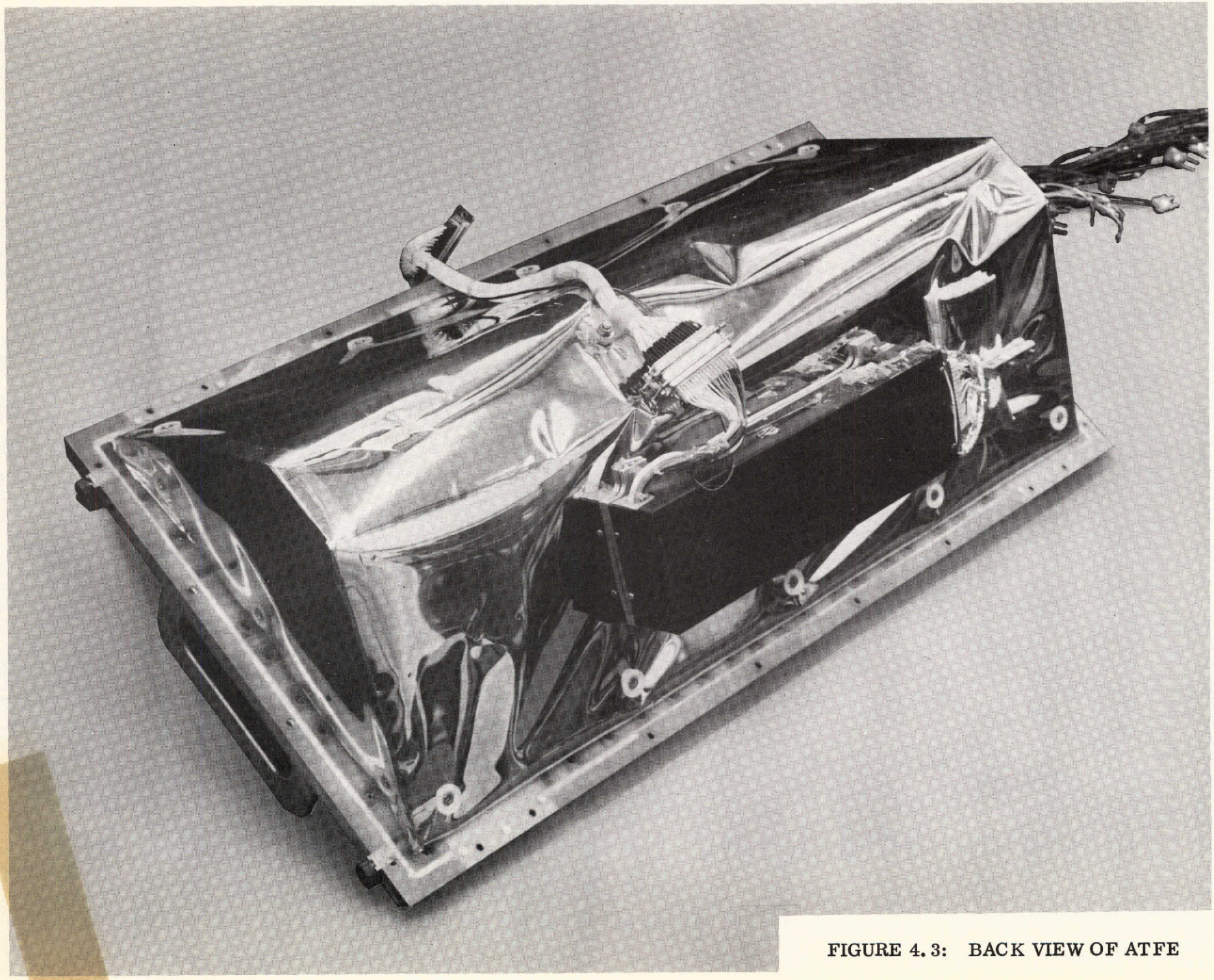

FIGURE 4.3: BACK VIEW OF ATFE

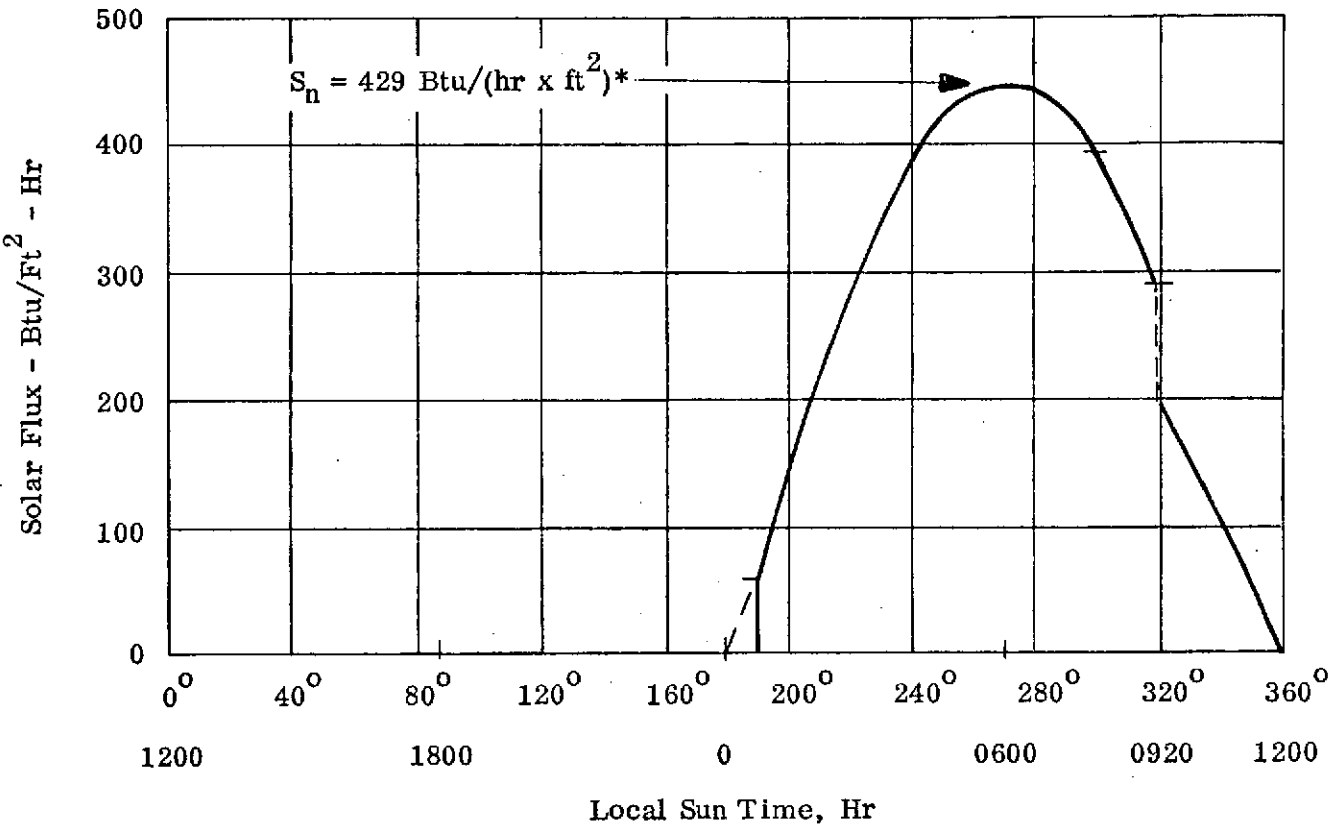

*Not plotted to scale

FIGURE 4.4

DESIGN SOLAR FLUX PROFILE, EAST FACE OF EVM

eclipse of the spacecraft and occurs only during periods of about 23 days before to 23 days after the Spring and Fall equinoxes. The timing and daily duration of these eclipses are given in Figure 4.5. Since only the duration after midnight affects the time of "sunrise" on the east wall, and since the maximum total duration of 70 minutes occurs at the equinoxes, the latest sunrise will take place at 00:35 hours.

Absorbed solar energy is used to simulate power dissipation during an electrical duty cycle and is transported from the absorber to the PCM box by the diode heat pipe. The energy first melts the PCM, which is octadecane and has a melting point of 28°C. When melting has been completed, the energy then passes through the PCM box to the FCHP which transports it to the space radiator. During the cycle, temperature control of the diode/PCM box interface is provided by the FCHP. The FCHP senses the temperature at the interface and, correspondingly, regulates the heat rejection to space to accommodate the variations in both the thermal load and the thermal boundary conditions at the radiator. As the shadow period is approached, the diode and FCHP decrease their conductance to minimize the heat loss from the PCM box to space. Thermal energy released by freezing the PCM is used to compensate for heat lost during the transient shutdown of the diode and FCHP and to provide temperature stability during part of the shadow period. When all the PCM has frozen, the temperature of the equipment shelf decreases at a rate that depends on the heat capacity of the PCM box and its parasitic heat leaks. The amount of octadecane provided in the PCM box is selected to permit cooling of the PCM box to about 0°C. This allows the evaluation of the PCM melting point stability in zero gravity.

A major design goal was to maintain the temperature at the diode/PCM box interface at 29 $\pm$ 3°C throughout the solar cycle and several hours of the shadowed period.

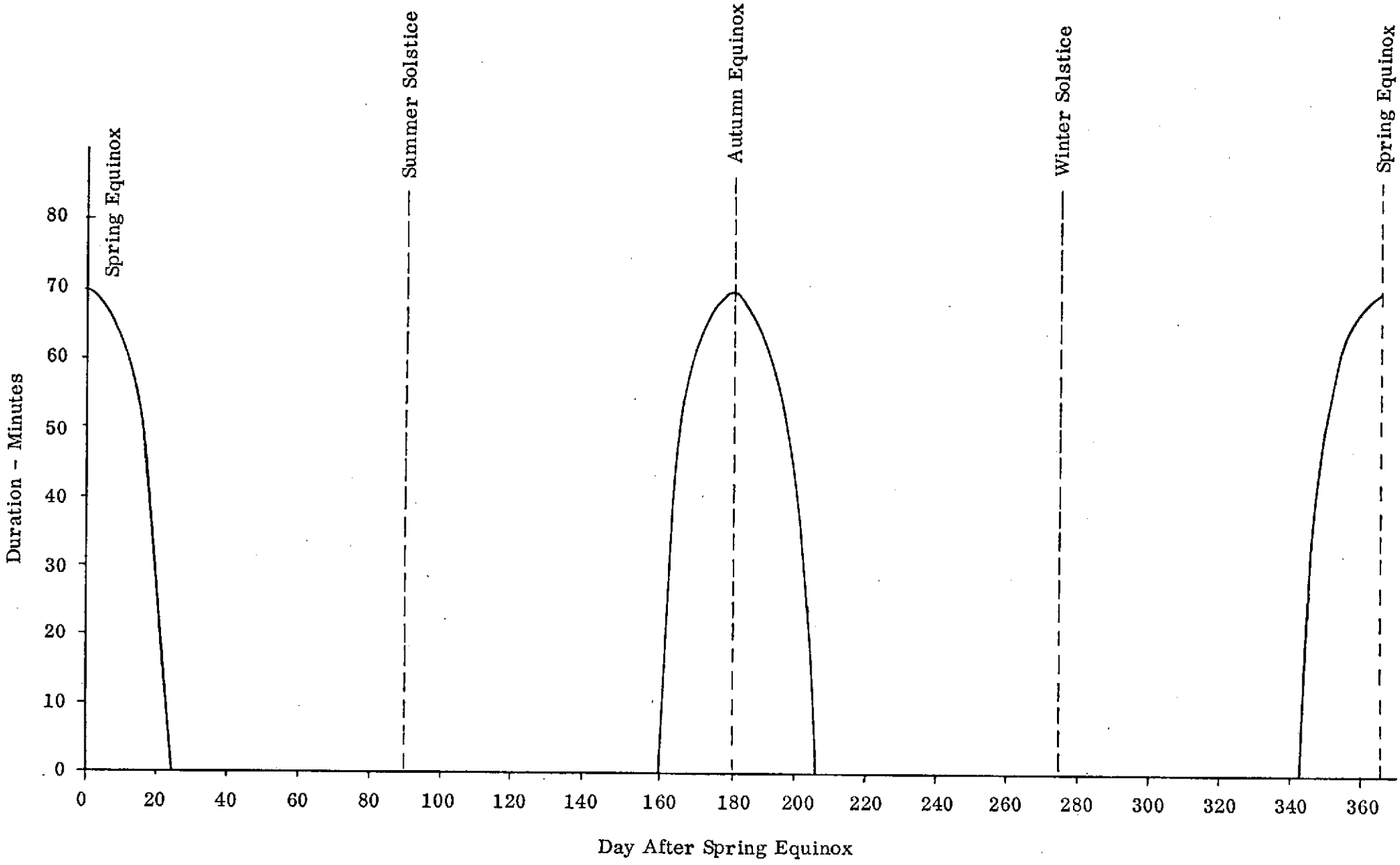

FIGURE 4.5

EARTH ECLIPSE TIME FOR ATS-F ORBIT

Other design goals and constraints on the system design and their impact on the experiment are listed in Table 4.1.

4.2 Component Design

4.2.1 Absorber

The absorber consists of a 0.040-inch (0.102 cm) thick aluminum substrate coated with Chemglaze Z306 (α/ε = 0.96/0.86) and has a 6 x 12 inch (15.24 x 30.48 cm) platform. The absorber and its interface with the thermal diode and FCHP reservoir are shown in Figure 4.6.

A black paint was chosen to maximize the solar absorption while minimizing the absorber's equilibrium temperature during peak solar conditions. Also, the high emittance results in a lower absorber temperature during the shadow, thereby providing a better test of diode performance. If the feedback controlled heat pipe (FCHP) should fail to transport the heat input, the absorber, diode, and PCM box would approach the equilibrium temperature of the absorber. The maximum allowable temperature in this failure mode was set at 127°C to guarantee a reasonable margin of safety for these components. Coatings with lower emissivities would have resulted in a more efficient absorber system, but their equilibrium temperatures would have been unacceptable. Six 1-inch (2.54 cm) square optical solar reflectors (OSR, α/ε = 0.10/0.82) are attached at one edge of the absorber to further guarantee the 127°C maximum temperature.

As indicated in Figure 4.6, the absorber has a 2-inch (5.08 cm) diameter well located near its center. This well runs the length of the absorber and accommodates the reservoir of the FCHP. Both sides of the well are insulated with multilayered insulation to minimize thermal interaction with the reservoir and to provide an essentially adiabatic surface. Adjacent to the well is a 5-inch (12.70 cm) long aluminum

Design Goals	Experiment Impact
1. Near room-temperature operation	1. Choice of PCM and heat-pipe working fluids
2. ±3°C control	2. FCHP reservoir size and thermal coupling
3. Maximum thermal throughput (approximately 20 W)	3. Absorber, radiator, and heat-pipe hydrodynamic designs
Constraints	
1. Meaningful 1-g testing of predicted 0-g performance	1. Overall ATFE configuration with heat pipes in common plane
2. Allowable envelope (24X12X6.0 in.) (60.96X30.48X15.24 cm)	2. Absorber and radiator sizes; with 1 (above), necessitated FCHP reservoir placed in absorber well
3. Minimum ATFE/ATS-F thermal interaction[a]	3. Structural design and insulation system
4. Limited spacecraft power	4. Use of solar energy as primary thermal input
5. Elimination of single point failures	5. Design of electronics module and use of auxiliary and backup heaters
6. ATS-F Project Experiment Interface and Environmental Test Specifications	6. Experiment design and test program

[a]The electronics module, however, is radiatively coupled to the EVM interior to avoid the temperature excursions experienced by the remainder of the ATFE.

TABLE 4.1

DESIGN GOALS, CONSTRAINTS, AND IMPACT

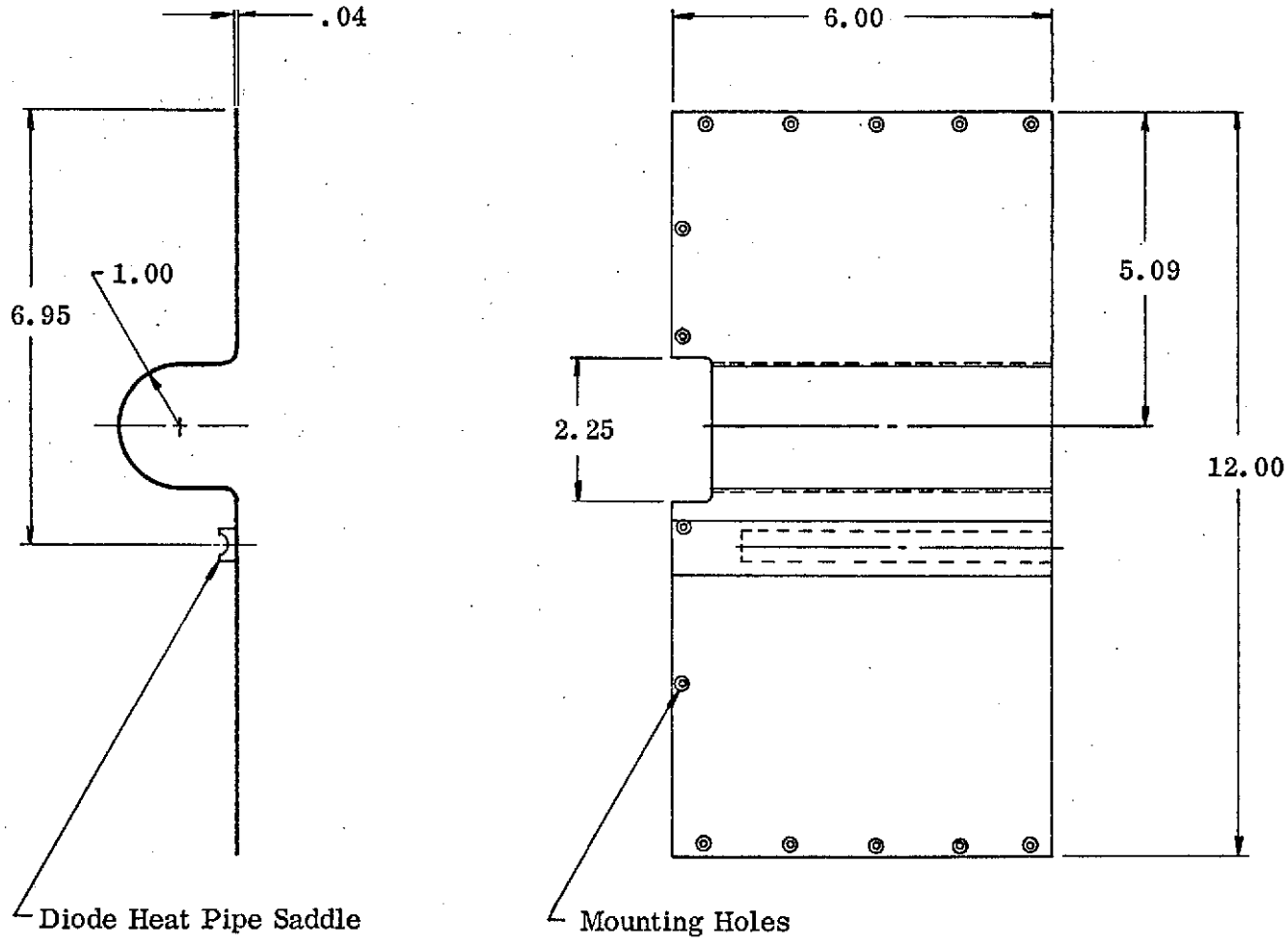

All Dimensions in Inches

FIGURE 4.6

DESIGN OF ABSORBER PANEL

saddle that was welded as an integral part of the absorber panel. The evaporator section of the diode is soldered to this saddle.

The total absorbing area is 60 inches^2 (387 cm^2), and the efficiency is approximately 45%. This results in a thermal throughput of approximately 20 watts for a maximum solar constant of 1418 watts/m^2. The length of the absorber was sized to maximize the net thermal input consistent with the experiment envelope and radiator heat-rejection requirements.

4.2.2 Thermal Diode Heat Pipe

The diode was provided to Dynatherm Corporation as Government Furnished Equipment by Grumman Aerospace Corporation for utilization in the ATFE. It is described in detail in Reference 7, and therefore only the major points will be discussed here.

From the various methods which exist for accomplishing diode heat pipe operation, excess liquid blockage was selected for the ATFE. This technique is based on the principle that excess liquid will accumulate as a slug in the cold section of the pipe. This slug inhibits vapor flow, thereby preventing "heat-piping" action in the blocked section and, except for relatively small conduction losses, effectively limits the heat transfer. A reservoir is located at the condenser end to accommodate excess liquid during the normal or forward heat-pipe mode.

In the ATFE, as the shadow period is approached, the absorber temperature drops below the temperature of the PCM box. When this happens, the liquid and vapor flows in the diode are reversed. (The normal condenser becomes an evaporator and the normal evaporator a condenser.) The excess liquid in the reservoir is vaporized by heat losses from the PCM box and flows to the reverse mode condenser (absorber

end). There it condenses, fills the vapor space, and effectively blocks further heat flow. The diode configuration is shown in Figure 4.7 and its design is summarized in Table 4.2.

The tunnel wick fabricated from 100-mesh screen is used as the primary capillary structure. The artery is centrally located and supported by a three-legged screen retainer-web assembly. This retainer also serves as a communication link between the artery and the screw thread grooves (90/inch or 31.5/cm) which provide circumferential distribution of the liquid around the tube. The spiral artery design permits relatively high heat transport capability in the normal mode with a small hydraulic diameter for the vapor flow. The small diameter is needed to support the liquid across the internal tube diameter in the blocked portion during shutdown in the one "g" environment. The smaller diameter also reduces the amount of excess liquid required, thereby decreasing the reservoir size and the transient energy losses during shutdown.

During shutdown, the vapor space in the evaporator, low "k", and transition sections must be blocked; hence, the smaller tube I.D. and vapor space thickness in these sections. The larger I.D. and corresponding vapor space thickness in the condenser section is used to reduce the vapor pressure drop in the forward mode. To minimize conduction losses, the low "k" section has a wall thickness of only 0.010 inch (0.0254 cm). It is reinforced with fiberglass to increase its burst pressure and protect it during handling.

The diode reservoir consists of 86 independent 0.063-inch (9.160 cm) diameter channels drilled in an aluminum cylinder 1.44 inches (3.66 cm) long. Aluminum was used to increase the heat transfer rates during the direct-to-reverse mode transient,

FIG. 4.7 ATFE DIODE HEAT PIPE

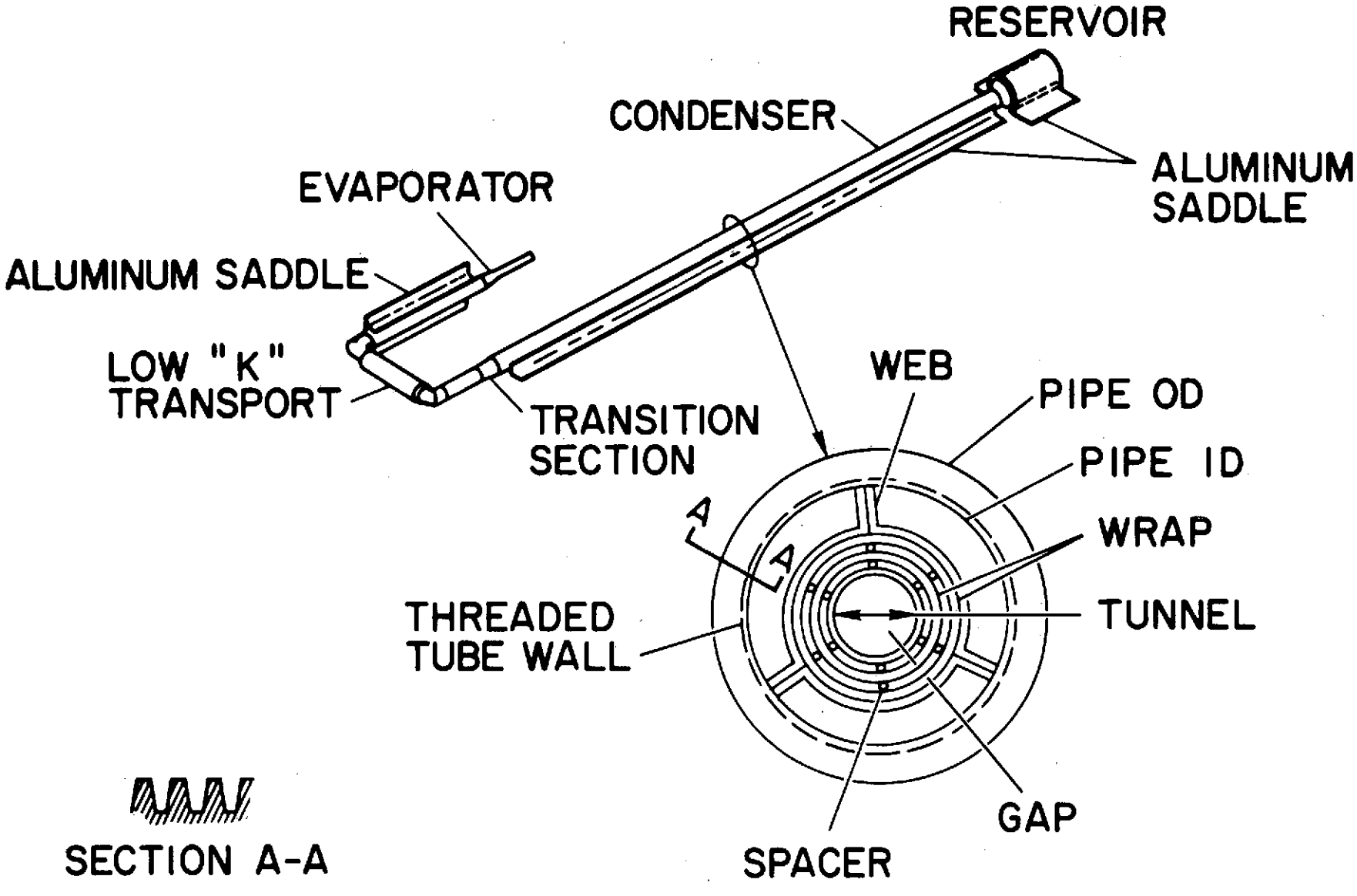

Envelope material – 304 stainless steel
Wick – 100-mesh stainless steel tunnel spiral artery
Working fluid – ammonia, 17.5 gm
Reservoir volume = 6.05 cm^3
Weight (diode only) = 286 gm

Section	Length, in. (cm)	O.D., in. (cm)	I.D., in. (cm)	Vapor space thickness, in. (cm)
Evaporator	4.90 (12.45)	0.377 (0.96)	0.309 (0.78)	0.025 (0.064)
Low "K"	1.88 (4.78)	0.329[a] (0.84)	0.309 (0.78)	0.025 (0.064)
Transition	1.42 (3.61)	0.375 (0.95)	0.309 (0.78)	0.025 (0.064)
Condenser	18.08 (45.92)	0.452 (1.15)	0.411 (1.04)	0.074 (0.190)
Reservoir	1.44 (3.66)	1.000 (2.54)	0.884 (2.25)	– –

[a]Tube without fiberglass reinforcement.

TABLE 4.2

ATFE DIODE HEAT PIPE SUMMARY

thereby reducing the shutdown time and the transient losses. The aluminum is press-fit into a stainless steel shell that is welded to the condenser tube. The arterial wick extends through the heat pipe tube but does not communicate with the liquid reservoir. Aluminum saddles are soldered to the reservoir and condenser to provide for attachment to and heat transfer to the PCM box.

4.2.3 Phase-Change Material (PCM) Box

Phase-change materials, also referred to as fusible materials, provide temperature stability by absorbing or rejecting heat nearly isothermally as they melt or freeze. In the ATFE, the latent heat of fusion released by freezing the PCM is used to compensate for both transient and steady-state parasitic losses from the PCM box. The transient losses are experienced during shutdown of the diode and FCHP components as the shadow period is approached. The parasitic losses occur during the shadow and are associated with (1) conduction leaks through the diode, FCHP, and structure; and (2) radiative coupling of the PCM box through its insulation to the cold absorber and radiator systems.

Figure 4.8 is a sketch showing the details of the PCM box. In addition to housing the PCM, the diode side of the box is used as a simulated equipment platform whose temperature is regulated by the FCHP during periods of heat input. The PCM box is a welded aluminum assembly with 0.040-inch (0.102 cm) thick walls. The box was designed to have a 10 watt/^{o}C conductance from diode to FCHP side.

Two identical compartments in the box contain the PCM, which is distributed in a partially expanded aluminum honeycomb core. Hysol adhesive is used to bond the honeycomb within the box.

FIG. 4.8 PCM BOX

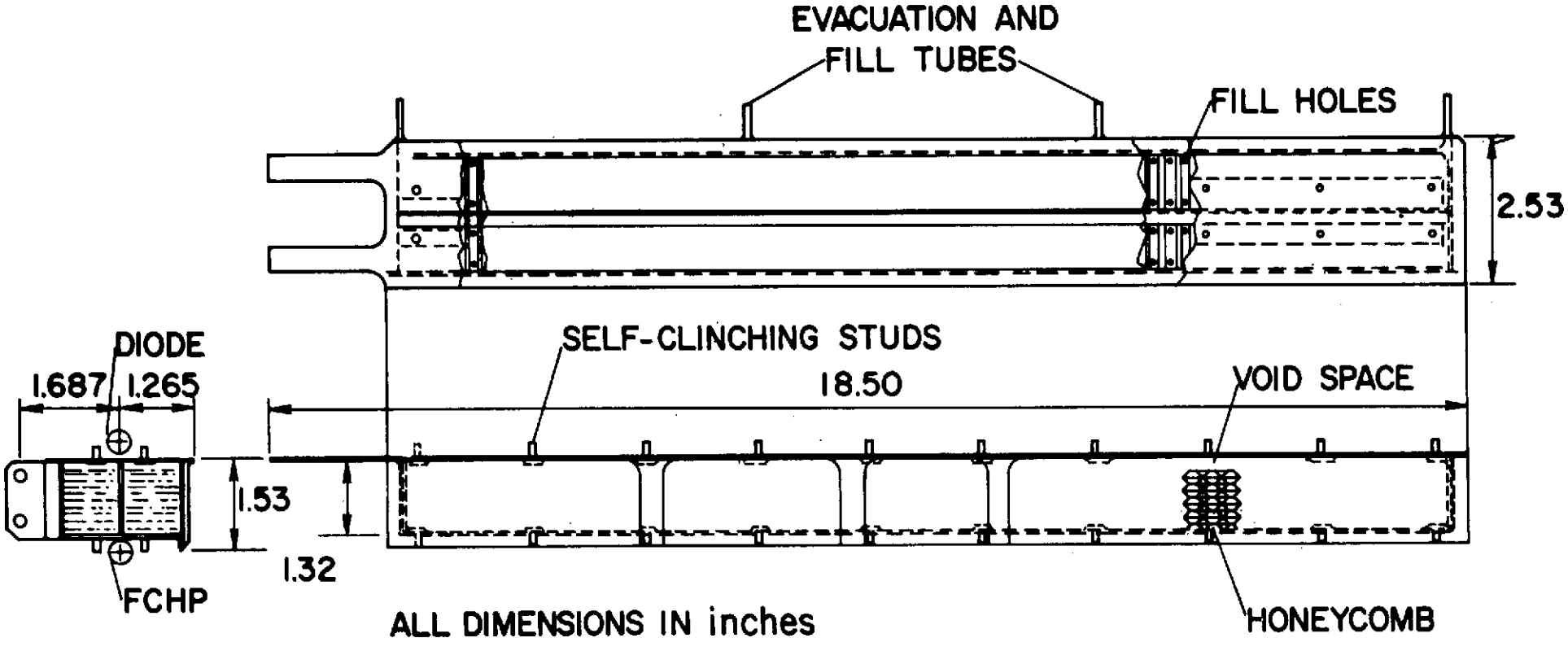

The honeycomb core is used to increase the thermal diffusivity of the PCM system and was designed in accordance with the procedure recommended in Reference 8. The individual compartments reduce the effective conduction length through the PCM/honeycomb core, thereby decreasing the amount of honeycomb required for optimum performance. In this system, the honeycomb cells have been oriented so that the primary conduction path is from the center shunt and side member to the center of the compartment. The side members and the center shunt are 0.040 inch (0.102 cm) and 0.031 inch (0.0787 cm) thick, respectively. The different thicknesses result in equal conductance paths through and around the box.

The PCM box contains 384 grams of octadecane, which is equivalent to 26 watt-hours of latent heat energy. Octadecane was chosen because its melting temperature ($28^{o}C$) was within the desired operating range and because it is an n-paraffin. These paraffins have a number of desirable features, including high heats of fusion and melting point stability (Ref. 9). Practical grade octadecane was used instead of a purer grade because the impurities provide more nucleation sites that facilitate solidification.

A void space of approximately 15% of the total internal volume is located above the honeycomb core at the diode side of the box to accommodate expansion of the octadecane up to a temperature well above the FCHP failure-mode temperature of $127^{o}C$. Two 0.0625-inch (0.159 cm) holes are drilled through each individual cell of the honeycomb to permit charging with the PCM and also to allow for expansion of the melted liquid into the void space. The void is purposely located near the heat input side of the box to allow the melting liquid to flow uninhibited toward a void. This prevents any localized excessive pressure buildup during liquefaction. For this same reason, the holes are located near the edges of the cells where the heat flows into the honeycomb from the

conduction members.

The smallest characteristic dimension of the void is substantially larger than the smallest characteristic dimension of the honeycomb cell. As a result, in zero "g", because of capillary action the liquid will preferentially fill the honeycomb. If the void has not been designed in this manner, a vapor space could have formed around the periphery of the individual compartments. This would have resulted in poor conduction to the PCM and possibly only partial melting or freezing.

Two 0.125-inch (0.3175 cm) charging tubes are welded to one side of the box. The box is first evacuated and then charged with the PCM at 125°C. A number of 0.125 inch (0.3175 cm) holes are located in the center member to allow charging of the individual compartments in a single operation. Self-clinching studs are inserted into the diode and FCHP faces of the PCM box to provide for mechanical attachment of these components. The PCM box is bolted to the support structure through flanges located at the end plates.

4.2.4 Feedback Controlled Heat Pipe

The basic ATFE FCHP configuration is shown in Figure 4.9 and its design is summarized in Table 4.3. Methanol was selected for the working fluid because it provides adequate self-priming and transport capability and its vapor pressure is substantially lower than that of ammonia. Consequently a significantly lighter reservoir can be used for containment resulting in more rapid response of the FCHP system to perturbations of the source temperature.

A composite slab wick was fabricated by wrapping 325-mesh screen around alternate layers of 325 and 20-mesh. It is centrally located in the heat pipe tube. The coarse screen permits high permeability within the limits of self-priming requirements,

FIG. 4.9 FEEDBACK CONTROLLED HEAT PIPE

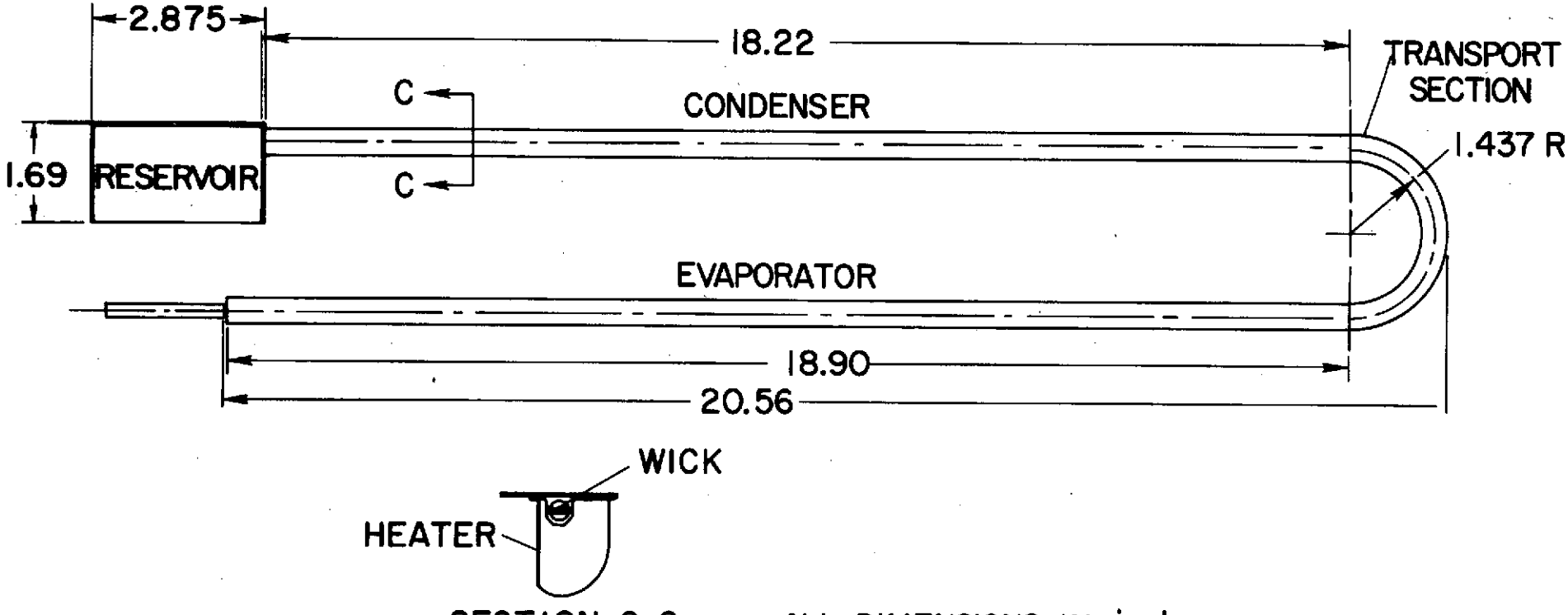

Envelope material – 304 stainless steel
Wick – 325/20 mesh stainless steel screen composite
(0.12 in. thick)
Working fluid – methanol, 28 gm
Control gas – helium, 2.08×10^{-3} gm
Reservoir volume – 78 cm^3
Reservoir volume/condenser and transport section
vapor space – 5.0 cm^3
Weight (including saddles) – 489 gm

Section	Length, in. (cm)	O.D., in. (cm)	I.D., in. (cm)
Evaporator	18.9 (48.00)	0.438 (1.113)	0.382 (0.970)
Transport	4.5 (11.43)	0.438 (1.113)	0.382 (0.970)
Condenser	15.7 (39.88)	0.375 (0.953)	0.319 (0.810)
Feed tube	2.5 (6.35)	0.375 (0.953)	0.345 (0.876)
Reservoir	2.9 (7.37)	N/A N/A	N/A N/A

TABLE 4.3

ATFE FCHP SUMMARY

whereas the fine screen is used to establish a high capillary pumping head. Screw thread grooves (36/inch or 14.17/cm) provide circumferential distribution of the liquid.

The evaporator and transport sections of the FCHP have a 0.382 inch (0.970 cm) I.D. and the condenser section has a 0.319 inch (0.810 cm) I.D. The larger I.D. is required to reduce viscous vapor losses and provide adequate transport capability, whereas the small condenser reduces the reservoir storage requirements. The feeder tube that extends from the condenser to the reservoir was reamed to a 0.015-inch (0.0381 cm) wall thickness to minimize conduction losses.

The reservoir's cross-section (Figure 4.9) was designed to minimize the self-priming requirements and to keep the reservoir radiator flush with the absorber to minimize solar input to the reservoir during maximum solar conditions, thereby allowing the reservoir to cool more efficiently. The reservoir has a 7.0-inch^2 (45.16 cm^2) OSR-covered radiating surface. The ratio of reservoir volume to condenser volume and the amount of noncondensible gas was chosen to provide temperature control of the PCM box at 28°C with the reservoir temperature varying from -8° to +8°C at maximum and minimum conditions, respectively.

A solid-state on/off electronic controller is used to provide regulation of the foil heater attached to the reservoir. A thermistor is used as the temperature sensor.

Aluminum saddles are soldered to the evaporator and condenser section to provide attachment to the PCM box and to the radiator panels. The condenser saddles are segmented to minimize conduction losses and establish a sharp gas-vapor interface.

4.2.5 Radiator

The radiator is shown in Figure 4.10. It consists of 10 separate aluminum panels 0.040 inch (0.102 cm) thick and 12.9 inches (30.48 cm) wide. The length of

All Dimensions in Inches

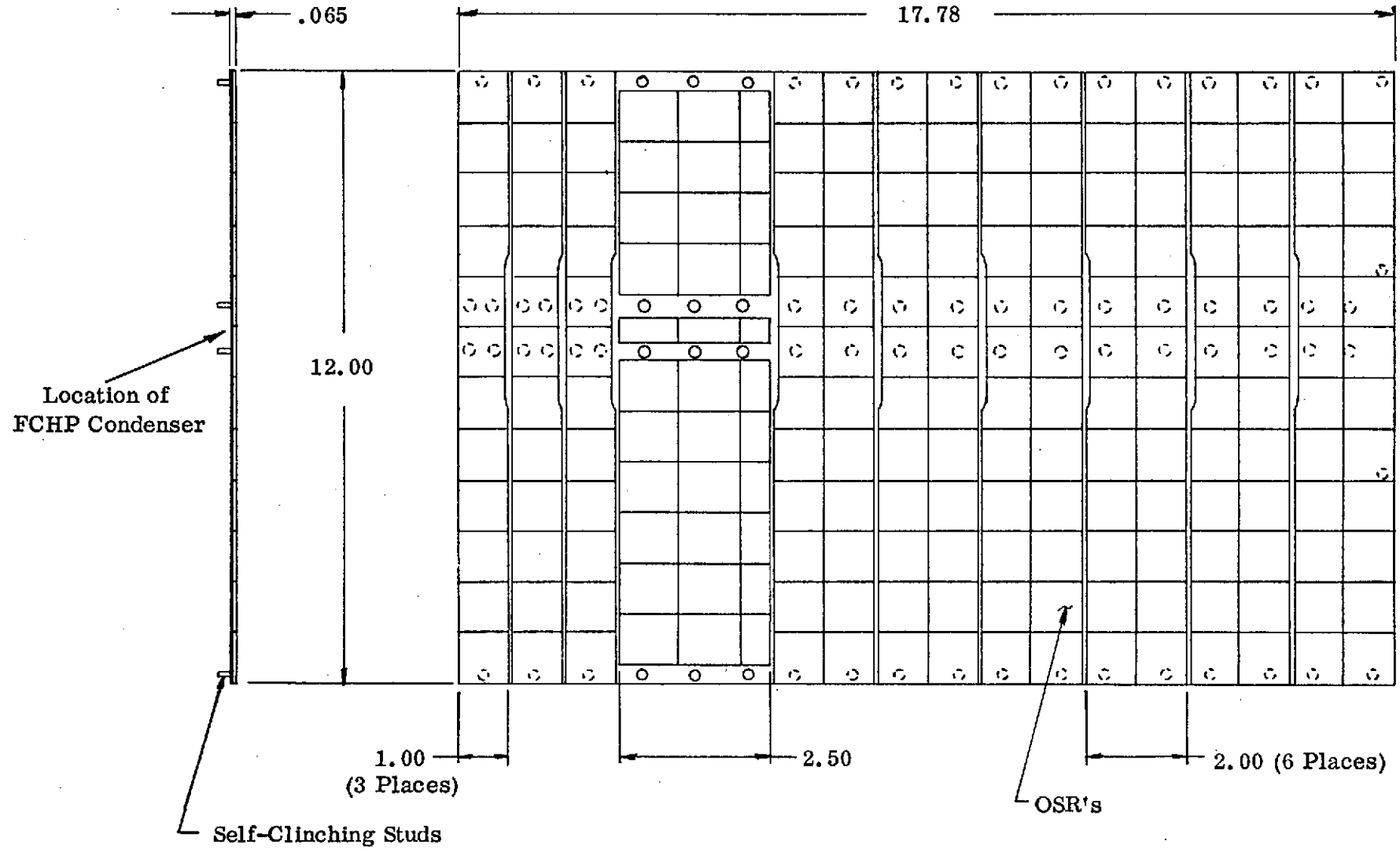

FIGURE 4.10

DESIGN OF RADIATOR PANEL

the panels near the transport section is 2.0 inches (5.08 cm) and 1.0 inch (2.54 cm) near the reservoir. The finer segmentation near the reservoir was chosen to establish a sharper gas-vapor interface and to reduce heat conduction into the reservoir during maximum condition. The size of the single 2.5-inch (6.35 cm) long panel was not selected because of thermal considerations but to ease assembly of the engineering model of the ATFE.

Since the radiator must reject its maximum energy during full sun, the panels are covered with OSR's whose specified optical properties are $\alpha/\varepsilon = 0.06/0.82$. However, an absorptivity of 0.10 has been used as a design value for all OSR surfaces to allow for spaces between the OSR's (i.e., packing factor), contamination, and potential infrared input from the spacecraft. Self-clinching studs are pressed into the panels to allow attachment to the FCHP condenser saddles and the ATFE support frame. Once installed, the radiator has a 17.75 x 12.0 inch (45.09 x 30.48 cm) platform.

4.2.6 Support Structure, Insulation, and Mechanical Integration

The support structure consists of an aluminum sheet metal housing riveted to a lexan frame. In addition to providing the main support for the PCM box, the housing also includes brackets and a baseplate for attaching the electronics module and filter box. The lexan frame supports the absorber and radiator panels and provides the mechanical interface with the spacecraft. Aside from being a lightweight material with good strength, lexan has low thermal conductivity that minimizes the thermal interaction between the ATFE and the spacecraft. Lightening holes were machined into the frame, which decreases its weight and thermal conductance by approximately 70%.

An insulation blanket is installed around the outside of the support structure to minimize the radiative coupling between the ATFE and the inside of the spacecraft.

The blanket consists of alternate layers of singly aluminized mylar and nylon mesh enclosed within singly aluminized kapton sheets. Similar insulation blankets are also installed within the ATFE to minimize component interactions.

Various aspects of the mechanical integration of the different components have been indicated in the preceding sections. Essentially all mechanical interfaces are bolted to permit maintainability of the individual components. A low outgassing conductive grease was applied at all heat pipe interfaces to reduce temperature drops through the system.

The condenser saddle of the diode is bolted to the PCM box which is, in turn, bolted to the FCHP evaporator saddle. Once instrumented and wrapped with insulation, this assembly is installed in the support structure and bolted to it at the flanges extending from the PCM box. Lexan washers are used at this interface to reduce conductive thermal losses from the PCM box. The individual radiator panels are then bolted to the FCHP and the lexan frame, as is the absorber panel. The main insulation blanket covers the support structure and is fastened to anchor nuts riveted to the structure. Finally, the electronics module and filter box are placed outside the insulation on the support-structure standoff to which they are bolted. The instrumentation harness plugs into the filter box via two connectors and establishes the electronic interface between the experiment and the electronics module.

The ATFE is fastened to the east wall of the ATS-F earth-viewing module (EVM) in several locations through a 0.50-inch (1.27 cm) wide lexan flange extending around the frame. Teflon inserts are provided within the spacecraft wall to minimize the conductance at the bolted joints. The lexan frame minimizes the conductive interaction with the spacecraft skin, and the main insulation blanket reduces the radiative coupling

between the ATFE and the inside of the spacecraft. The outside of the electronics module is black anodized so that it is radiatively coupled to the inside of the spacecraft in order to avoid the fluctuating thermal environment experienced by the ATFE absorber and radiator. The electronic interface is established by mating the experiment connector to the spacecraft connector. This contains all power, command, and telemetry functions.

4.2.7 Controls and Telemetry

A simplified block diagram of the command and telemetry functions of the ATFE is shown in Figure 4.11. Basically, it consists of the following components:

- Controller for the reservoir heater
- Auxiliary heater and back-up heaters
- Commands to execute various operating modes
- Telemetry and signal conditioning

The controller for the reservoir heater is an on/off regulator. It uses a signal from a thermistor attached to the diode side of the PCM box to control the heat input to the FCHP reservoir.

An auxiliary heater and back-up heater are employed in the ATFE. The auxiliary heater has an output of 20.1 watts at 28 VDC and is attached to the PCM box alongside the diode condenser saddle. It will be activated periodically if the diode fails to transport the absorbed solar energy. This heater will also be used in conjunction with the diode during the shadow period to activate the FCHP when it is normally in an off condition. The back-up heater has an output of 2.87 watts at 28 VDC and is attached to the FCHP reservoir. It is identical to the main reservoir heater that is regulated by the

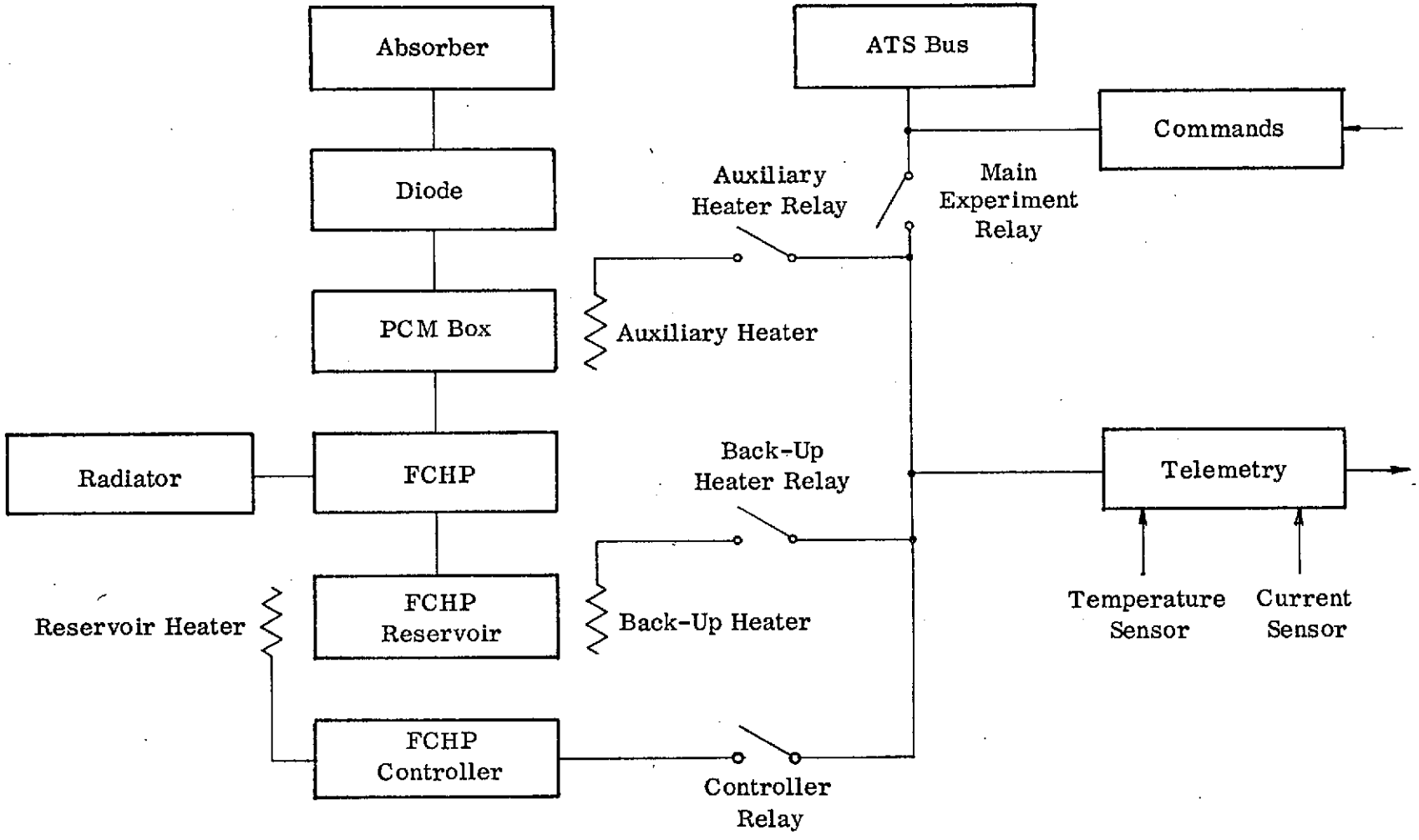

FIGURE 4.11

CONTROL AND TELEMETRY BLOCK DIAGRAM

controller. This heater will be used to provide manual control of the FCHP if the controller should fail.

The command circuitry provides for the execution of the eight discrete functions listed in Table 4.4. Each command is designed to accept inputs from either of two redundant spacecraft decoders. The Experiment ON/OFF command circuitry is totally redundant to prevent a single point failure resulting in loss of telemetry and therefore loss of the experiment. The Experiment ON/OFF circuitry also includes holding relays to permit independent operation of the ATFE which shares a 28-VDC load interface circuit (LIC) with the Quartz Crystal Microbalance Experiment. Loss of power from the LIC will cause a dropout to an Experiment OFF condition. Power can then be applied from the LIC only by exercising the Experiment ON command.

The Controller ON command activates the electronic controller for the FCHP reservoir. During normal mode of operation, the controller will be turned on to provide automatic feedback control. If the controller should fail in the ON condition it can be controlled manually by exercising Controller ON/OFF commands, as necessary, for regulation. Otherwise, the back-up heater can be controlled manually to simulate the controller function. Finally, ON/OFF control of the auxiliary heater will be used to provide auxiliary heat input to the PCM box in addition to, or instead of, the solar input provided by the thermal diode.

The locations of the temperature and reservoir heater current sensors are shown in Figure 4.12. There are a total of 20 temperature sensors; most of them are located in pairs and each pair is assigned one common telemetry channel. The current output from the electronic controller is monitored by a single sensor and is allocated a separate telemetry channel.

Command title	Command function
Experiment ON	Applies 28 vdc from the spacecraft to the experiment bus
Experiment OFF	
Controller ON	Applies 28 vdc from the experiment bus to the controller
Controller OFF	
Backup heater ON	Applies 28 vdc from the experiment bus to the backup heater
Backup heater OFF	
Auxiliary heater ON	Applies 28 vdc from the experiment bus to the auxiliary heater
Auxiliary heater OFF	

[a]Each of the OFF command functions removes the 28 vdc applied by the corresponding ON command.

TABLE 4.4

ATFE COMMAND ASSIGNMENTS

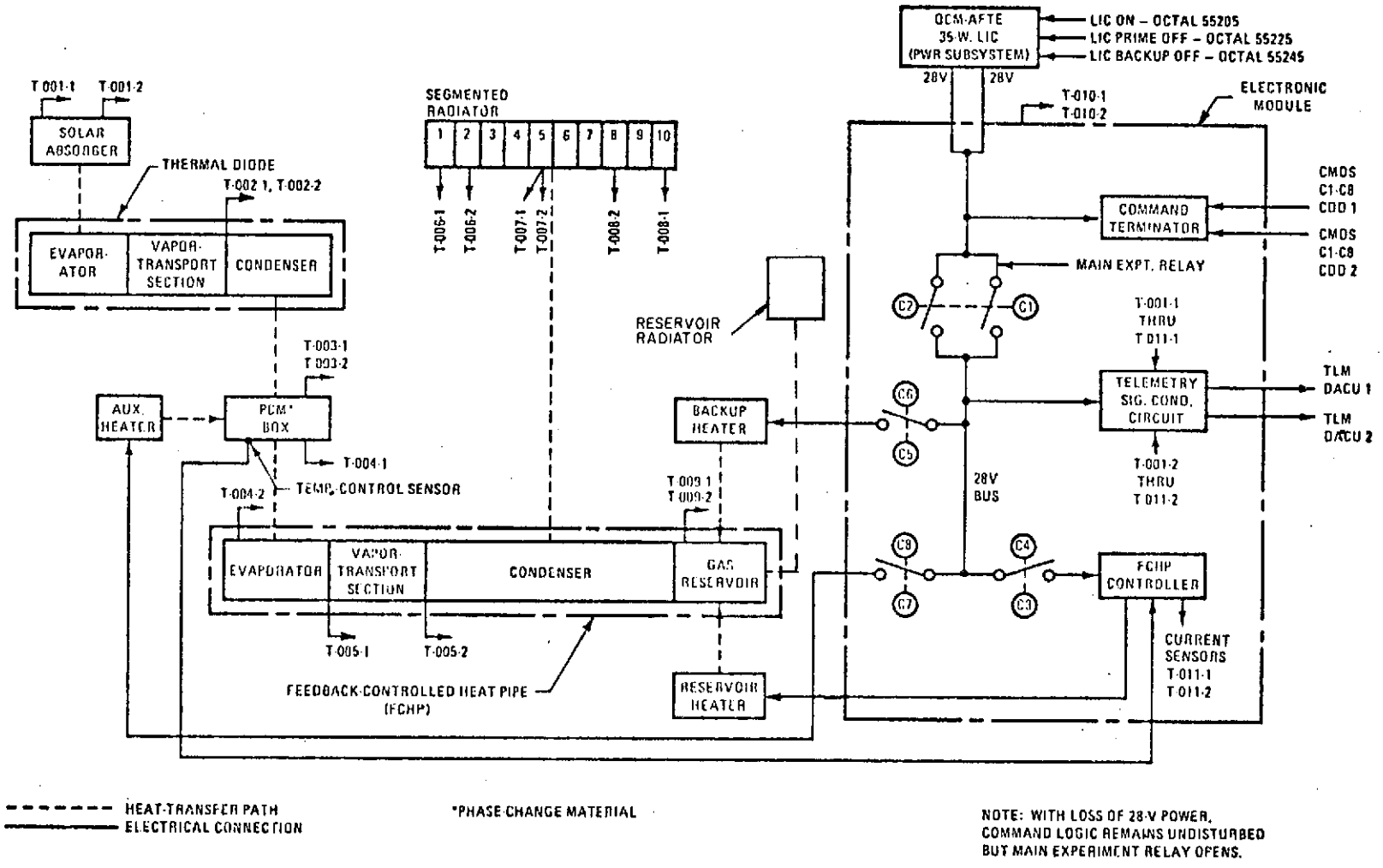

FIGURE 4.12

ATFE FUNCTIONAL AND RELIABILITY LOGIC DIAGRAM

Platinum transducers are used to measure the absorber and radiator temperatures which drop below that acceptable for thermistors. The remaining temperature data are sensed by single thermistors or thermistor composites. The transducer signal conditioning includes operational amplifiers, whereas the thermistor signal conditioning utilizes passive resistor divider networks.

The different telemetry channels are listed in Table 4.5. Each of the channels can be used with either one of two different spacecraft encoders. Thus, except for the current sensor, the system is totally redundant in terms of sensors, signal conditioning, and output. Only the output is redundant for the current sensor.

The ATS-F is an advanced communications satellite whose antenna transmits at exceptionally high intensities over a broad frequency range. The ATFE is subjected to external electromagnetic radiation as high as 50 volts/m with discrete frequencies in the range from 40 MHz to 6 GHz. Preliminary tests indicated that the absorber and radiator telemetry channels were susceptible to EMI radiated both external and internal to the spacecraft. This susceptibility was experienced primarily at lower frequencies and manifested itself in unacceptable output voltage excursions that were apparently due to amplification of the EMI by the operational amplifiers in the signal conditioning circuits.

An aluminum box containing ferrite was installed as shown in Figure 4.13 to filter EMI coming from the experiment harness. Three ferrite beads were also installed on each of the leads of the ATFE harness at the connector to filter EMI input from the spacecraft harness. The ATFE harness is wrapped with several layers of an electrically conductive cloth that is grounded to the connector and the electronic module to shield the ATFE harness from the internal EMI involvement of the space-

	Channel	Range, °C
1[a]	Absorber, near diode	-125 to +40
2	Absorber, near diode	
1	Diode adiabatic section	0 to +130
2	Diode adiabatic section	
1	PCM box, diode side	0 to +50
2	PCM box, diode side	
1	PCM box, FCHP side	0 to +50
2	FCHP saddle, upstream end	
1	FCHP, adiabatic section	-70 to +30
2	FCHP, adiabatic section	
1	Radiator, fin 1	-150 to +30
2	Radiator, fin 2	
1	Radiator, fin 5	-150 to +30
2	Radiator, fin 5	
1	Radiator, fin 10	-150 to +30
2	Radiator, fin 8	
1	FCHP gas reservoir	-75 to +30
2	FCHP gas reservoir	
1	Electronics module	-50 to +50
2	Electronics module	
1	Reservoir-heater current	0 to 200
2	(incl. fault-logic bias)	mA

[a]1 denotes spacecraft encoder #1, 2 denotes spacecraft encoder #2.

TABLE 4.5

ATFE TELEMETRY CHANNEL LIST

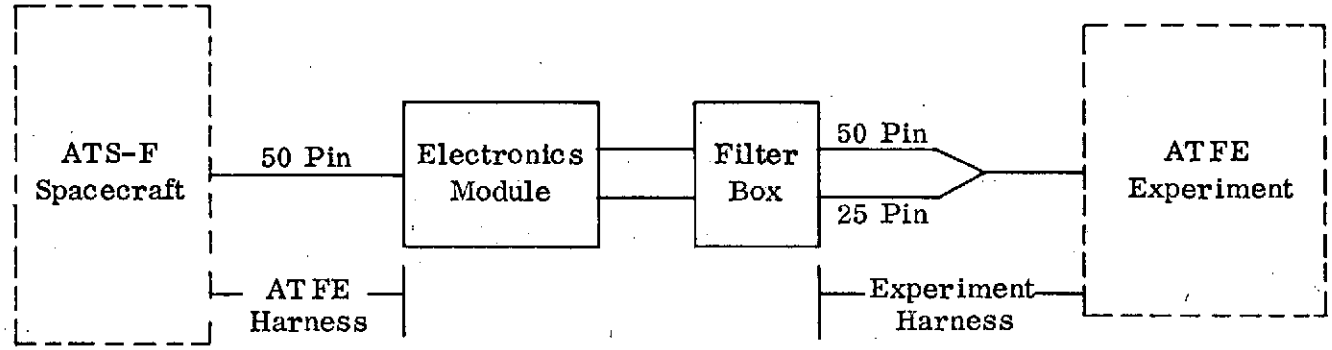

FIGURE 4.13

ELECTRICAL INTERFACE

craft. The experiment harness is similarly wrapped. The entire inboard side of the absorber and radiator was covered with three layers of the conductive cloth to reduce the EMI to the sensors. The cloth was grounded with conductive epoxy to the ATFE chassis. This combination of shielding and filters has reduced the susceptibility of the telemetry to EMI to within acceptable tolerances.

4.3 Failure Mode Analysis

A Failure Mode Effects and Criticality Analysis (FMECA) was conducted in accordance with the requirements of NASA-ARC document AHB 5326-1 dated May 1971. The results are summarized in Table 4.6. From this table it is seen that two failure modes have the highest criticality rating (4), because they result in complete loss of the experiment. These two failure modes are:

(1) Loss of Experiment ON Command

(2) Loss of Telemetry

Because of their criticality, total redundancy is provided in the experiment ON/OFF circuitry and the signal conditioning unit.

4.4 Qualification and Flight Acceptance Testing

The ATFE has been qualified and accepted for flight in accordance with the ATS-F Environmental Test Specifications for Components and Experiments (S-320-ATS-2). The tests performed are listed in Table 4.7 and are described in the following sections.

4.4.1 Functional and Environmental Tests

The test for EMI susceptibility was performed at National Scientific Laboratory (NSL) in Virginia. For this test, the ATFE was mounted in its flight configuration to a

TABLE 4.6: FAILURE MODE EFFECTS AND CRITICALLITY ANALYSIS CHART.

ITEM IDENTIFICATION						FAILURE EFFECT ON					
NAME	I. D. NO.	DWG. REF. DESIGNATION	RELIABILITY LOGIC DIAGRAM NO.	FUNCTION	FAILURE MODE & CAUSE	COMPONENT/ FUNCTIONAL ASSEMBLY	SUBSYSTEM	SYSTEM	FAILURE DETECTION METHOD	CORRECTIVE ACTION	COMPONENT CRITICALLITY CATEGORY
ABSORBER PANEL	1039	034-1039	1*	ABSORB SOLAR ENERGY.	DEGRADED ABSORPTIVITY.	NONE.	REDUCED ENERGY TO THERMAL DIODE.	NEGLIGIBLE.	NOT REQ'D.	NONE.	I
THERMAL DIODE	1005	034-1005		TWO OPERATIONAL MODES: ON-TRANSFER ABSORBED SOLAR ENERGY.	HEAT PIPE LEAK-LOSS OF WORKING FLUID.	LOSS OF OPERATIONAL MODE.	AUXILIARY HEATER PROVIDES REDUNDANCY.	LIMITED EXP. OBJECTIVES.	TELEMETRY T-001 AND T-002.	NONE.	2
				OFF-MINIMIZE HEAT LEAK TO ABSORBER PANEL.	SAME AS ABOVE	LOSS OF OPERATIONAL MODE.	NONE.	LIMITED EXP. OBJECTIVES.	T-001 AND T-002.	NONE.	2
PCM-ES	1035	034-1035		PROVIDE TEMPERATURE CONTROL DURING SHADOW.	LEAK IN THE EQUIPMENT SHELF-LOSS OF PCM.	LOSS OF TEMPERATURE CONTROL DURING SHADOW PERIOD.	NONE.	LIMITED EXP. OBJECTIVES.	T-003 AND T-004.	NONE.	2
FCHP	1084	034-1084		PROVIDE TEMPERATURE CONTROL OF PCM-ES THROUGHOUT ORBITAL CYCLE.	TWO POTENTIAL FAILURE MODES						
					1. LOSS OF WORKING FLUID DUE TO LEAK.	LOSS OF FUNCTION.	LOSS OF TEMPERATURE CONTROL OF PCM-ES DURING SOLAR INPUT.	MAJOR LOSS OF EXPERIMENT OBJECTIVES.	TELEMETRY T-004 AND T-005.	NONE.	3
					2. CONTROLLER FAILS-ELECTRONICS FAIL.	BACK-UP HEATER PROVIDES PARTIAL REDUNDANCY.	LOSS OFF TEMPERATURE CONTROL FOR 90% OF MISSION.	REDUCED EXPERIMENT OBJECTIVES.	TELEMETRY T-009, T-005, T-011.	COMMAND CONTROLLER OFF-GROUND CONTROL OF BACK-UP HEATER.	2
ELECTRONIC MODULE	1090	034-1090		A. COMMANDS							
				A.1 EXP. ON.	ELECTRONIC FAILURE.	LOSS OF POWER AND TELEMETRY.	LOSS OF TEMPERATURE CONTROL.	LOSS OF EXP. OBJECTIVES.	LOSS OF TELEMETRY.	REDUNDANT RELAY.	4
				A.2 EXP. OFF.	ELECTRONIC FAILURE.	NONE.	NONE.	NONE.	TELEMETRY WILL BE ON.	TURN S/C LIC. POWER. OFF.	I
				A.3 CONTROLLER ON.	ELECTRONIC FAILURE.	SAME AS 1084-2 ABOVE.	SAME AS 1084-2 ABOVE	SAME AS 1084-2 ABOVE	T-011.	SAME AS 1084-2 ABOVE.	2
				A.4 CONTROLLER OFF.	ELECTRONIC FAILURE.	NONE	NONE	SMALL REDUCTION IN EXP. OBJECTIVES.	T-011.	NONE.	I
				A.5 BACK-UP HEATER ON.	ELECTRONIC FAILURE.	FCHP WITHOUT REDUNDANT HEATER.	LOSS OF REDUNDANCY OF TEMPERATURE CONTROL.	USED ONLY IN EVENT OF CONTROLLER FAILURE, FMECA NOT APPLICABLE.	T-009.	NONE.	NA
				A.6 BACK-UP HEATER OFF.	ELECTRONIC FAILURE.	NONE.	FCHP CAN NO LONGER OPERATE IN NORMAL MODE.	REDUCED EXP. ERIMENT OBJECTIVES.	T-009.	NONE.	2
				A.7 AUXILIARY HEATER ON.	ELECTRONIC FAILURE.	NONE.	REDUCED EXERCISE OF FCHP.	SLIGHTLY REDUCTION IN EXP. OBJECTIVE.	T-003 AND T-004.	NONE.	I
				A.8 AUXILIARY HEATER OFF.	ELECTRONIC FAILURE.	NONE	LOSS OF TEMP. CONTROL DURING PART OF ORBIT. NO FREEZING OF PCM.	REDUCTION IN EXP. OBJECTIVE.	T-003 AND T-004.	NONE.	2
				B. TELEMETRY.							
				B.1. INDIVIDUAL SENSOR.	MECH. DAMAGE OR LOSS OF CALIBRATION.	LOSS OF FUNCTION.	REDUCED DATA FROM AFFECTED SUBSYSTEM.	MINOR REDUCTION IN EXP. OBJECTIVE.	TELEMETRY.	USE DATA FROM SECOND ENCODER.	I
				B.2 SIGNAL CONDITIONING UNIT.	ELECTRONIC FAILURE.	LOSS OF TELEMETRY.	NA	LOSS OF EXP. OBJECTIVE.	LOSS OF TELEMETRY.	TOTALLY REDUNDANT.	4
				C. CONTROLLER	ELECTRONIC FAILURE.	SAME AS 1084-2 ABOVE.	SAME AS 1084-2 ABOVE.	SAME AS 1084-2 ABOVE.	T-011	SAME AS 1084-2 ABOVE.	2

* SEE FIGURE 4.12 FOR IDENTIFICATION OF ITEMS.

TEST	ENVIRONMENT	
	QUALIFICATION	ACCEPTANCE
Electromagnetic Interference	Simulated RF	Simulated RF
First Functional Test	Ambient	Ambient
Second Functional Test	Ambient	Ambient
Thermal Vacuum (Phase I)		
Hot Soak	$51 \pm 2^{o}C$	$51 \pm 2^{o}C$
Controller Calibration	Nominal Orbit	Nominal Orbit
Baseline Orbital Cycle	Nominal Orbit	Nominal Orbit
Cold Soak	$-10 \pm 1^{o}C$	$-10 \pm 1^{o}C$
First Leak Test	Vacuum	Vacuum
Vibration	Sine & Random	Sine & Random
Second Leak Test	Vacuum	Vacuum
Third Functional Test	Ambient	Ambient
Storage Temperature Test	60^{o} to $-30^{o}C$	---
Fourth Functional Test	Ambient	---
Instrumentation Calibration	-90^{o} to $+50^{o}C$	-90^{o} to $+50^{o}C$
Thermal Vacuum (Phase II)		
Automatic Feedback Control	Max., Nominal, Min. Orbit	Max., Nominal, Min. Orbit
Manual Feedback Control	Nominal Orbit	Nominal Orbit
Passive Gas Control	Nominal Orbit	Nominal Orbit
Automatic Feedback with Auxiliary Heater	Nominal Orbit	Nominal Orbit
Third Leak Test	Vacuum	Vacuum
Weight and CG Determinations	Ambient	Ambient

TABLE 4.7

QUALIFICATION AND ACCEPTANCE TESTS

simulated east wall and irradiated with RF energy at Qualification level frequencies and intensities associated with both the exterior and interior of the spacecraft.

The first functional test was performed at Dynatherm prior to shipment of the experiment to NASA-ARC. All subsequent testing was done at ARC. The functional tests were performed in the ambient and verified only the correct operation of the ATFE rather than providing quantitative performance data. The tests consisted of checking all command and telemetry channels, verifying the operation of all heaters, and establishing an interface between vapor and gas in the FCHP. The latter test served as a qualitative verification that the FCHP was charged with the correct amount of noncondensing gas. The melting of the PCM was also verified.

Leak testing was performed before and after environmental testing and before and after the thermal vacuum performance test. The entire ATFE was placed in a vacuum chamber; and a mass spectrometer and a helium leak detector were used to detect ammonia working fluid from the diode, methanol from the FCHP, octadecane PCM, and helium control gas from the FCHP.

The ATFE was subjected to both sine and random vibrations in all three spacecraft axis on a Ling Model A 300 B Vibration System. The maximum level during sinusoidal vibration was 12 "g" in the 22 to 200 Hz range (qualification and acceptance) and 17 "g-rms" and 11.3 "g-rms" during random qualification and acceptance vibration, respectively. Storage temperature tests and instrumentation calibration were performed in an isothermal temperature-altitude chamber backfilled with dry nitrogen gas at near ambient pressure. Hot and cold soak tests were performed in a thermal vacuum chamber with liquid-nitrogen cooled walls. After exposure to each of the environments described above, either the functional test or the thermal vacuum test performance with

simulated orbital conditions was performed. Except for a slight shift in the controller set point on the flight unit, no degradation of the ATFE from environmental exposure was detected.

4.4.2 Thermal Performance Tests

The performance of the ATFE under simulated orbital conditions for various operational modes was of major interest and, therefore, comprised a significant portion of the test program. The ATFE was mounted in a panel representing the east wall of the spacecraft. This panel formed one side of a box that radiatively simulated the internal cavity of the spacecraft. The temperature of this box was then controlled to the desired spacecraft temperature. Foil heaters bonded to the inboard sides of the absorber and radiator were used to simulate absorbed solar energy. Voltage to the heaters was automatically stepped at 20-minute intervals to the correct level corresponding to the solar energy cycle. Throughout the entire orbit, the absorber and radiator viewed the cold chamber walls. In addition to the flight instrumentation, 63 thermocouples were attached to various locations within the ATFE and the test setup to provide additional temperature data during qualification tests. Fifty thermocouples were used during the acceptance tests. All data was automatically logged at regular intervals with a commercial data-logging system.

The engineering model, the qualification model, and the flight unit were subjected to several simulated solar cycles under various environmental conditions and operational modes. The test conditions for the qualification and flight model are listed in Table 4.8. The engineering model was tested in a similar way; but, since several modifications were made to the subsequent models, the engineering model tests are not representative for the final configuration of the experiment.

	SOLAR CYCLE	SOLAR INTENSITY	SPACECRAFT TEMP. ^{o}C	OPERATIONAL MODE
Qualification Unit	1	Nominal +5%	35	Automatic Feedback Control
	2	Nominal -5%, -8%	35	Automatic Feedback Control
	3	Nominal -5%, -8%	5	Automatic Feedback Control
	4	Nominal +5%	5	Automatic Feedback Control
	5	Nominal -5%	20	Automatic Feedback Control
	6	Nominal -5%	20	Passive Temperature Control
	7	Nominal -5%	20	Passive + Auxiliary Heater
	8	Nominal -5%	20	Automatic Feedback + Auxiliary
	9	Nominal -5%	20	Automatic Feedback + Auxiliary Heater + Backup Heater
	10	Nominal -5%	40	Automatic Feedback + Auxiliary Heater
	11	Nominal -5%	40	Passive Temperature Control
Flight Unit	1	Nominal +5%	35	Automatic Feedback Control
	2 to 6	Nominal +5%	20	Partial Cycles
	7	Nominal +5%	35	Automatic Feedback Control
	8	Nominal -5%, -8%	5	Automatic Feedback Control
	9	Nominal -5%	20	Automatic Feedback Control
	10	Nominal -5%	20	Passive Temperature Control
	11	Nominal -5%	20	Automatic Feedback Control + Intermediate Auxiliary Heater

TABLE 4.8

SOLAR CYCLE QUALIFICATION AND ACCEPTANCE TESTS

The cycles with automatic feedback control (1-5 for qualification unit and 1-9 for flight unit) served to establish the expected performance over the probable range of solar inputs and spacecraft temperatures. Nominal solar input $\pm 5\%$ corresponds to the uncertainty of solar absorption. The additional -8% used in cycles 2 and 3 (qualification) and 8 (flight) accounts for seasonal variations due to change in the angle of incidence.

During the cycles with passive temperature control (6 and 11 for qualification unit and 10 for flight unit), the reservoir heater was turned off and the FCHP operated as a conventional variable conductance heat pipe. The effect of additional heat input into the PCM box was studied in cycles 7 through 10 (qualification) and 11 (flight). In these cycles, the auxiliary heater attached to the PCM box was activated (either continuously or intermittently) to augment the heat input by the thermal diode and to evaluate the ability of the FCHP to regulate during the shadow period. Cycles 2 through 6 of the flight unit were experimental cycles during which minor adjustments of the insulation and thermal coupling were made.

Performance of the ATFE qualification and flight units is discussed in the following section. For the purpose of easy identification of the symbols used in the following graphs, a simplified instrumentation block diagram is shown in Figure 4.14.

4.4.2.1 Solar Cycles with Automatic Feedback Control

The transient performance with automatic feedback control is shown for two typical cycles in Figures 4.15 and 4.16 (cycle 1 of qualification unit and cycle 9 of flight unit). The general trend of the temperature transients is the same in both cases. As the ATFE moves from the end of the shadow period into sunlight, the absorber quickly rises to a maximum of 32 to 35°C near maximum solar input. It then decreases in

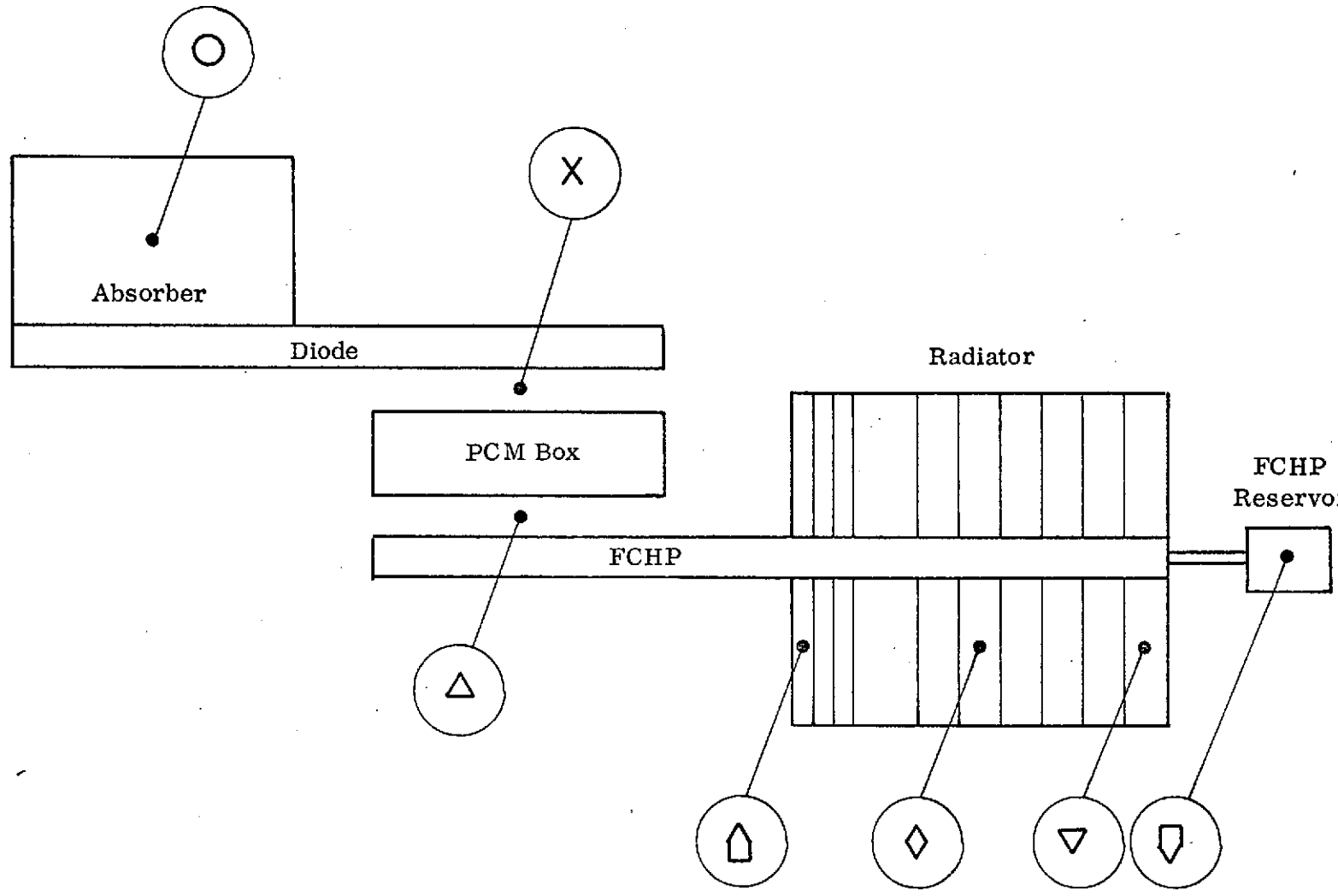

FIGURE 4.14

SENSOR LOCATIONS AND SYMBOLS FOR ORBITAL CYCLES

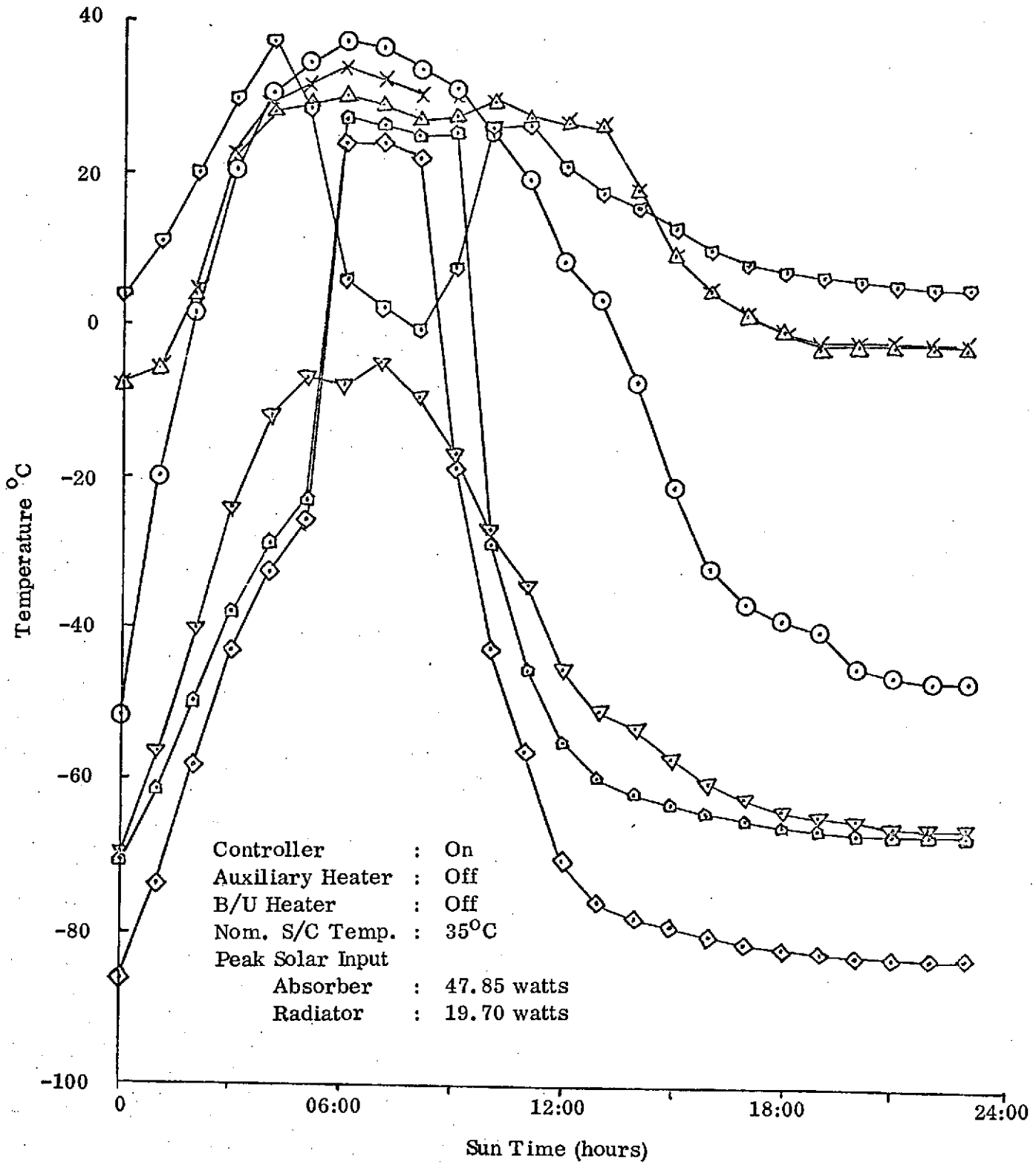

FIGURE 4.15

ATFE BACKUP UNIT RETEST (ORBIT CYCLE NO. 1)

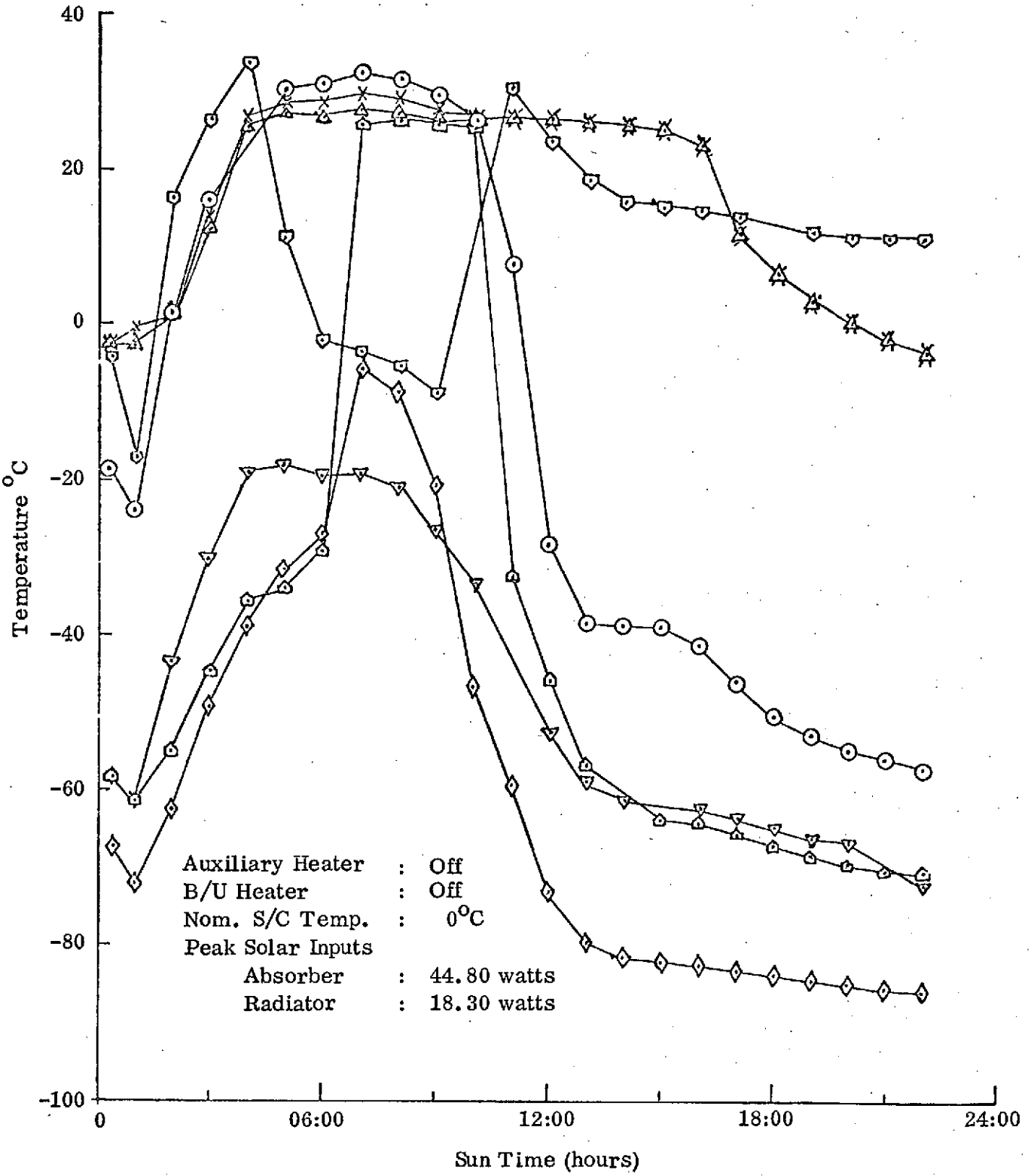

FIGURE 4.16

ATFE FLIGHT UNIT RETEST (ORBIT CYCLE NO. 9)

temperature as the sun "goes down" until the diode completes its reversal. In the flight unit, the absorber temperature decreases at the same rate as the solar input until it reaches a plateau at -39°C where it remains until the PCM has all frozen and the PCM box drops in temperature. The absorber temperature is held at this plateau by heat leaks from the constant temperature PCM box and spacecraft. In the qualification unit, the absorber temperature decreases very slowly and does not reach -40°C until 18:00 hours sun time. This latter behavior is indicative of incomplete diode shutdown and is coupled with a shorter period of energy storage in the PCM box. Various degrees of diode shutdown have been observed with both models. Partial shutdown manifests itself by higher temperature plateaus and sometimes even by a warming trend of the absorber after the sun has set. This latter phenomenon is shown in Figure 4.17 (cycle 7 of flight unit). Note that the absorber temperature begins to again rise at 14:00 hours sun time. It is not clear what caused the sudden increase in diode conductance at that time. It appears that the extreme sensitivity (to temperature profiles along the pipe) of the fluid inventory remaining in the noncommunicating diode reservoir may be a major factor.

The PCM box also increases rapidly in temperature as the diode begins transferring energy to it early in the solar cycle. It then becomes stabilized near 28°C (octadecane melting point) with a sufficient temperature gradient (approximately 2°C) from the diode to FCHP side to assure that all the PCM is melted. It should be recognized that the temperature stability of the system can be no better than the temperature gradients required in the PCM box to assure melting and freezing of the PCM. For the ATFE, this minimum range is approximately 26° to 30°C.

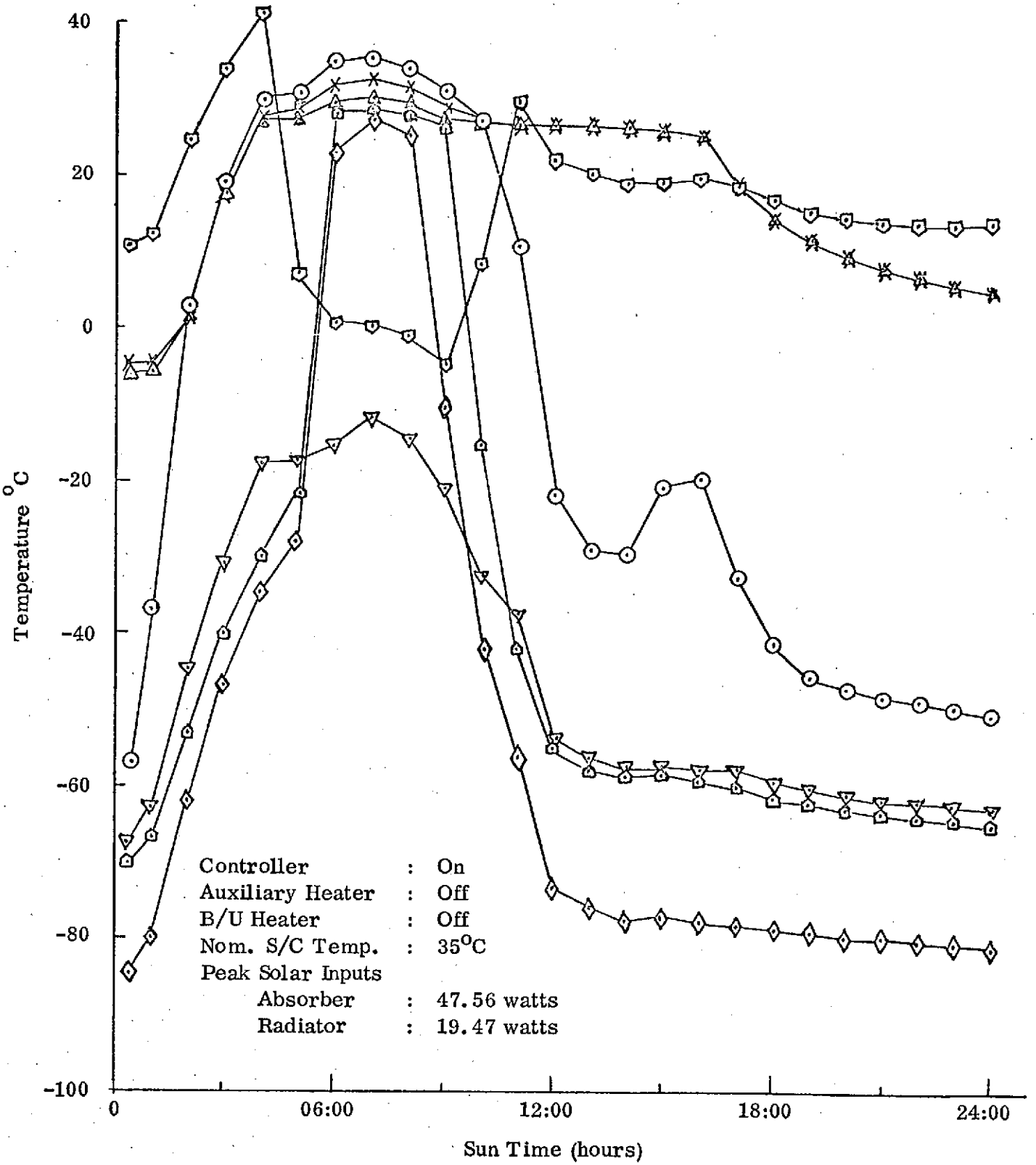

FIGURE 4.17

ATFE FLIGHT UNIT RETEST (ORBIT CYCLE NO. 7)

As the absorber temperature drops below that of the PCM box, the freezing PCM provides energy to reverse the diode and to compensate for parasitic heat leaks. Because of the relatively small parasitic heat loss from both sides of the PCM box (<5 watts total), the temperature gradient across the PCM box disappears at that time.

The influx of solar energy to the FCHP reservoir radiator, during the initial portions of the cycle, supplements the heater power within the reservoir and results in a rapid increase in temperature. When the diode side of the PCM box (controller sensor location) reaches the control set point (28°C), the reservoir heater turns off and the reservoir temperature begins to decrease. The transient response of the reservoir during this period is perhaps the single most important factor in the FCHP's transient performance. If the reservoir temperature drops slowly and to an insufficiently low level, the control gas is not allowed to recede into the reservoir quickly enough to allow the FCHP condenser to open up enough to reject the required heat load. A temperature overshoot then occurs at the heat source (PCM box). For example, the ATFE design is such that each 3°C increase in reservoir temperature near peak solar input results in approximately a 1°C overshoot on the diode side of the PCM box. A major difficulty with the ATFE was thermally decoupling the FCHP reservoir from the absorber which, by necessity, surrounded it on three sides.

Before leaving the shadowed period, the entire radiator is inactive and at -60°C to -90°C. Note that radiator fin #10, which is closest to the reservoir, is slightly warmer than the other fins. This is the result of a small conduction heat leak from the reservoir to the heat pipe condenser. As the experiment moves into the sunlight, the radiator temperature rises to approximately -25°C which is consistent with the directly absorbed

solar energy. When the control set point is reached and the reservoir temperature drops, the radiator quickly becomes active. The effect of only 10% difference in solar radiation can be seen by comparing Figures 4.15, 4.16, and 4.17. In the solar cycles of 4.15 and 4.17 the solar input was 5% higher than nominal, and in 4.16 it was 5% lower than nominal. In the first two cases, the radiator opens at least up to the fifth fin (but not including the tenth). With 10% lower input the fifth fin never fully opens.

As the solar cycle progresses toward the shadow, the controller is seen to turn the reservoir heater back on with a resulting increase in FCHP reservoir temperature. This temperature, however, begins to decrease to a quasi steady-state level during the shadow. If the reservoir temperature drops too low while the vapor temperature remains stabilized by the PCM, the FCHP condenser shows a tendency to partially open and allow the remaining energy in the PCM material to be rejected. The temperature control of the FCHP reservoir, therefore, is a careful compromise to achieve as low a temperature as possible during peak solar conditions while maintaining a sufficiently high temperature during shadow. For the ATFE, this resulted in an important trade-off between heater power, heat rejection capability, thermal capacitance, and thermal coupling to other portions of the experiment.

In the flight unit, the temperature of the PCM box remains stable for six hours after the solar input from the absorber stops (from 10:00 to 16:00 hours sun time). In the qualification unit, where the diode does not completely reverse, the stabilized time is only four hours (from 09:00 to 13:00 hours sun time). The difference is, of course, due to heat leakage from the PCM through the diode to the absorber.

Perhaps the interaction of the various components as a system is better visualized in Figure 4.18. During peak solar input, the absorber and diode are nearly iso-

FIG.4-18 TYPICAL TEMPERATURE PROFILES WITH FEEDBACK CONTROL

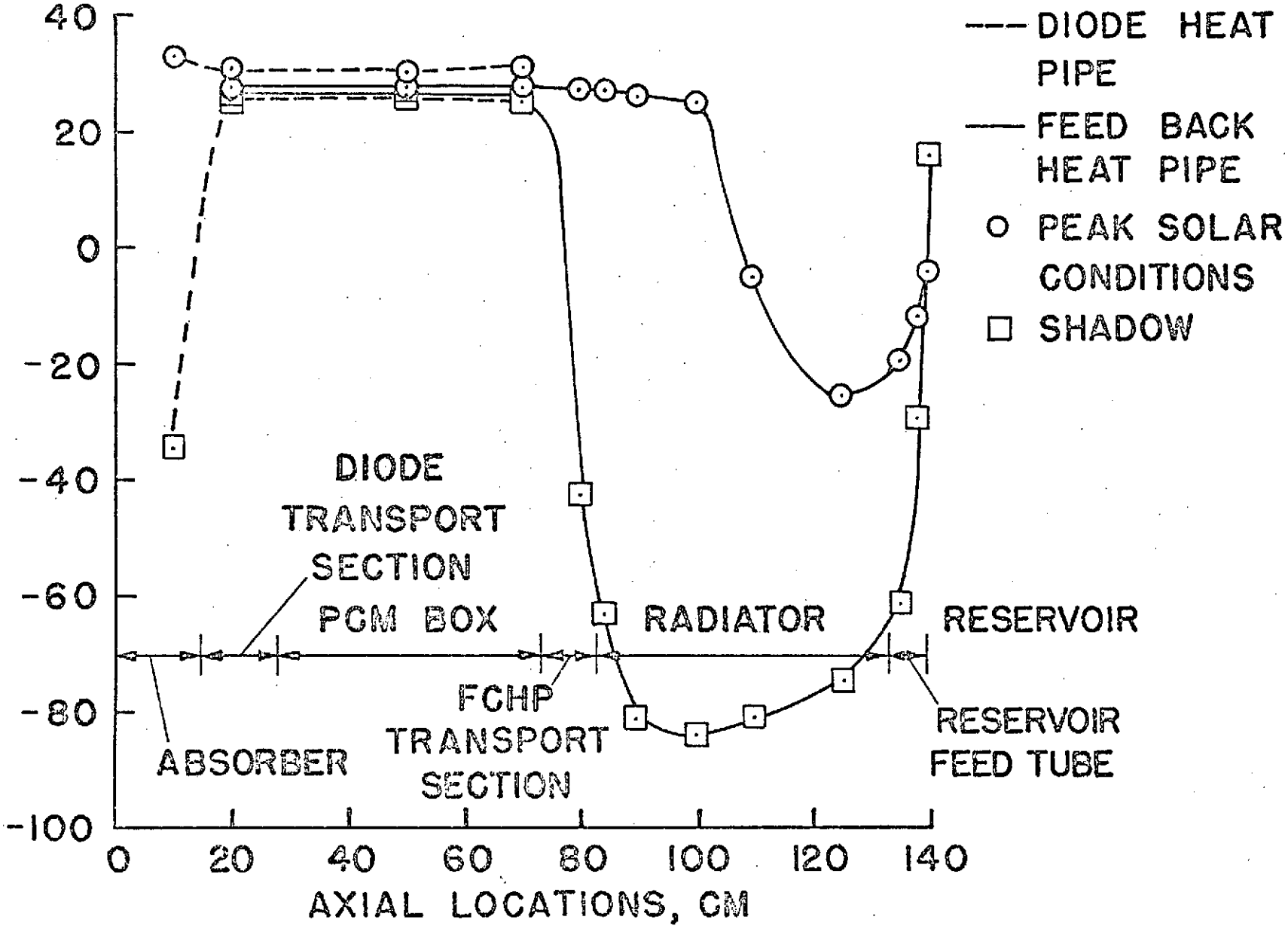

thermal. A temperature drop of a few degrees exists through the PCM box to the feedback pipe, whose profile is nearly linear until the gas-blocked region of the condenser is reached. The reservoir heater is off, allowing the reservoir to approach equilibrium with the external environment and the remainder of the ATFE. On the other hand, during the shadow period, the PCM holds the PCM box at its freezing point while the diode allows the absorber to drop to its low temperature. The feedback reservoir heater is on, thereby raising the reservoir temperature and forcing additional amounts of gas into the condenser which it blocks completely. The large temperature drops from the PCM box to the absorber (62^{o}C) and the the radiator (110^{o}C) demonstrate the effectiveness of these new thermal control tools.

The FCHP's ability to maintain temperature stability is indicated by the variation in temperature of the diode side of the PCM box during peak solar conditions. The peak temperatures for the feedback control orbital cycles are listed in Table 4.9.

The high peak temperatures of the qualification unit and cycles 1 and 7 of the flight unit are overshoots and result from the inability of the FCHP reservoir to cool to a sufficiently low temperature during peak solar input. As shown in Table 4.9, the minimum temperatures which the reservoir attained were generally higher for the qualification unit; hence the larger overshoot.

4.4.2.2 Passive Gas Control

The temperature transients of two cycles without feedback control are shown in Figures 4.19 and 4.20. Only a small portion of the PCM material was melted. Significant melting did not occur since the unheated, cold reservoir allowed the FCHP condenser to reject energy from the solar absorber at a level below the PCM melting temperature; whereas, in the feedback mode, the controller does not allow heat rejection until the PCM

UNIT	CYCLE NO.	PEAK PCM BOX TEMPERATURE °C	MIN. FCHP RESERVOIR TEMPERATURE °C
Qualification	1	34.0	0
Qualification	2	33.0	+5
Qualification	3	32.5	+10
Qualification	4	36.0	+12
Qualification	5	36.0	+6
Flight	1	33.0	-2
Flight	7	33.0	-4
Flight	8	28.0	-3
Flight	9	30.0	-9

TABLE 4.9

PEAK PCM BOX TEMPERATURES
DURING FEEDBACK CONTROL CYCLES

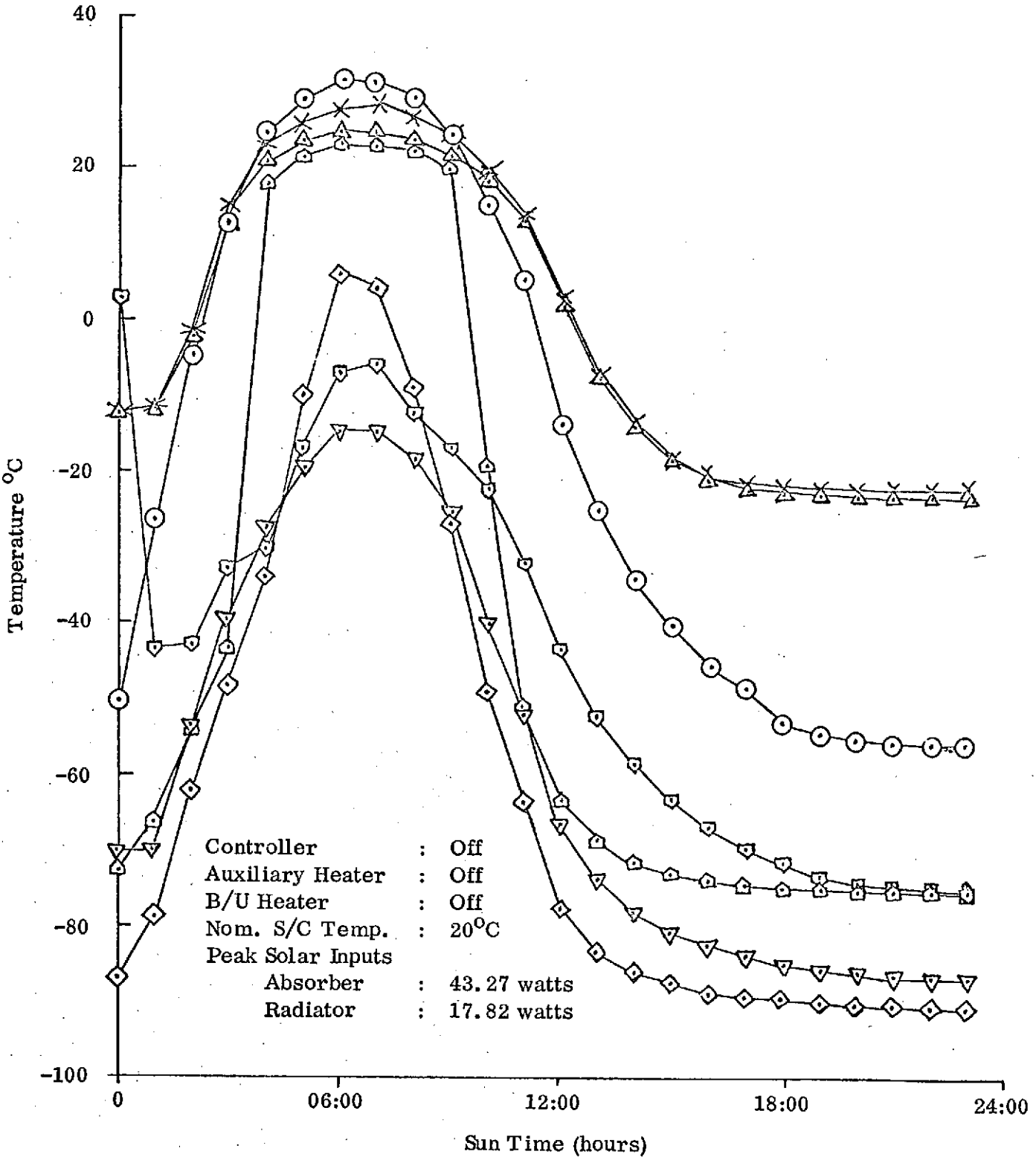

FIGURE 4.19

ATFE BACKUP UNIT RETEST (ORBIT CYCLE NO. 6)

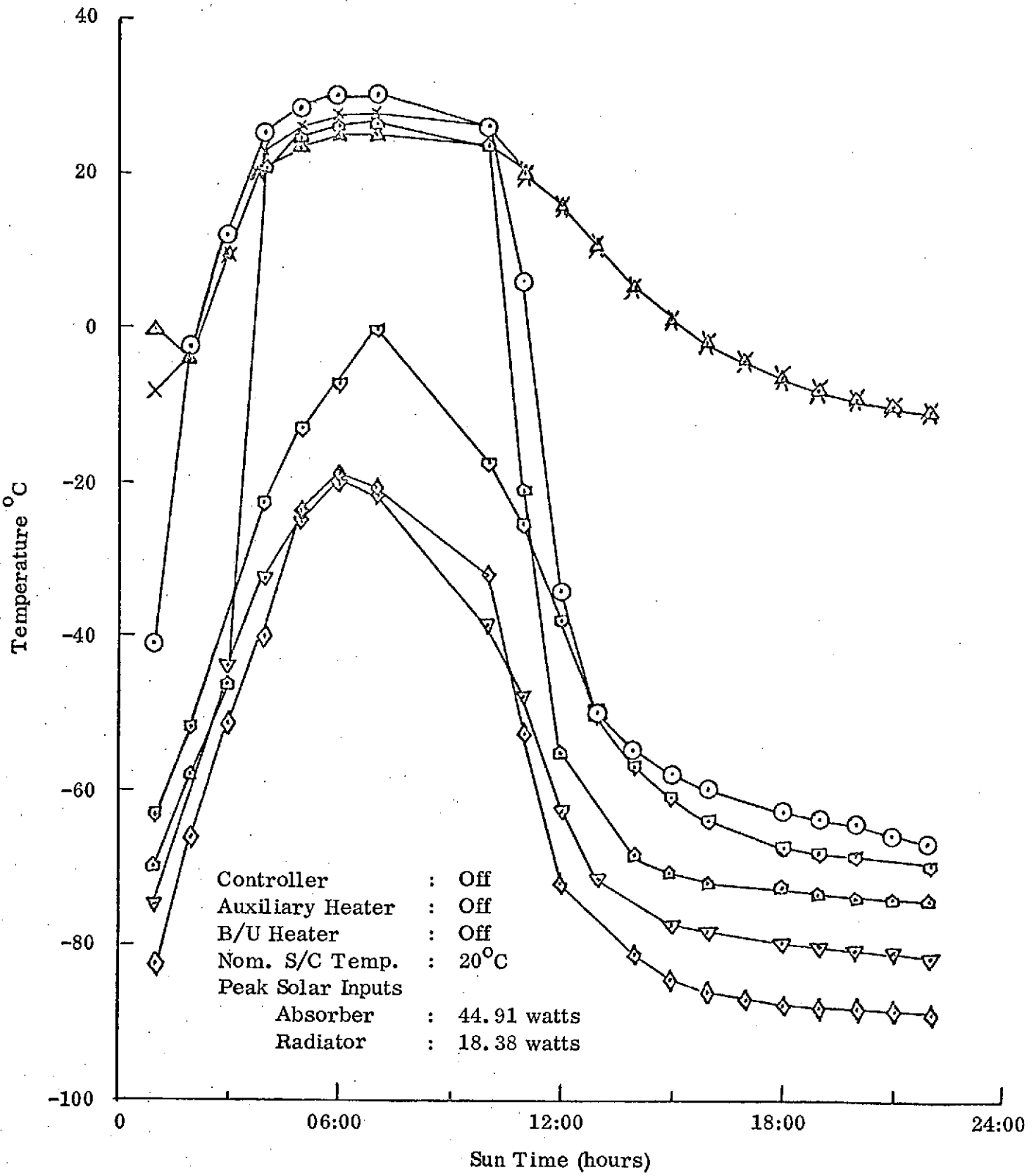

FIGURE 4.20

ATFE FLIGHT UNIT RETEST (ORBIT CYCLE NO. 10)

was melted. This can be clearly seen by comparing Figures 4.16 and 4.20. In the feedback control mode, the radiator (fin 1) does not "open" until 06:00 hours sun time. In the passive mode, it opens at 03:00 hours when the PCM box temperature is only $23^{\circ}C$.

4.4.2.3 Feedback Control with Auxiliary Heater

To exercise the FCHP beyond the capacity provided by the natural orbital environment, a 20-watt auxiliary heater was used (Figure 4.21). At about 04:00 hours sun time, the combined inputs from the absorber and auxiliary heater exceed the heat rejection capability of the radiator and the PCM box temperature rises above the control print. During the shadow period, the PCM box is stabilized at $28^{\circ}C$.

In the cycle shown in Figure 4.22, the auxiliary heater was turned off between the hours of 04:00 and 08:00 sun time in order to avoid the overdriving of the radiator. Except for a small overshoot at 04:00 hours (when the auxiliary heater was turned off), the FCHP stabilized the diode side of the box at approximately $28^{\circ} \pm 0.5^{\circ}C$.

4.5 Specifications and Documentation

The Flight and Qualification Units of the ATFE conform with the following NASA generated specifications:

S-320-ATS-2	Environmental Test Specification for Components and Experiments, ATS-F and ATS-G
S-460-ATS-64	ATFE Interface Specification

The design of Flight and Qualification Units is documented in Dynatherm drawings which are listed in Table 4.10. A list of Dynatherm generated specifications and procedures is provided in Table 4.11.

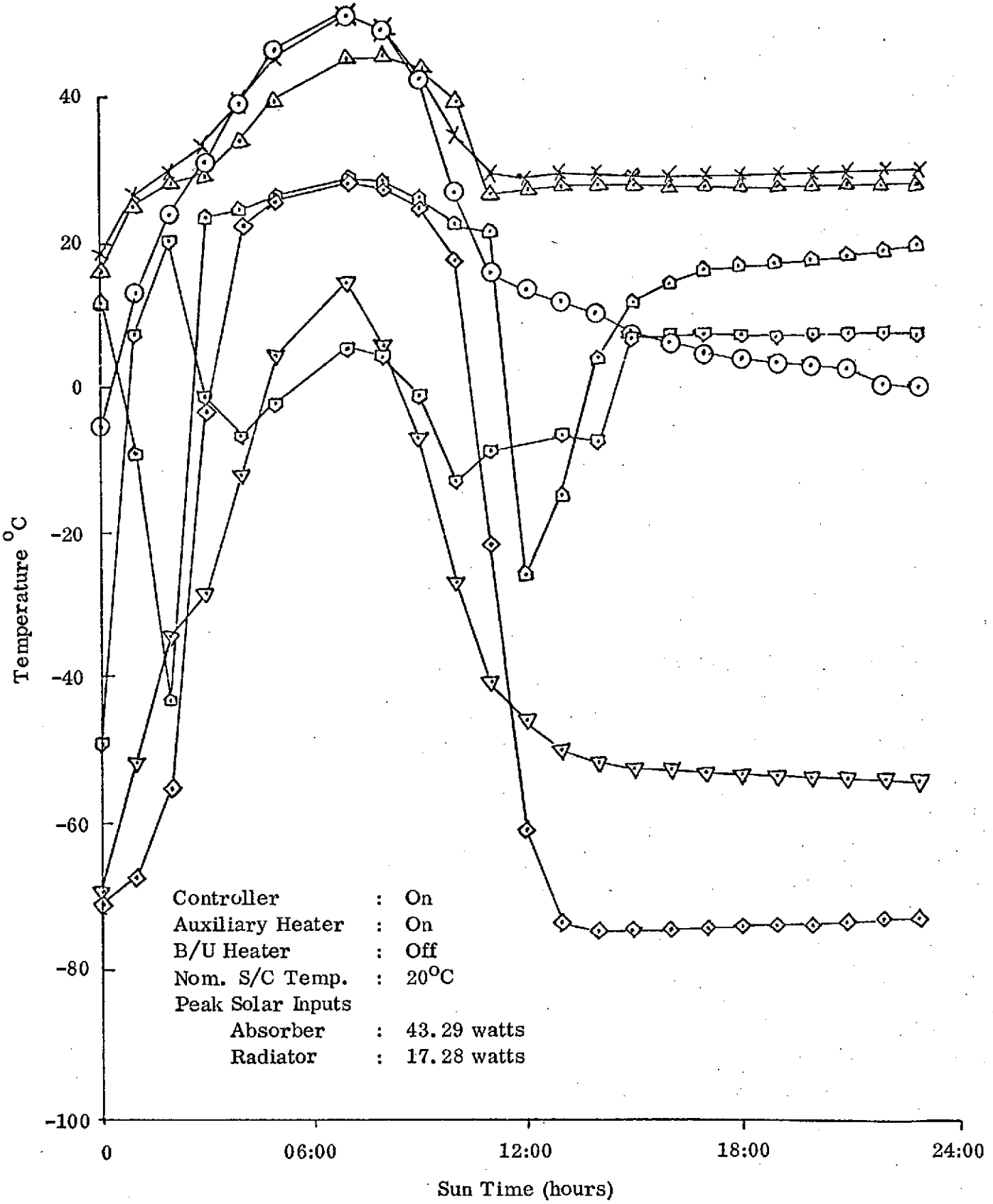

FIGURE 4.21

ATFE BACKUP UNIT RETEST (ORBIT CYCLE NO. 8)

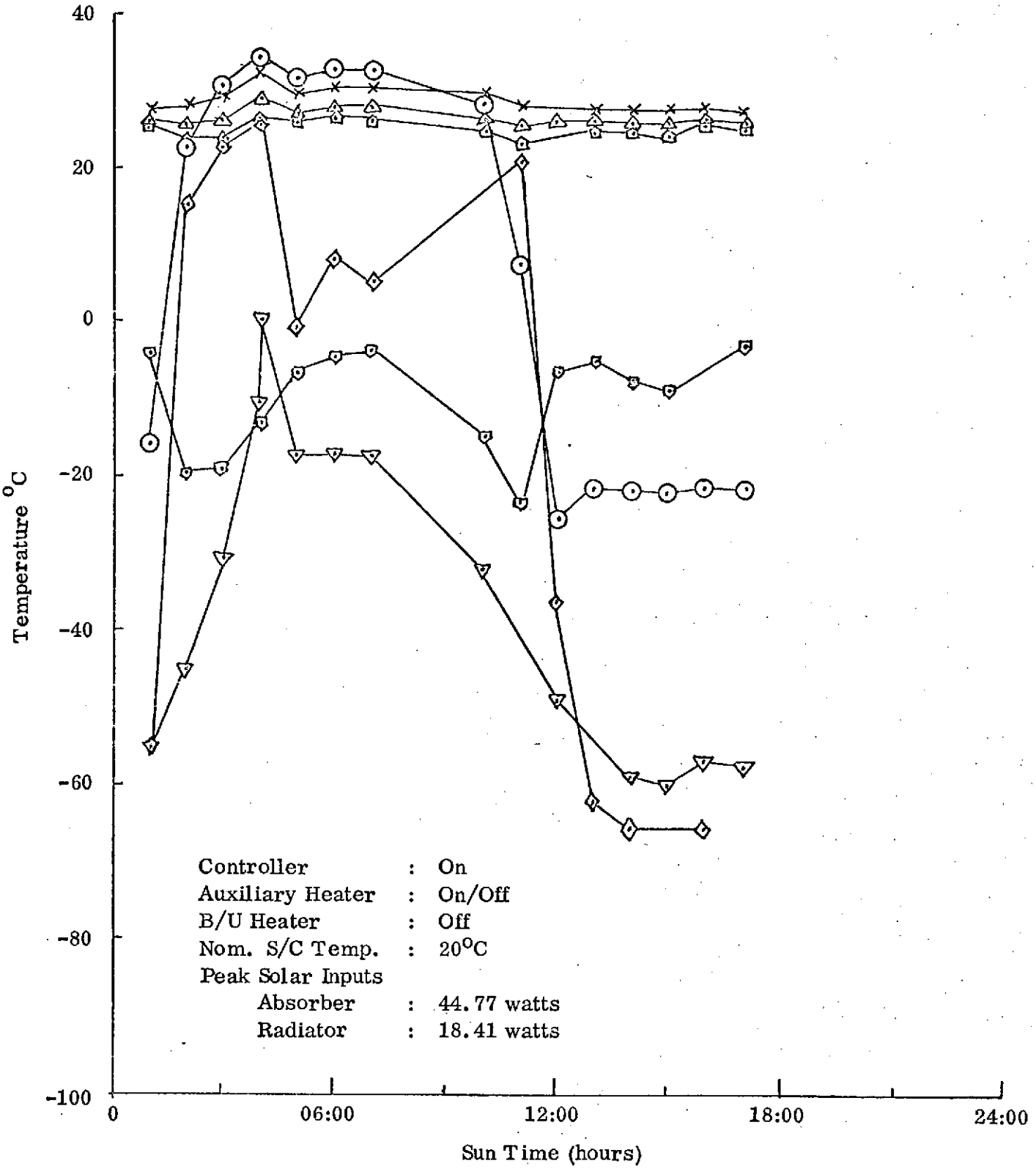

FIGURE 4.22

ATFE FLIGHT UNIT RETEST (ORBIT CYCLE NO. 11)

Drawing Number	Latest Revision	Number Sheets	Nomenclature or Description
G460-F-071 (GSFC)	E	2	I.C.D. ATS-F-AMES ATFE
G460-F-072 (GSFC)	-	1	I.C.D. Spacecraft Drill Template for ATFE
G460-F-073 (GSFC)	B	1	I.C.D. Cover and Stand for ATFE
DTM 034-1005	D	1	I.C.D. AMES ATFE Thermal Diode Heat Pipe
DTM 034-1010	D	1	ATFE Cover and Stand (Ground Support Equipment)
DTM 034-1033	B	1	ATFE Radiator Panel Assemblies
DTM 034-1035	E	2	ATFE Phase Change Material Equipment Shelf
DTM 034-1036	E	1	ATFE Saddle Details
DTM 034-1039	C	1	ATFE Absorber Panel Assembly
DTM 034-1041	E	1	ATFE FCHP Assembly
DTM 034-1044	C	1	ATFE Internal Insulations
DTM 034-1072	-	-	ATFE List of Specifications, Procedures, Source Control Drawings
DTM 034-1073	A	1	ATFE Project Parts, Devices, and Material List
DTM 034-1076	-	-	ATFE Tool and Fixture List

TABLE 4.10

ATFE QUALIFICATION AND FLIGHT UNITS DRAWING LIST

Drawing Number	Latest Revision	Number Sheets	Nomenclature or Description
DTM 034-1080	F	2	ATFE General Assembly
DTM 034-1081	H	4	ATFE Structural Assembly
DTM 034-1082	E	3	ATFE PCM-ES with Heat Pipe Assembly
DTM 034-1083	-	1	ATFE Isolator Details
DTM 034-1084	C	1	ATFE FCHP/Saddles Assembly
DTM 034-1085	C	1	ATFE Clip and Bracket Details
DTM 034-1087	B	2	ATFE Main Insulation Assembly
DTM 034-1089	-	1	ATFE Functional Diagram
DTM 034-1092	A	1	ATFE FCHP Straight Heat Pipe Assembly
ITE E07004-002	C	1	ATFE Schematic Diagram for Electronics Module
ITE C-7004-005	-	-	ATFE Ferrite Box
ITE D-7004-034-1091	A	-	ATFE Electronic Module Assembly
ITE PLD-7004-034-1091	-	-	ATFE Electronic Module Parts List
ITE DL-7004-034-1091	-	-	ATFE Electronic Module Drawing List

TABLE 4.10 (Continued)

ATFE QUALIFICATION AND FLIGHT UNITS DRAWING LIST

Drawing Number	Latest Revision	Number Sheets	Nomenclature or Description
DTM 001-1003	-	3	Pinch-Off Procedure
DTM 001-1007	-	3	Cleaning Procedure of Aluminum (6061) for Welding
DTM 001-1008	-	3	Cleaning Procedure for Methanol/SST Heat Pipe Tubes
DTM 001-1010	-	6	Gas Charging Procedure for VCHP
DTM 001-1011	-	3	Cleaning Procedure for Methanol/SST Heat Pipe with Wick
DTM 001-1012	-	3	Cleaning Procedure for 304 SST Parts for Heat Pipe Assemblies
DTM 001-1013	-	3	Procedure for Surface Preparation of Aluminum and Aluminum Parts for Adhesive Bonding
DTM 001-1020	-	2	Thermistor Bonding Procedure
DTM 034-1050	B	4	Procedure for the Assembly of the ATFE Phase Change Material Equipment Shelf
DTM 034-1051	B	7	Charging Procedure for the ATFE Phase Change Material Equipment Shelf
DTM 034-1052	A	3	Procedure for Bonding Second Surface Thermal Control Mirror to an Aluminum Substrate

TABLE 4.11

ATFE QUALIFICATION AND FLIGHT UNITS SPECIFICATION AND PROCEDURE LIST

Drawing Number	Latest Revision	Number Sheets	Nomenclature or Description
DTM 034-1053	-	4	PEM Studs and Splines, Fasteners Installation Procedure
DTM 034-1056	B	-	NASA AMES ATFE Inspection Plan
DTM 034-1057	-	8	Specification for ATFE Electronic Controller
DTM 034-1058	-	13	Specification for the ATFE Electronics Module
DTM 034-1062	-	9	Specification for ATFE Command and Signal Conditioning Unit
DTM 034-1063	-	1	Second Surface Thermal Control Mirror
DTM 034-1064	-	1	Regimesh Slab
DTM 034-1065	-	7	Methanol Charging Procedure
DTM 034-1068	-	6	Test Procedure for the ATFE FCHP
DTM 034-1069	-	3	Test Procedure for the ATFE PCM-ES
DTM 034-1075	-	-	ATFE Functional Test Procedure

TABLE 4.11 (Continued)

ATFE QUALIFICATION AND FLIGHT UNITS SPECIFICATION AND PROCEDURE LIST

At NASA-ARC, qualification and acceptance testing was performed in accordance with the following plans and procedures:

TPL-PES-ATS-1	ATFE Qualification and Acceptance Test Plan
TP-PES-ATS-4	ATFE Leak Test Procedure
TP-PES-ATS-5	ATFE Functional Test Procedure
TP-PES-ATS-6	ATFE Thermal Vacuum Test Procedure
PERS-P-1088	ATFE Environmental Test Procedure (includes weight and center of gravity, vibration, storage temperature, and thermocouple calibrations)

Records of all inspections and tests conducted at Dynatherm were submitted to NASA with the delivery of each heat pipe as part of a documentation package. After completion of the Qualification and Acceptance Testing at NASA-ARC, a Data Package was prepared which contains a complete record of all NASA conducted inspections and tests. For reference purposes, the Summary of this Data Package follows:

"The Advanced Thermal Control Flight Experiment (ATFE) has successfully completed qualification and acceptance testing at the Ames Research Center in accordance with Specification S-320-ATS-2, Rev. D."

"Qualification tests were performed on unit S/N 034-1080-003 during the period August 12 - September 2, 1972. Acceptance testing of the flight unit S/N 034-1080-019 occupied the period January 10 - February 10, 1973. Near the end of the Acceptance Program the thermal diode was found to be functioning below expectations. The unit was returned to the contractor for repair, at which time steps were also taken to reduce its susceptibility to electromagnetic interference. Differences between the qualification and flight units are detailed in the section "Flight Configuration." Repetition of acceptance testing began on May 29 and was completed on June 24, 1973."

"With slight modifications of the heat transfer associated with the reservoir of the feedback-controlled heat pipe (FCHP) (ECO included under "Flight Configuration"), the unit met or exceeded all test criteria and performed to the satisfaction of the Principal Investigator."

5. REFERENCES

1. Bienert, W. B., "Study to Evaluate the Feasibility of a Feedback Controlled Variable Conductance Heat Pipe", Dynatherm Corporation Technical Summary Report DTM-70-4 under NASA Contract NAS2-5722

2. Marcus, B. D., "Theory and Design of Variable Conductance Heat Pipes", NASA Contractor Report CR-2018, April 1972

3. Bienert, W. B., Brennan, P. J., and Kirkpatrick, J. P., "Feedback Controlled Variable Conductance Heat Pipes", AIAA Paper No. 71-421, April 1971

4. Bienert, W. B. and Brennan, P. J., "Transient Performance of Electrical Feedback-Controlled Variable Conductance Heat Pipes", ASME Paper 71-Av-27

5. Heat Pipe Design Handbook, prepared for NASA-MSC by Dynatherm Corporation, August 1972

6. Bienert, W. B., "Heat Pipes for Temperature Control", Proc. 4th Intersociety Energy Conversion Engineering Conference, Washington, D. C., 1969

7. Swerdling, B. et al., "Development of a Thermal Diode Heat Pipe for the Advanced Thermal Control Flight Experiment (ATFE)", AIAA Progress in Astronautics: Thermal Control and Radiation, Vol. 31, edited by C. L. Tien, The MIT Press, Cambridge, Mass., 1972, pp. 35-50

8. Bentilla, E. W. et al., "Research and Development Study on Thermal Control by Use of Fusible Materials", Northrop Space Labs, N66-26691, April 1966, NASA

9. Hale, D. V. et al., "Phase Change Material Handbook", CR-61363, Sept. 1971, NASA

APPENDIX A

STEADY-STATE PERFORMANCE EQUATION OF FCHP

In Section 3.1 of this report, a set of equations is developed which define the required reservoir size for a specified control performance (ΔT_v) and variation in the sink temperature ($T_{o,l}$ and $T_{o,h}$). If the vapor temperature variations are small, these equations can be solved explicitly for ΔT_v. These "inverted" equations can then be used to evaluate the control performance of a FCHP for specified sink variations.

In the most general case, the reservoir temperature at the low condition is less than the vapor temperature (not all gas is expelled from the reservoir). At the high condition, the reservoir temperature is higher than the sink temperature (which requires a larger than optimum reservoir). For this case, the control performance is given by:

$$\Delta T_v = \frac{\frac{V_c}{V_r}\left[1 - \frac{p_v(T_{o,l})}{p_v(T_{v,n})}\right] + \frac{T_{o,l}}{T_{r,l}}\left[1 - \frac{p_v(T_{r,l})}{p_v(T_{v,n})}\right] - \frac{T_{o,l}}{T_{r,h}}\left[1 - \frac{p_v(T_{r,h})}{p_v(T_{v,n})}\right]}{\frac{1}{2}\ln\frac{dp_v}{dT_v}\left[\frac{V_c}{V_r} + \frac{T_{o,l}}{T_{r,h}} + \frac{T_{o,l}}{T_{r,l}}\right]} \qquad \text{(A-1)}$$

The following special cases are frequently of interest:

1. The reservoir temperature at the high condition is equal to the sink temperature but at the low condition is less than the vapor temperature.

$$T_{r,h} = T_{o,h} \quad \text{and} \quad T_{r,l} < T_{v,l} \qquad \text{(A-2)}$$

$$\Delta T_v = \frac{\frac{V_c}{V_r}\left[1 - \frac{p_v(T_{o,l})}{p_v(T_{v,n})}\right] + \frac{T_{o,l}}{T_{r,l}}\left[1 - \frac{p_v(T_{r,l})}{p_v(T_{v,n})}\right] - \frac{T_{o,l}}{T_{o,h}}\left[1 - \frac{p_v(T_{o,h})}{p_v(T_{v,n})}\right]}{\frac{1}{2}\ln\frac{dp_v}{dT_v}\left[\frac{V_c}{V_r} + \frac{T_{o,l}}{T_{o,h}} + \frac{T_{o,l}}{T_{r,l}}\right]} \qquad \text{(A-3)}$$

2. The reservoir temperature at the low condition is equal to the vapor temperature but at the high condition is higher than the sink temperature.

$$T_{r,h} > T_{o,h} \qquad \text{and} \qquad T_{r,l} = T_{v,l} \tag{A-4}$$

$$T_{v,l} = T_{v,n} - \frac{\Delta T_v}{2} \sim T_{v,n} \tag{A-5}$$

$$\Delta T_v = \frac{\frac{V_c}{V_r}\left[1 - \frac{p_v(T_{o,l})}{p_v(T_{v,n})}\right] - \frac{T_{o,l}}{T_{r,h}}\left[1 - \frac{p_v(T_{r,l})}{p_v(T_{v,n})}\right]}{\frac{1}{2}\ln\frac{dp_v}{dT_v}\left[\frac{V_c}{V_r} + \frac{T_{o,l}}{T_{r,h}} + \frac{T_{o,l}}{T_{v,n}}\right]} \tag{A-6}$$

3. In the ideal FCHP (minimum reservoir requirement), the reservoir temperature at the low condition is equal to the vapor temperature and at the high condition is equal to the sink temperature.

$$T_{r,h} = T_{o,h} \qquad \text{and} \qquad T_{r,l} = T_{v,l} \tag{A-7}$$

$$\Delta T_v = \frac{\frac{V_c}{V_r}\left[1 - \frac{p_v(T_{o,l})}{p_v(T_{v,n})}\right] - \frac{T_{o,l}}{T_{o,h}}\left[1 - \frac{p_v(T_{o,h})}{p_v(T_{v,n})}\right]}{\frac{1}{2}\ln\frac{dp_v}{dT_v}\left[\frac{V_c}{V_r} + \frac{T_{o,l}}{T_{o,h}} + \frac{T_{o,l}}{T_{v,n}}\right]} \tag{A-8}$$

4. If the reservoir temperature equals the sink temperature under all conditions, the FCHP becomes a passive VCHP.

$$T_{r,h} = T_{o,h} \qquad \text{and} \qquad T_{r,l} = T_{o,l} \tag{A-9}$$

$$\Delta T_v = \frac{\left(\frac{V_c}{V_r} + 1\right)\left[1 - \frac{p_v(T_{o,l})}{p_v(T_{v,n})}\right] - \frac{T_{o,l}}{T_{o,h}}\left[1 - \frac{p_v(T_{o,h})}{p_v(T_{v,n})}\right]}{\frac{1}{2} \ln \frac{dp_v}{dT_v}\left[\frac{V_c}{V_r} + 1 + \frac{T_{o,l}}{T_{o,h}}\right]} \qquad \text{(A-10)}$$

APPENDIX B

COMPUTER PROGRAM FEDCON - FEEDBACK CONTROLLED VARIABLE CONDUCTANCE HEAT PIPE TRANSIENT ANALYSIS

1. Introduction

This appendix describes the theory and utilization of the computer program FEDCON which has been developed to analyze the transient behavior of an electrical feedback-controlled variable conductance heat pipe. In principle, the feedback mechanisms monitor the source temperature and adjust the gas storage volume. As in the case of conventional thermal control heat pipes, a noncondensing gas is employed to control the heat rejection area of the heat pipe; but now the effective storage volume is variable and related to the heat source. The noncondensible gas volume and therefore the conductance is adjusted by varying the partial pressure of the working fluid within the storage volume. The heat source is monitored electrically, and the signal drives a small heater at the storage volume which in turn controls the temperature of the saturated working fluid. The use of feedback permits the heat source temperature to be monitored directly. As a result, the effect of changes in heat load, environmental conditions, etc., on source temperature are attenuated.

2. Theory

A functional block diagram for the system is shown in Figure B-1. An actuating signal related to the error between the reference and actual source temperature drives the auxiliary heater which controls the temperature of the storage reservoir. Conservation of the mass of the noncondensible in the storage reservoir and the inactive part of the condenser (consistent with storage and sink conditions and the system pressure) dictates the active length of the condenser (Y). An energy balance for the active part

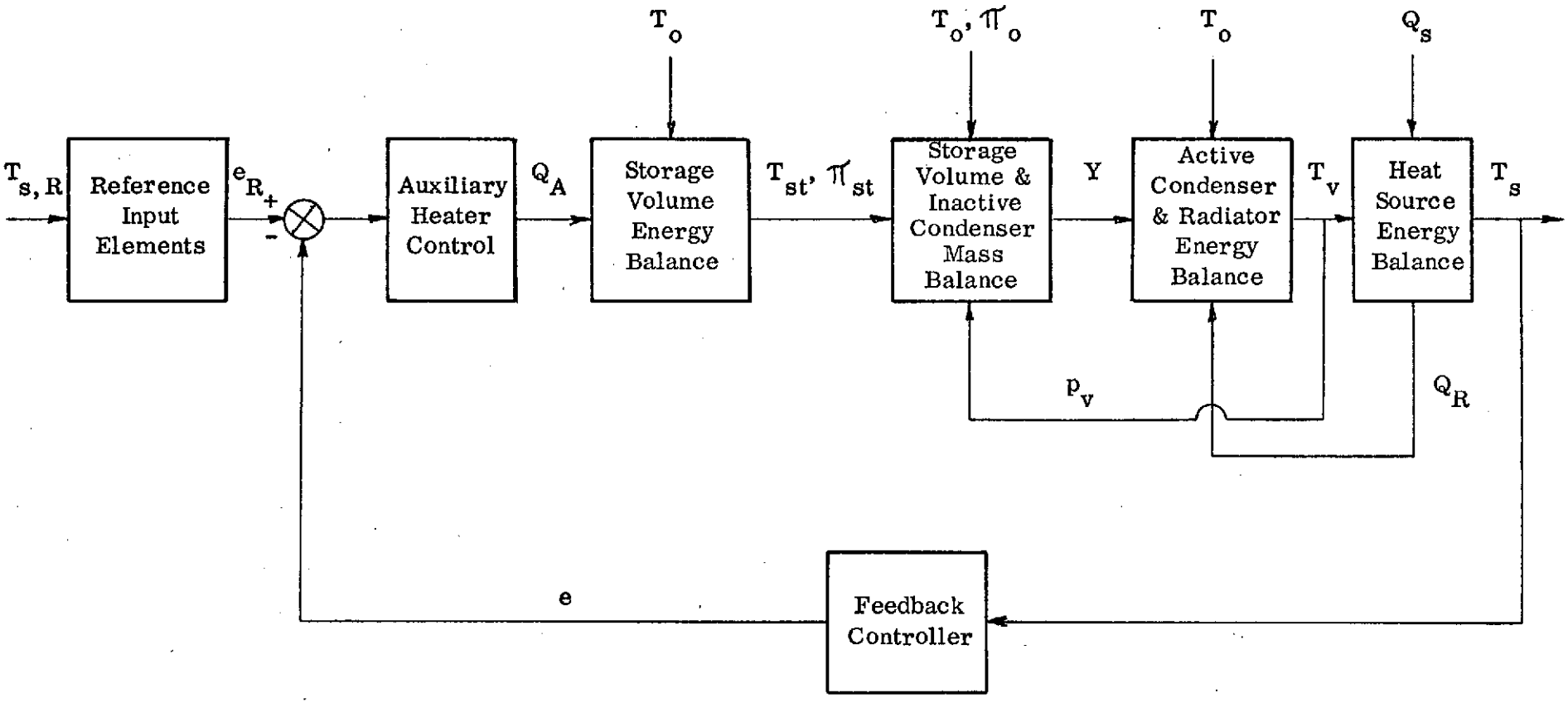

FIGURE B-1

FUNCTIONAL BLOCK DIAGRAM FOR AN ACTIVE FEEDBACK CONTROLLED VARIABLE CONDUCTANCE HEAT PIPE SYSTEM

of the condenser establishes the vapor temperature. Similarly, with the vapor temperature established, an energy balance at the heat source determines the temperature of the heat source. The output heat source temperature is monitored and input to the feedback controller which moderates the signal and feeds it back to the auxiliary heater.

The mathematical model which simulates the transient response of this system is shown in Figure B-2.

The following assumptions have been used in defining the model:

- The noncondensible gas obeys the ideal-gas equation of state.
- Mass diffusion is negligible -- i.e., a sharp interface exists between the working fluid vapor and the noncondensible gas at the beginning of the inactive part of the condenser.
- Conduction along the heat pipe wall is negligible.
- The inactive part of the condenser instantaneously assumes the sink temperature when it becomes inactive. As an option, the inactive condenser temperature may be calculated as a mean temperature between active condenser and sink temperature.
- Heat dissipation to the sink can be described by either the convection equation or radiation exchange.
- The entire condenser length is active at the high power/high sink condition.

The mathematical model based on these assumptions consists of the following system of simultaneous nonlinear differential equations. At the heat source (node 1):

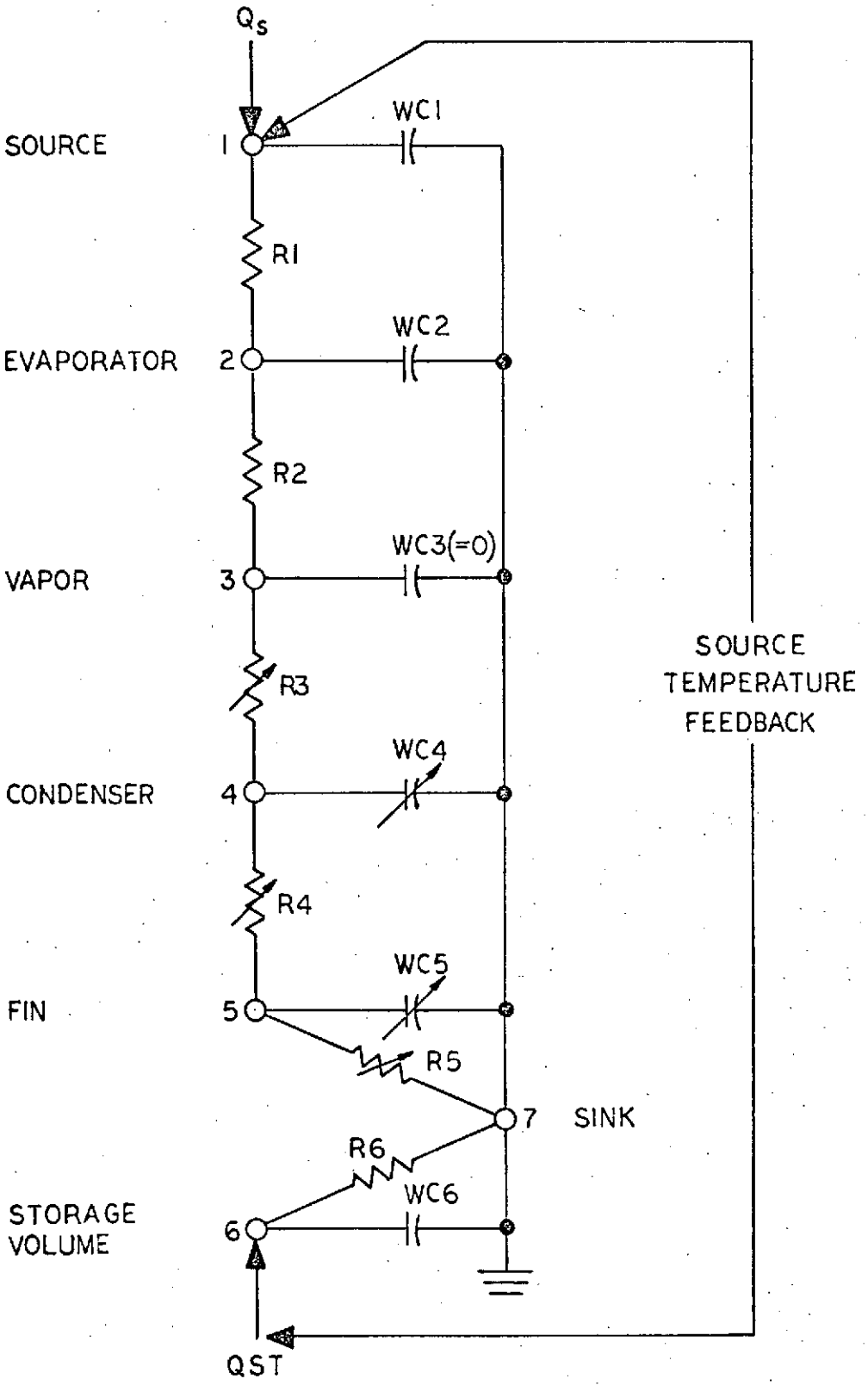

FIGURE B-2

THERMAL MODEL FOR ELECTRICAL FEEDBACK CONTROLLED HEAT PIPE SYSTEM

$$Q_s = (m\,c_p)_1 \frac{dT_1}{dt} + \frac{T_1 - T_2}{R_1} \tag{B-1}$$

At the evaporator wall (node 2):

$$\frac{T_1 - T_2}{R_1} = (m\,c_p)_2 \frac{dT_2}{dt} + \frac{T_2 - T_3}{R_2} \tag{B-2}$$

At the vapor (node 3):

$$\frac{T_2 - T_3}{R_2} = (m\,c_p)_3 \frac{dT_3}{dt} + \frac{T_3 - T_4}{R_3} \tag{B-3}$$

where $(m\,c_p)_3$ is usually set to zero. At the condenser wall (node 4):

$$\frac{T_3 - T_4}{R_3} = (m\,c_p)_4 \frac{dT_4}{dt} + \frac{T_4 - T_5}{R_4} \tag{B-4}$$

At the cooling fin (node 5):

$$\frac{T_4 - T_5}{R_4} = (m\,c_p)_5 \frac{dT_5}{dt} + \frac{T_5 - T_0}{R_5} \tag{B-5}$$

where T_0 = sink temperature. At the gas storage reservoir (node 6):

$$Q_{st} = (m\,c_p)_6 \frac{dT_6}{dt} + \frac{T_6 - T_0}{R_6} \tag{B-6}$$

In addition to satisfying the above heat balances, the following mass balance must be maintained:

$$m_g = m_{ic} + m_{st} \tag{B-7}$$

Substitution of the Ideal Gas Law gives:

$$m_g = \frac{(P_v - \pi_o)}{R_g T_0} V_{ic} + \frac{(P_v - \pi_{st})}{R_g T_{st}} V_{st} \qquad \text{(B-8)}$$

where:

$$V_{ic} = \frac{\pi D_v^2}{4} (L_c - Y) \qquad \text{(B-9)}$$

In the above equations, the thermal resistances and capacitances R_3, R_4, R_5, $(m\,c_p)_3$, $(m\,c_p)_4$, $(m\,c_p)_5$ are a function of Y which is the length of the active part of the condenser. The nonlinearities of this system are associated with the variable length "Y" required for variable conductance. Thus, the resistances and capacitances associated with the variable condenser length are given by:

$$R_y = R_L \times \frac{L_c}{Y} \qquad \text{(B-10)}$$

$$(m\,c_p)_y = (m\,c_p)_L \times \frac{Y}{L_c} \qquad \text{(B-11)}$$

The value of Q_{st} in Equation B-6 is a function of the type of electronic controller and the controller's bandwidth. Either ON/OFF or proportional control can be evaluated.

A simplified flow diagram for this program called FEDCON (Feedback Controlled Variable Conductance Heat Pipe Transient Analysis) is shown in Figure B-3. Basically, the program performs an initialization in which all constant coefficients and the initial heat pipe temperature profile are determined. Upon completion of the initialization, the transient analysis is begun. Any combination of heat source power, sink temperature, or auxiliary power will drive the system. The differential equations (Equations B-1 thru

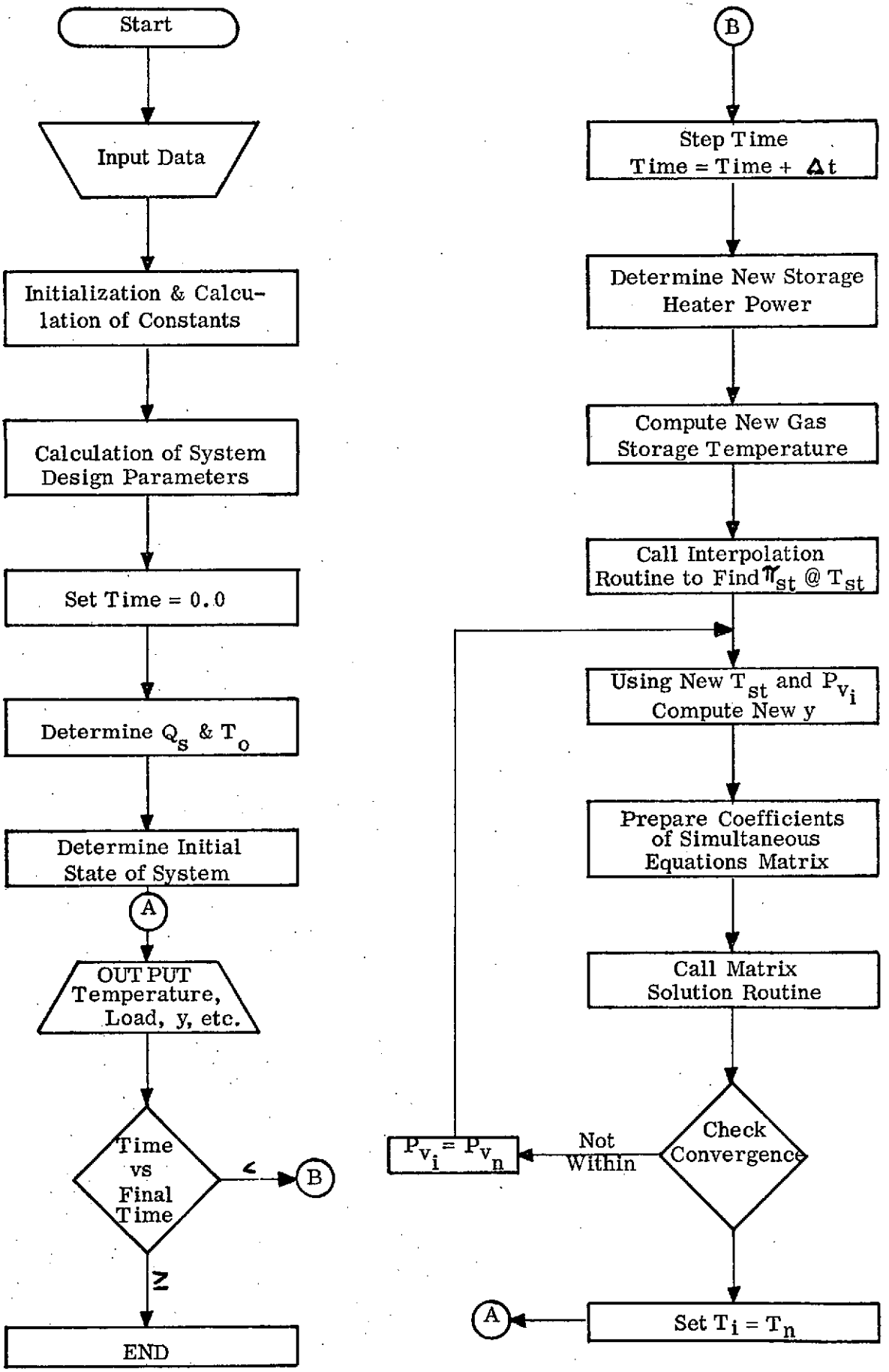

FIGURE B-3

FLOW DIAGRAM FOR TRANSIENT ANALYSIS OF ELECTRICAL FEEDBACK CONTROLLED HEAT PIPE SYSTEM

B-6) are approximated by a third order Runga-Kutta equation. Temperatures are determined for a calculated value of "Y" based on satisfying the mass balance with the vapor temperature and pressure related to the preceding calculation. A matrix inversion which utilizes the Gaussian Elimination Method is used to solve for the temperatures. Because of the nonlinearities associated with the variable conductance, it is necessary to iterate within a given time step in order to guarantee simultaneous solution of both the heat balance equations and the mass balance. Convergence is obtained at a given time step when:

$$\frac{|p_v - p_{v,i}|}{p_v} \leq \delta \qquad \text{(B-12)}$$

where:

p_v = Vapor pressure corresponding to the vapor temperature determined from the present calculation within a given time step.

$p_{v,i}$ = Vapor pressure corresponding to a vapor temperature which is related to the vapor temperature determined in the preceding calculation within the same time step.

δ = Specified convergence increment.

Three subroutines are included within the main program:

FINDP - Interpolates in the vapor pressure versus temperature tables

FINDQT - Interpolates in the source load and sink temperature versus time tables

ELIMI - Inverts the matrix by Gauss Elimination Method

3. Input

Depending on the type of problem, there are a maximum of ten input cards which are:

CARD #1 : TITLE CARD (Up to 80 characters) [Format 80H]

CARD #2 : CONTROL CARD - IP, IQS, ITO, IRAD, INACT [Format 515]

CARD #3 : THERMAL RESISTANCES - R_1 thru R_6 (^oK/watt) [Format 6E12]

CARD #4 : THERMAL CAPACITANCES - WC_{p1}, WC_{p2}, WC_{p4}, WC_{p5}, WC_{p6} (watt-sec/^oK) [Format 12E6]

CARD #5 : DV, XLC, RMW, QSMX, QSMI, QOAO, GAM3, TOM, TOMI, TSTH, TSTL (See Card #5 description below) [Format 12E6]

CARD #6 : POI, FTIME, DT, TSR, GAIN, QSTN, VST, WGAS (See description below) [Format 12E6]

CARD #7 : TEMPERATURE VS WORKING FLUID VAPOR PRESSURE CURVE (^oK, Atmospheres) [Format 12E6]

CARD #8 : TIME VS SOURCE DISSIPATION (Q_s) {Only if IQS > 0} (seconds, watts) [Format 12E6]

CARD #9 : TIME VS SINK TEMPERATURE (T_o) {Only if IT > 0} (seconds, ^oK) [Format 12E6]

CARD #10 : CONTINUATION CARD More > 0 for continuation - new case
More ≤ 0 to end

3.1 Detailed Description of Input Cards

CARD #2 : Control Card

IP = Number of table points for vapor pressure curve

IQS = Number of table points for Q_s curve; if < zero - no input and CARD #8 is skipped, QS is set equal to QSMX

ITO = Number of table points for T_o curve; if ≤ zero - no input and CARD #9 is skipped, TO is set equal to TOMI

IRAD $>$ 0, Radiation is mode of heat transfer from condenser to sink R(5) = $_5A_5$; IRAD = 0 for convection or conduction to sink

INACT $\leq$ 0, the temperature in inactive section of the condenser is set equal to the sink temperature (T_o); if >0, the temperature in inactive section is calculated as a function of the percent of inactivity and vapor temperature as well as sink temperature.

CARD #5

DV = Equivalent Vapor Diameter, cm

XLC = Total Length of Condenser, cm

RMW = Molecular Weight of Noncondensible Gas

QSMX = Maximum Source Load, watts

QSMI = Minimum Source Load, watts

QOAD = Auxiliary Heater Power for ON/OFF Control, watts; equal to zero for proportional control

GAM3 = Deadband Tolerance ($T_{sr} \pm$ GAM3) for ON/OFF Control, ^oK; equal to maximum auxiliary heater power for proportional control

GAM2 = $P_v/P_{v,i}$ (~ 0.01 for H_2O; ~ 0.005 for Ammonia)

TOM = Maximum Sink Temperature, ^oK

TOMI = Minimum Sink Temperature, ^oK

TSTH = Storage Temperature at High Power/High Sink (Minimum), ^oK

TSTL = Storage Temperature at Low Power/Low Sink (Maximum), ^oK

CARD #6

PoI = Printout Interval, seconds

FTIME = Final Time, seconds

DT = Calculating Increment, seconds (~0.5)

TSR = Source Control Temperature, ^{o}K

GAIN = Proportional Control Gain, watt/^{o}K

QSTN = Proportional Controller Nominal Auxiliary Power, watt

VST = Storage Volume, cc; if < 0 - calculates and uses ideal design

WGAS = Noncondensible Gas Charge, gms
(if WGAS = 0, using calculated value)

4. Program Listing

The program listing for FEDCON is presented in the following pages.

```
      PROGRAM FEDCON(INPUT,OUTPUT,TAPE5=INPUT,TAPE6=OUTPUT)
C  **********  REVISION AS AUGUST 27,1971 **********
      DIMENSION  R(6),WC(6),D(6),TN(6),A(6),ER(6),TI(7),TP(20),P(20),TQ(
     120),Q(20),TM(20),T(20),C(6,6),PD(6),IC(7)
    1 FORMAT (1H1,26X,*FEEDBACK  CONTROLLED  VARIABLE  CONDUCTANCE  HEAT
     1  PIPE  TRANSIENT  ANALYSIS*/////)
    2 FORMAT (47X,*T Y P E   O F   C O N T R O L L E R*//)
    3 FORMAT (59X,*PROPORTIONAL*)
    4 FORMAT (61X,*ON - OFF*)
    5 FORMAT (47X,*MAXIMUM HEATER POWER = *,F7.1,* WATTS*)
    6 FORMAT (51X,*GAIN = *,F9.2,* WATTS/DEG K*)
    7 FORMAT (////54X,*S O U R C E   D A T A*//)
    8 FORMAT (49X,*MAXIMUM DISSIPATION = *,F5.1,* WATTS*)
    9 FORMAT (49X,*MINIMUM DISSIPATION = *,F5.1,* WATTS*)
   10 FORMAT (49X,*TEMP. CONTROL POINT = *,F5.1,* DEG K*///)
   11 FORMAT (54X,*D E S I G N   D A T A*//)
   12 FORMAT (52X,*VAPOR DIAMETER = *,F6.3,* CM*)
   13 FORMAT (48X,*TOTAL CONDENSER LENGTH = *,F6.2,* CM*///)
   14 FORMAT (48X,*NON-CONDENSIBLE  GAS  PARAMETERS*//)
   15 FORMAT (53X,*MOLECULAR WEIGHT = *,F6.3)
   16 FORMAT (51X,*STORAGE VOLUME = *F6.2,* CU CM*)
   17 FORMAT (49X,*TOTAL WEIGHT OF GAS = *,F7.4,* GMS*)
   18 FORMAT (44X,*GAS VOLUME FOR IDEAL DESIGN = *,F6.2,* CU CM*///)
   19 FORMAT (40X,*THERMAL  RESISTANCE*,10X,*THERMAL  CAPACITANCE*)
   20 FORMAT (43X,*DEG K/WATT*,19X,*WATT-SEC/DEG K*//)
   21 FORMAT (30X,I1,12X,F10.5,21X,F10.5/)
   22 FORMAT (F7.2,F10.2,6F12.2,3F13.3)
   23 FORMAT (6H1 TIME,5X,*T  R  A  N  S  I  E  N  T     T  E  M  P  E
     1R  A  T  U  R  E  S  (D  E  G  C)     Q(SOURCE)     Q(STORAGE)     L
     2ENGTH(C)*/)
   24 FORMAT (* (MIN)*,5X,*SOURCE     EVAPORATOR      VAPOR     CONDENSER
     1  RADIATOR      STORAGE       SINK*,9X,*WATTS*,8X,*WATTS*,9X,*CM*//)
   25 FORMAT (6E12.4)
   26 FORMAT (12E6.4)
   27 FORMAT (3I2,8E6.4)
   28 FORMAT (44X,*GAS WEIGHT FOR IDEAL DESIGN = *,F6.4,* GMS*)
  299 FORMAT (1H1)
  300 FORMAT (80H
     1                                  )
  301 FORMAT (//  47X,*I N P U T    T A B L E S*//)
  302 FORMAT(34X,*WORKING  FLUID  VAPOR  PRESSURE  VERSUS TEMPERATURE*/)
  303 FORMAT (47X,I2,F12.1,F14.5)
  304 FORMAT (48X,*N*,6X,*TEMP(K)*,6X,*PV(ATM)*)
  305 FORMAT (48X,*N*,4X,*TIME(SEC)*,4X,*QS(WATTS)*)
  306 FORMAT (48X,*N*,4X,*TIME(SEC)*,4X,*TO(DEG K)*)
  307 FORMAT (//34X,*VARIATION  IN  SOURCE  HEAT  LOAD  VERSUS  TIME*/)
  308 FORMAT (//34X,*VARIATION  IN  SINK  TEMPERATURE  VERSUS  TIME*/)
  309 FORMAT (12BX,I2)
  671 FORMAT (////10X,*THIS IS THE STEADY STATE RESULTS AT ZERO TIME WHI
     1CH WAS ONLY REQUESTED----------*)
```

```
 30   READ (5,300)
      READ (5,27) IP,IQS,ITO,IRAD,INACT
      READ (5,25)(R(N),N=1,6)
      READ (5,25) WC(1),WC(2),WC(4),WC(5),WC(6)
      READ (5,26) DV,XLC,RMW,QSMX,QSMI,QOAO,GAM3,GAM2,TOM,TOMI,TSTH,TSTL
      READ(5,26)POI,FTIME,DT,TSR,GAIN,QSTN,VST,WGAS
      READ (5,26)(TP(N),P(N),N=1,IP)
      WRITE (6,299)
      WRITE (6,300)
      WRITE (6,301)
      WRITE (6,302)
      WRITE (6,304)
      WRITE (6,303)(N,TP(N),P(N),N=1,IP)
      IF (IQS) 32,32,33
 32   QS=QSMX
      GO TO 34
 33   READ (5,26)(TQ(N),Q(N),N=1,IQS)
      WRITE (6,307)
      WRITE (6,305)
      WRITE (6,303)(N,TQ(N),Q(N),N=1,IQS)
 34   IF (ITO) 35,35,36
 35   TO=TOMI
      GO TO 37
 36   READ (5,26)(TM(N),T(N),N=1,ITO)
      DO 337 N=1,ITO
337   T(N)=T(N)+273.
      WRITE (6,308)
      WRITE (6,306)
      WRITE (6,303)(N,TM(N),T(N),N=1,ITO)
 37   PIE=3.141592
      SIGMA=5.67E-12
      WC(3)=0.0
      GAM1=0.5
      RGAS=81.929/RMW
      JS=0
      BAS=20.
      ER(1)=R(1)
      ER(6)=R(6)
      DO 39 N=2,5
      M=N-1
 39   ER(N)=R(M)*R(N)/(R(M)+R(N))
      VC=PIE*DV**2*XLC/4.
      TVL=TSR-(R(1)+R(2))*QSMI
      TVH=TSR-(R(1)+R(2))*QSMX
      CALL FINDP(IP,TOMI,PO,P,TP)
      CALL FINDP(IP,TVL,PVL,P,TP)
      CALL FINDP(IP,TVH,PVH,P,TP)
      CALL FINDP(IP,TSTH,PSTH,P,TP)
      CALL FINDP(IP,TSTL,PSTL,P,TP)
      CALL FINDP(IP,TOM,POM,P,TP)
```

```
      IF (IP) 999,42,42
   42 X1=(1.-PO/PVL)*TSTL*VC/TOMI
      X2=(1.-PSTH/PVH)*PVH*TSTL/(PVL*TSTH)-(1.-PSTL/PVL)
      VSTI=X1/X2
      WGAI=(PVL-PO)*VC/(RGAS*TOMI)+(PVL-PSTL)*VST/(RGAS*TSTL)
      IF (VST) 441,441,442
  441 VST=VSTI
  442 IF (WGAS) 443,443,444
  443 WGAS=WGAI
  444 VSTO=VST
      VSTH=WGAS*RGAS*TOM/(PVH-POM)
      TIME=0.0
      TIMM=0.0
   43 IF (IQS) 999,45,44
   44 CALL FINDQT(IQS,TIME,QS,Q,TQ)
      IF (IQS) 999,999,45
   45 IF (ITO) 999,47,46
   46 CALL FINDQT(ITO,TIME,TO,T,TM)
      CALL FINDP(IP,TO,PO,P,TP)
      IF (ITO) 999,999,48
   48 IF (IP) 999,999,47
   47 IF (TIME) 49,49,71
   49 TV=TSR-(R(1)+R(2))*QS
      CALL FINDP(IP,TV,PV,P,IP)
      IF (IRAD)351,351,350
  350 RR5=R(5)
      RR6=R(6)
      R(5)=1./(RR5*SIGMA*(TV+TO)*(TV**2+TO**2))
  351 Y=(R(3)+R(4)+R(5))*QS*XLC/(TV-TO)
      VCY=PIE*DV**2*(XLC-Y)/4.
      IF(INACT)341,341,340
  340 TA=TV*Y/XLC+TO*(XLC-Y)/XLC
      GO TO 342
  341 TA=TO
  342 CALL FINDP(IP,TA,PA,P,IP)
      WGST=WGAS-(PV-PO)*VCY/(RGAS*TO)
      ER(3)=R(2)*R(3)/(R(2)+R(3)*XLC/Y)
      DO 40 N=1,6
      PQ(N)=0.0
      A(N)=1.0
      IF (WC(N)) 401,401,41
   41 A(N)=1.0-0.5*DT/(WC(N)*ER(N))+(DT/(WC(N)*ER(N)))**2/6.
  401 A(N)=WC(N)/(A(N)*DT)
   40 ER(N)=A(N)+1./ER(N)
      J=0
      TSTI=TV-10.
      CALL FINDP(IP,TSTI,PST,P,TP)
   50 TSTN=VST*(PV-PST)/(RGAS*WGST)
      BIT=TSTN-TSTI
      ABIT=ABS(BIT)
```

```
      PPP=ABIT-GAM1
      IF (PPP) 52,52,51
   51 IF (BIT) 502,52,501
  501 JS=JS+1
      GO TO 503
  502 JS=JS-1
  503 IF (JS) 505,506,504
  504 JS=1
      GO TO 507
  505 JS=-1
      GO TO 507
  506 BAS=BAS/3.
  507 BBIT=ABS(BIT+1.)
      IF (ABIT-BAS) 509,508,508
  508 TST=TSTI + BAS*(BBIT-ABIT)
      GO TO 510
  509 TST=TSTI + BIT/4.
  510 CALL FINDP(IP,TST,PST,P,TP)
      TSTI=TST
      J=J+1
      IF (J-40) 511,512,512
  512 WRITE(6,500)  ABIT
  500 FORMAT(//15X,*INITIAL TST LOOP REACHED 40 ITERATIONS*,F12.5)
      GO TO 999
  511 IF (IP) 999,999,50
   52 TI(1)=TSR
      TI(2)=TSR-QS*R(1)
      TI(3)=TV
      IF (Y) 521,521,522
  521 TI(4)=TV
      TI(5)=TV
      GO TO 523
  522 TI(4)=TV-R(3)*XLC*QS/Y
      TI(5)=TI(4)-R(4)*XLC*QS/Y
  523 IF (IRAD) 353,353,352
  352 R(6)=1./(RR6*SIGMA*(TSI+T0)*(TST**2+T0**2))
  353 IF (QOAO) 53,53,54
   53 QST=(TSI-T0)/R(6)
      QSTM=(TSTL-T0)/R(6)
      GO TO 55
   54 QST=QOAO
   55 WRITE (6,1)
      WRITE (6,2)
      IF (QOAO) 56,56,57
   56 WRITE (6,3)
      WRITE (6,5) QSTM
      WRITE (6,6) GAIN
      GO TO 58
   57 WRITE (6,4)
      WRITE (6,5) QOAO
```

```
58    WRITE (6,7)
      WRITE (6,8) QSMX
      WRITE (6,9) QSMI
      WRITE (6,10) TSR
      WRITE (6,11)
      WRITE (6,12) DV
      WRITE (6,13) XLC
      WRITE (6,14)
      WRITE (6,15) RMN
      WRITE (6,16) VST
      WRITE (6,17) WGAS
      WRITE (6,28) WGAI
      WRITE (6,18) VSTI
      WRITE (6,19)
      WRITE (6,20)
      WRITE (6,21)(N,P(N),WC(N),N=1,6)
      WRITE (6,23)
      WRITE (6,24)
      PTIME=0.0
      TI(6)=TST
      TI(7)=TO
      YY=Y
59    DO 69 N=1,7
69    TC(N)=TI(N) -273.0
      WRITE (6,22)TIMM,(TC(N),N=1,7),QS,QST,YY
      IF (FTIME) 669,669,670
669   WRITE (6,671)
      GO TO 999
670   PTIME=PTIME + POI-.0001
      IF (TIME-FTIME) 60,999,999
60    IF (QOAO) 61,61,63
61    QST=QSTN+ GAIN*(TSR-TI(1))
      IF (QST) 62,70,78
78    IF (QST-GAM3) 70,70,79
79    QST=GAM3
      GO TO 70
62    QST=0.0
      GO TO 70
63    DTEMP=TI(1)-TSR
      IF (DTEMP-GAM3) 64,67,67
64    IF (DTEMP) 65,66,66
65    IF (DTEMP+GAM3) 66,67,67
66    QST=QOAO
      GO TO 70
67    QST=0.0
70    TIME=TIME + DT
      TIMM=TIME/60.0
      GO TO 43
 71   IF (IRAD) 355,355,354
```

```
  354 R(5)=1.0/(RR5*SIGMA*(TI(5)+T0)*(TI(5)**2+T0**2))
      R(6)=1.0/(RR6*SIGMA*(TI(6)+T0)*(TI(6)**2+T0**2))
      ER(5)=R(4)*R(5)/(R(4)+R(5))
      ER(6)=R(6)
      DO 356 N=5,6
      A(N)=1.0
      IF (WC(N)) 357,357,358
  358 A(N)=1.0-.5*DT/(WC(N)*ER(N))+(DT/(WC(N)*ER(N)))**2/6.
  357 A(N)=WC(N)/(A(N)*DT)
  356 ER(N)=A(N)+1.0/ER(N)
  355 TST=(QST+T0/R(6)+A(6)*TI(6))/ER(6)
      CALL FINDP(IP,TST,PST,P,TP)
      J=1
      PQ(1)=QS
      PQ(5)=T0/R(5)
      IF (IP) 999,999,72
   72 VCY=RGAS*T0*WGAS/(PV-PQ)-(PV-PST)*T0*VST/((PV-PQ)*TST)
      Y=XLC-4.*VCY/(PIE*DV**2)
      YY=Y
      VST=VSTO
      IF (Y) 700,700,701
  700 Y=0.0001
      GO TO 704
  701 IF (Y-XLC) 704,704,702
  702 Y=XLC
      VCY1=VC
  705 VSTO=VSTO+VC-.5*(VCY+VCY1)
      VRAT=ABS(VSTO-VST)/VST
      IF (VRAT-0.01) 707,707,706
  706 VST=VSTO
      VCY1=VCY
      VCY=RGAS*T0*WGAS/(PV-PQ)-(PV-PST)*T0*VST/((PV-PQ)*TST)
      GO TO 705
  707 YY=XLC-4.*VCY/(PIE*DV**2)
  704 DO 38 N=1,6
      TN(N)=0.0
      DO 38 K=1,6
   38 C(N,K)=0.0
      DO 68 N=1,5
      C(N,N)=ER(N)
      D(N)=PQ(N)+A(N)*TI(N)
      M=N+1
      C(N,M)=-1.0/R(N)
   68 C(M,N)=C(N,M)
      C(3,2)=-XLC/(R(2)*Y)
      C(3,3)=A(3)+(R(2)+R(3)*XLC/Y)/(R(2)*R(3))
      HARB=0.0
      CALL ELIMI(5,C,D,TN,HARB)
      IF (HARB) 999,73,999
   73 CALL FINDP(IP,TN(3),PVN,P,TP)
```

```
      IF (IP) 999,999,74
74    PDIF=ABS(PVN-PV)/PV
      DIV=J
80    IF (PDIF-GAM2) 76,76,75
75    TI(3)= TI(3) + (TN(3) - TI(3))/DIV
      CALL FINOP(IP,TI(3),PV,P,TP)
      J=J+1
      IF (J-20) 72,720,720
720   WRITE (6,721)
 721  FORMAT(//15X,*Y-PV CONVERGENCE LOOP REACHED 20 ITERATIONS*)
      GO TO 999
76    DO 77 N=1,5
77    TI(N)=TN(N)
      PV=PVN
      TI(6)=TST
      TI(7)=TO
      IF (TIME-PTIME) 60,59,59
999   READ (5,27) MORE
      IF (MORE) 100,100,30
100   STOP
      END
```

```
      SUBROUTINE FINDOT(IP,TFD,PFD,P,TP)
C  PROGRAM FINDP INTERPOLATES BETWEEN POINTS OF AN INPUT TABLE
      DIMENSION P(20),TP(20)
      I=1
    1 IF (I-IP) 4,2,2
    2 WRITE (6,3)
      WRITE (6,33) I,TP(I),TFD
   33 FORMAT (I5,2E20.4)
    3 FORMAT (//8X,*POINT   EXCEEDS   TABLES*//)
      IP=-1
      RETURN
    4 IF (TFD-TP(I+1)) 6,6,5
    5 I=I+1
      GO TO 1
    6 PFD=P(I) + (TFD-TP(I))*(P(I+1)-P(I))/(TP(I+1)-TP(I))
      RETURN
      END
      SUBROUTINE FINDP(IP,TFD,PFD,P,TP)
C  PROGRAM FINDP INTERPOLATES BETWEEN POINTS OF AN INPUT TABLE
      DIMENSION P(20),TP(20)
      I=1
    1 IF (I-IP) 4,2,2
    2 WRITE (6,3)
    3 FORMAT (//8X,*POINT  EXCEEDS  TABLES*//)
      IP=-1
      RETURN
    4 IF (TFD-TP(I+1)) 6,6,5
    5 I=I+1
      GO TO 1
    6 PFL=ALOG(P(I))+(TFD-TP(I))*(ALOG(P(I+1))-ALOG(P(I)))/(TP(I+1)-
     1TP(I))
      PFD=EXP(PFL)
      RETURN
      END
```

```
      SUBROUTINE ELIMI(NN,C,D,TN,HARB)
C  PROGRAM ELIMI SOLVES SIMULTANEOUS EQUATIONS BY GAUSS ELIMINATION METHOD
      DIMENSION C(6,6),D(6),TN(6),DUM(6)
      N1=NN-1
      DO 51 I=1,N1
      DD=C(I,I)
      IF(DD)47,41,47
   41 JS=I+1
      DO 42 J=JS,NN
      IF(C(J,I))43,42,43
   42 CONTINUE
      HARB=1.0
      WRITE (6,6)
    6 FORMAT (//6X,*MATRIX--- PROBLEM*//)
      RETURN
   43 DO 44 J1=I,NN
   44 DUM(J1)=C(I,J1)
      DM=D(I)
      DO 45 J1=I,NN
   45 C(I,J1)=C(J,J1)
      D(I)=D(J)
      DO 46 J1=I,NN
   46 C(J,J1)=DUM(J1)
      D(J)=DM
      DD=C(I,I)
   47 DO 48 J=I,NN
   48 C(I,J)=C(I,J)/DD
      D(I)=D(I)/DD
      K=I+1
      DO 51 L=K,NN
      R=C(L,I)
      IF(R)49,51,49
   49 DO 50 J=I,NN
   50 C(L,J)=C(L,J)-R*C(I,J)
      D(L)=D(L)-R*D(I)
   51 CONTINUE
      TN(NN)=D(NN)/C(NN,NN)
      K=NN
   52 NN=NN-1
      N=NN
      IF(N)53,53,54
   53 NN=K
      RETURN
   54 TN(N)=D(N)
      NP=N+1
      DO 55 I=NP,K
   55 TN(N)=TN(N)-C(N,I)*TN(I)
      GO TO 52
      END
```